Model Predictive Control for Formation Flying Spacecraft

by

Louis Scott Breger

Bachelor of Science Aeronautics and Astronautics
Massachusetts Institute of Technology, 2002

Submitted to the Department of Aeronautics and Astronautics
in partial fulfillment of the requirements for the degree of

Master of Science in Aeronautics and Astronautics

at the

MASSACHUSETTS INSTITUTE OF TECHNOLOGY

June 2004

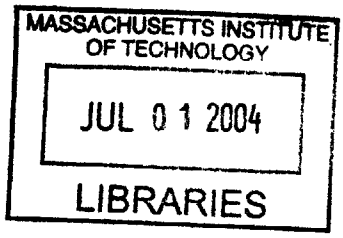

Author .....
Department of Aeronautics and Astronautics
May 21, 2004

AERO

Certified by .....
Jonathan P. How
Associate Professor
Thesis Supervisor

Accepted by .....
Edward M. Greitzer
H.N. Slater Professor of Aeronautics and Astronautics
Chair, Committee on Graduate Students

Model Predictive Control for Formation Flying Spacecraft

by

Louis Scott Breger

Submitted to the Department of Aeronautics and Astronautics
on May 21, 2004, in partial fulfillment of the
requirements for the degree of
Master of Science in Aeronautics and Astronautics

Abstract

Formation flying is an enabling technology for many future space missions. This thesis addresses some of the key dynamics and control issues expected in future missions by pursuing two areas of advancement: extensions of relative linear dynamics models and assessment and mitigation of sensor noise effects on control systems. Relative dynamics models play an important role in finding drift-free initial conditions for spacecraft formations and for designing feedback controllers. This thesis presents extensions to the equations of relative motion expressed in both Cartesian reference frames and Keplerian orbital elements, including new initialization techniques for widely spaced passive apertures with very general formation configurations. Also, a new linear time-varying form of the equations of relative motion is developed from Gauss' Variational Equations, and the linearizing assumptions for these equations are shown to be consistent with typical formation flying scenarios. The second area considers the impact of sensor noise, predicted by several researchers to have a significant effect on the fuel-use for formation flying control. This thesis analyzes the impact of carrier-phase differential GPS sensor noise using a new analytical method for predicting the effects of disturbances on a model predictive control formulation. Previous work used an "open-loop" planning approach to achieve robustness in the presence of sensor noise, but was limited to short planning horizons. This thesis employs a "closed-loop" approach which accounts for future replanning, enabling longer planning horizons and more general terminal constraints. This MPC formulation guarantees the robustness of the planning system to both process and sensing noise with fuel costs that are shown to be comparable to the previous approach.

Thesis Supervisor: Jonathan P. How
Title: Associate Professor

Acknowledgments

Many thanks to everyone who has assisted me thus far in my academic career. I would particularly like to mention my parents, Joel and Carol, my sister, Julia, and my graduate academic and research advisor, Jonathan How. Also, in conducting and documenting the research contained in this thesis, the assistance of two of my labmates, Arthur Richards and Megan Mitchell, has been greatly appreciated. The camaraderie provided by the whole lab and by my other friends at MIT has amplified the pleasure and excitement of the graduate experience.

This research was supported by NASA Grants #NCC5-704 and #NCC5-729.

I dedicate this thesis to the memory of my grandparents.

Contents

List of Figures

List of Tables

Chapter 1

Introduction

In the early years of space flight, most satellites were launched with individual purposes and worked independently of one another. Often they were controlled manually via commands uplinked from specialized ground stations. Less than ten years after the launch of Sputnik, the *c*onstellation emerged as another form of space mission, one in which satellites are launched with a common purpose, but do not require coordinated control. The Transit constellation (begun in the 1960s) and the GPS constellation are examples of satellites that were designed to provide common services for navigation [71]. The spacecraft in these constellations are operated individually from ground stations and controlled periodically through station-keeping maneuvers designed to maintain specific orbits. More recently, constellations of satellites have been launched for communications (Iridium) and science gathering (EO1, Cluster, and LISA) [4, 49, 83]. Many space missions planned for the near-future fall into a new class of *f*ormation flying missions. These are missions which require coordinated control to maintain a desired relative geometry between the satellites. Formation flying missions are well-suited to applications requiring simultaneous observations from multiple locations (such as interferometry and synthetic aperture radar).

Formation flying missions are being designed to fly in many different types of orbits: TechSat-21 and Orion in Low Earth Orbit (LEO) [2,5], Magnetospheric Multiscale Mission (MMS) (see Figure 1) in High Earth Orbit (HEO) [51], and Stellar Imager in L2 [74]. A recent paper [73] identifies these three missions as *benchmark*

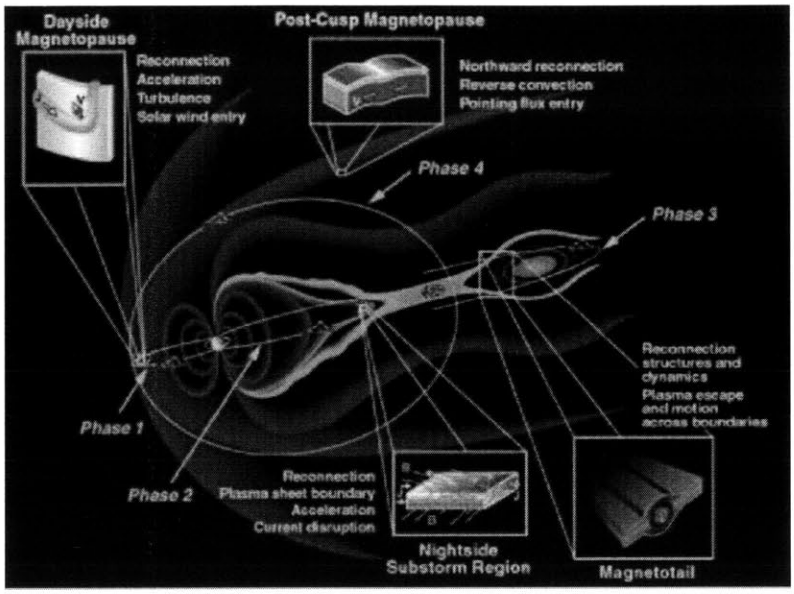

Fig. 1–1: Artist's depiction of the Magnetospheric Multiscale Mission [80]

problems for formation flying. Each poses unique challenges to the present state-of-the-art in spacecraft orbit design and control. This thesis focuses on the particular challenges posed by missions designed for LEO and HEO.

This thesis addresses two spacecraft formation flying control challenges: control of widely separated formations in highly elliptical orbits and the prediction and mitigation of the effects of sensor noise on spacecraft control. First, the problem of using linearized dynamics for *initialization* and *control* of widely-separated spacecraft formations is examined using linear perturbation states to capture the effects of second order nonlinearities. Control in highly elliptical orbits is addressed by developing and using a set of linear, time-varying dynamics based in the LVLH frame and valid for elliptic orbits. Next, linearized dynamics based in the Keplerian orbital element frame are applied in a model predictive formulation and are shown to be valid for typical state error separations. Formation initialization and coordination techniques in a differential orbital element frame are also discussed. To address the problem of predicting/mitigating the effects CDGPS sensor noise might have on the control performance, a new technique based on a robust, closed-loop model predictive control formulation is developed. Realistic simulations using the closed-loop technique are

implemented based on a bounded noise model developed for CDGPS sensor noise and expected process noise in LEO.

1.1 Previous Work and Contributions

The *dynamics of relative motion* for circular orbits are described by a set of linear, time-invariant equations, now known as the Hill's or Clohessy-Wiltshire equations [75, 76]. Much work has been done in the past thirty years studying relative dynamics of orbital motion of elliptical orbits [10, 13, 11, 12, 35, 18, 72], and as a result, Lawden's equations of motion and their parameter-varying closed form solution have also become commonplace for use in relative orbital dynamics problems [18]. However, with recent interest in closed-loop control for formation flying, several time-explicit forms of the relative equations of motion have also been developed. In Ref. [35], both the equations of motion and a state transition matrix are derived that are linearized in eccentricity, making them valid for orbits with $e < 0.3$. More recently, Ref. [72] presented a form of the state transition matrix which propagates relative motion and is valid for all eccentricities. This form is useful for propagating open-loop, however no control effect matrix is given, so it is not sufficient for discrete control. This thesis derives a new set of equations of motion based in an LVLH frame that are valid for all eccentricities and can be numerically discretized for the purposes of control, yielding both the state transition matrix and the control effect matrix. This form of the relative dynamics is useful for fixed-time step propagation, closed-loop discrete control, and discrete online planning.

Initialization techniques for spacecraft formations typically attempt to achieve two goals: place spacecraft in a desired formation geometry and create a formation that requires as little fuel as possible to maintain. Typical desired formation geometries in LEO are in-track separations and projected circles. For example, the TechSat-21 mission, a formation flying passive aperture radar system, sparked a great deal of interest in *passive aperture formations.* The problem of creating a passive aperture in a circular orbit has a well-known solution based on Hill's equations [26]. Ref. [18]

developed a closed-form solution for creating a passive aperture in a general elliptical orbit from Lawden's equations. Both of these approaches rely on the assumption that the spacecraft in the formation are close to the origin of the reference frame. Ref. [48] extends those approaches to handle larger separations between spacecraft using a set of second order perturbation states. However, their approach was limited to a specific class of passive aperture orbits that does not include a tetrahedron, which is a common formation geometry for HEO missions [51]. This thesis extends Ref. [48] to initialize widely separated formations that have arbitrary relative geometry. The approach taken is to re-derive the second order perturbation solution using a general drift-free solution to Hill's equations, This new form of the long-baseline correction is capable of initializing tetrahedron geometries. The general long-baseline correction is demonstrated on LEO orbits and evaluated in terms of a tetrahedron quality metric.

Ref. [43] specifies a formation configuration using relative orbital elements (as opposed to a relative Cartesian frame such as LVLH). This approach assigns each spacecraft to a desired orbital element offset from one spacecraft in the formation. Assigning all spacecraft to have the same orbital energy (*i.e.,* have the same semimajor axis, one the Keplerian elements) creates a drift-free formation for any amount of separation. This thesis introduces a linear optimization approach for specifying drift-free initial conditions for arbitrary Cartesian geometries using differential orbit elements. This approach is demonstrated on a tetrahedron-shaped formation. Alternative orbit initialization approaches for a tetrahedron geometry are discussed in Refs. [45,49]. Those approaches create drift-free formations, but choose some of the degrees of freedom in the initialization problem without optimizing. The method introduced in this thesis optimizes the choice of all variables (*e.g.,* velocity direction, tetrahedron orientation, scaling, and position) in order to minimize the fuel-use required to achieve the desired initial conditions.

Many formation control approaches have been suggested in recent years [82,14,4, 30,54,39,40,43,81,38], spanning a large range of techniques, including PD, LQR, LMI, nonlinear, Lyapunov, impulsive, and model predictive. Typically, it is assumed that a formation is initialized to a stable orbit and deviations caused by disturbances such

as differential drag and/or differential J_2 must be corrected. Some approaches, such as Lyapunov and PD controllers [40], require that control be applied continuously, a strategy both prone to high fuel use and difficult to implement when thrusting requires attitude adjustment. Other approaches, such as the impulsive thrusting scheme introduced in Ref. [44], require spacecraft to thrust at previously specified times and directions in the orbit, ensuring that some of the maneuvers will not be fuel-optimal.

Model Predictive Control (MPC) with online linear programming (LP) optimization is used for control in this thesis [30]. This approach to control has several advantages for the spacecraft formation flying problem. It is a planning type of controller, which makes explicit use of natural dynamics and known disturbance models to minimize fuel use. MPC is capable of including hard state constraints naturally, such as error boxes for science performance and thrust magnitude constraints to capture limitations of the satellites. The use of LP optimization with MPC allows a piecewise linear performance metric (the one-norm of fuel use) to be chosen, which captures the cost of maneuvering using differential velocity changes. Also, the LP form creates a discontinuous control law which allows for periods of drifting during a plan, when natural dynamics are being used. This type of control law is similar to the "bang-off-bang" solution typical of a fuel-minimizing optimal control problem. Lastly, linear programs can be solved rapidly, enabling a real-time implementation with commercial software [53].

Sensor noise has been identified as an issue for spacecraft control using GPS measurements. For a formation relying of CDGPS for relative state sensing, expected estimate standard deviations for an LVLH frame are 0.01 m for position and 0.0005 m/s for velocity [56, 57, 70]. References [77, 32, 78] identify similar levels of sensing noise as a driver of fuel use expected to exceed other disturbances present in the spacecraft formation flying problem. The inability of a spacecraft controller to know its state accurately prevents correct initial conditions from being attained. Thus, some level of drift will occur between the spacecraft in the formation. Continuous control strategies deal with this drift through constant correction, possibly leading to a large

fuel use. Another approach is to create a deadband or error box centered around the desired state [30, 78], in which a spacecraft will not apply control until it nears or exceeds the bounds of the box. In addition to the error box approach, Ref. [30] presents a robustness method which relies on online planning to generate trajectories that are valid for a range of possible initial conditions encompassed by the sensor error. This "open-loop" robustness approach creates plans that are guaranteed to be inside a box at the end of a fixed time horizon. However, the open-loop approach is limited in the length of planning horizon it can use for a given box size by the necessity of retaining problem feasibility. An alternative "closed-loop" approach to noise robustness is presented in Ref. [59], in which planning occurs regularly to ensure a spacecraft never exits the error box by explicitly considering not only the present initial conditions, but also the effects of future replanning. This additional consideration enables longer planning horizons and more general terminal constraints. Work in this thesis applies the new closed-loop robustness approach to a realistic spacecraft formation flying problem and also applies an analytic method to predict performance in the presence of sensor noise for a simplified problem.

1.2 Thesis Overview

This thesis focuses on extending the application of model predictive control (MPC) to the spacecraft formation flying problem. The MPC formulation developed in Ref. [30] is used in Chapters 2 and 3 and the formulation developed in Ref. [59] is used in Chapter 4.

Chapter 2 presents several extensions to the dynamics of relative motion in Cartesian frames, including the derivation of:

- Generalized initial conditions and linear time-invariant (LTI) equations of motion that enable widely separated formations to be initialized in drift-free configurations and propagated. These dynamics extensions are demonstrated in the context of a LEO mission, where they provide a significant improvement, and an MMS-like orbit and formation geometry, where nonlinearity effects are

minimal compared to eccentricity effects.

- A linear time-varying set of equations of spacecraft relative motion that are valid for elliptic orbits and based in an LVLH frame. Enabling planning in fixed time steps in the LVLH frame eliminates the need for real-time frame conversion of inputs during the implementation of the plan and also shifts the computation of the nonlinear mapping between time and true anomaly to the plan formulation stage, rather than the time-critical plan implementation stage. These dynamics are demonstrated on a realistic HEO mission scenario and shown to be practical both in terms of expected fuel use and optimization formulation and solution times.

Chapter 3 discusses the use of Gauss' Variational Equations (GVEs) for model predictive control of spacecraft formations. Extensions include:

- A linear, time-varying form of relative dynamics is developed using the GVEs and its range of validity is established for typical LEO and HEO reference orbits.
- Used the GVE-based relative dynamics to derive a MPC controller. Demonstrated its efficiency compared to a previously published GVE-based planning technique. Presented a nonlinear simulation of the control of a tetrahedron formation using a GVE-based model predictive controller.
- Derived a new linear optimization formulation for choosing the relative orbital element initial conditions based on a desired Cartesian formation geometry. This approach allows for the optimization of velocity direction, rotation, translation, and scaling to minimize the fuel required to maneuver into a formation and it is applied to an MMS-like formation geometry.
- Extended the *virtual center* approach to formation flying in Ref. [42] to a GVE formulation with a decentralized implementation.

Chapter 4 addresses the impact of sensing noise on a model predictive control system. This is accomplished using a form of "closed-loop" model predictive control which has predictable performance under certain constraints [67]. Extensions include:

- Used the predictive method to identify the performance sensitivity of several parameters in the MPC formulation: error box size, planning horizon length, and expected sensor noise level.
- Demonstrated that the "closed-loop" robustness method can be used to ensure both sensor noise and process noise robustness in a realistic environment with realistic constraints. Investigated the effect that more general controller terminal constraints (*i.e.,* those enabled by the longer planning horizons used in the closed-loop method) have on performance. A simulated mission showed average fuel use per spacecraft of 2.2 mm/s per orbit for a four-spacecraft formation in LEO.

Chapter 5 describes a new "hardware-in-the-loop" formation flying testbed created using hardware at the Goddard Space Flight Center (GSFC). Key points:

- This testbed uses a GPS signal generator connected to Orion GPS receivers to create a realistic sensor output, which is then used for control. The testbed was modified to use a commercially available propagator to drive the signal generator. The dynamics model is nonlinear, includes realistic disturbances, and can be used for testing at both MIT and GSFC.
- The testbed is MATLAB-based and uses separate computers to simulate each spacecraft in the fleet, introducing communication considerations into the decentralized control and estimation algorithms. Initial closed-loop control results are presented.

Chapter 2

Relative Dynamics Extensions

Spacecraft formations are often specified and controlled using relative dynamics of orbital motion. The reason for this is that the relative dynamics about an orbit can be linearized [8], creating a system in which linear control can be applied. Hill's equations is an often-used set of linearized dynamics, which is linearized about a circular reference orbit. An advantage of Hill's equations is that they are partially decoupled, neutrally stable, and linear time-invariant, making the application of control straightforward. Lawden's equations [10] are time-varying system of relative dynamics, also linearized in terms of separation, which are valid for eccentric orbits.

In recent literature [26, 14, 18], a number of methods of creating drift-free formations were established. These methods rely assigning all spacecraft in a formation the same semimajor axis or orbital energy. In a circular orbit, this requirement is equivalent to eliminating the secular term in Hill's equations [8]. Ref. [18] developed initial conditions for a drift-free formation in an eccentric orbit. However, neither the circular nor the eccentric orbit conditions account for nonlinearities unmodeled by Hill's or Lawden's dynamics and, as a result, fail to produce drift-free motion in widely separated spacecraft.

This chapter presents extensions to Hill's equations, which allow the second-order terms of the relative motion of a drift-free formation to be modeled as linear perturbations on the original solution. This is a generalization of work presented in Ref. [48]. This work is evaluated in the context of a widely separated tetrahedron-shaped for-

mation, similar to the MMS mission [51]. This chapter also develops an approach to modeling relative dynamics for eccentric orbits as a function of time in an LVLH frame, rather than in equal periods of true anomaly as it was demonstrated applied to a Lawden frame in Refs. [16, 18]. This simplifies the implementation of the model predictive control system of the type described in Ref. [30].

2.1 Long-baseline Initialization Technique

A number of future spacecraft formation flying missions will require spacecraft to maintain specified separations or relative geometries [49]. These requirements stem from the need to obtain scientific data simultaneously from widely separated locations or the need to take data in the same location at frequent intervals [6].

To minimize control effort, orbits can be chosen that naturally prevent the spacecraft from separating. One type of drift-free orbit, a *passive aperture*, is based on the elimination of secular terms from Hill's equations [9]. The general solution to Hill's equations has six initial conditions that define a satellite's orbit relative to the origin of the Hill's frame, where x is the radial direction, y is the along-track direction, and z is the across-track direction. It can be seen that the only term contributing to secular drift is $-(3\dot{y}(0) + 6n_{\text{ref}}x(0))t$, where n_{ref} is the period of the osculating orbit and t is elapsed time. The condition to prevent spacecraft separation over time is

$$3\dot{y}(0) = -6n_{\text{ref}}x(0) \tag{2.1}$$

This approach works well for formations in circular orbits where the separation between spacecraft is on the order of 100 m. However, the accuracy of Hill's equations degrades as the inter-spacecraft separation is extended, therefore, choosing initial conditions based on Eq. 2.1 will no longer eliminate secular drift. Ref. 48 recently proposed an approach that extends the validity of Hill's equations to larger inter-spacecraft separations by adding a set of second order perturbations. This approach is derived for a specific solution to Hill's equations with initial conditions that restrict

the formation to a projected circle in the y-z plane. In this case, the radius of the projected circle is the same for all satellites in the formation and the position of the satellites in the circle is chosen by an angular offset.

That approach is shown to work well, but it is overly restrictive, as the formation geometry is specified by only two initial conditions. The MMS mission will require a widely separated regular tetrahedron geometry to fulfill its science objectives, and the two initial conditions available are not sufficient to fully describe a tetrahedron. To use the nonlinearity correction for an MMS-like mission, the following extends the basic approach in Ref. [48] to a more general solution of Hill's equations:

$$\begin{aligned} x(t) &= x(0)\cos(n_{\text{ref}}t) + \frac{\dot{x}(0)}{n_{\text{ref}}}\sin(n_{\text{ref}}t) \\ y(t) &= y(0) + \frac{2\dot{x}(0)}{n_{\text{ref}}}\big[\cos(n_{\text{ref}}t) - 1\big] - 2x(0)\sin(n_{\text{ref}}t) \\ z(t) &= z(0)\cos(n_{\text{ref}}t) + \frac{\dot{z}(0)}{n_{\text{ref}}}\sin(n_{\text{ref}}t) \end{aligned} \tag{2.2}$$

where the relative orbit of each spacecraft in the Hill's frame is defined by five initial conditions, $x(0)$, $y(0)$, $z(0)$, $\dot{x}(0)$, and $\dot{z}(0)$. The Hill's solution in Eq. 2.2 can be used to define initial conditions corresponding to the corners of a tetrahedron, because the initial x, y, and z coordinates can be specified independently. Using Eq. 2.2, any initial velocity conditions will produce a recurring tetrahedron formation in the Hill's frame, but the nonlinearity correction derived herein can be applied to other geometries that may require specific initial velocities as well as positions. Optimizing the choice of initial conditions to account for other effects is discussed at the end of the subsection and a similar initial condition optimization development can be found in Section 3.5.

Figure 2–1 shows a regular tetrahedron with a spacecraft at each vertex. The lines are shown just to highlight the geometry. Tetrahedron examples used in this Chapter

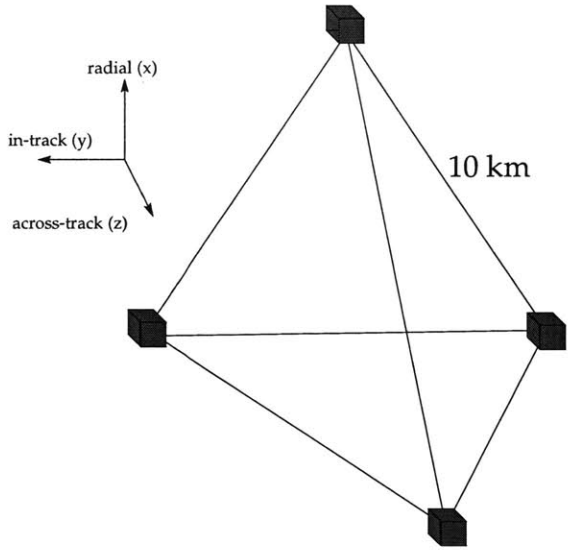

Fig. 2–1: Regular 10 km tetrahedron formation.

use the (x, y, z) initial position conditions (in kilometers)

$$\begin{aligned} \text{Sat}_1 &= (0, 0, \frac{\sqrt{3}}{3}10) & \text{Sat}_2 &= (0, \frac{1}{2}10, -\frac{\sqrt{3}}{6}10) \\ \text{Sat}_3 &= (0, -\frac{1}{2}10, -\frac{\sqrt{3}}{6}10) & \text{Sat}_4 &= (\frac{\sqrt{6}}{3}10, 0, 0) \end{aligned} \tag{2.3}$$

The nonlinearity correction only accounts for second order effects. The fully nonlinear relative equations of motion (not shown) can be reduced in terms of eccentricity and nonlinearity into the following second order equations of motion [48]

$$\begin{aligned} \ddot{x} - 2n_{\text{ref}}\dot{y} - 3n_{\text{ref}}^2 x &= \epsilon\left[\frac{y^2}{2} + \frac{z^2}{2} - x^2\right] \\ \ddot{y} - 2n_{\text{ref}}\dot{x} &= \epsilon xy \\ \ddot{z} - n_{\text{ref}}^2 \dot{z} &= \epsilon xz \end{aligned} \tag{2.4}$$

where $\epsilon = 3\mu/a_c^4$, μ is the gravitational parameter, and a_c is the semi-major axis of the reference orbit. Assuming the radial direction solution (and corresponding solutions in the in-track and cross-track directions)

$$\ddot{x} = \ddot{x}_{\text{h}} + \epsilon\ddot{x}_{\text{cn}}, \quad \dot{x} = \dot{x}_{\text{h}} + \epsilon\dot{x}_{\text{cn}}, \quad x = x_{\text{h}} + \epsilon x_{\text{cn}} \tag{2.5}$$

where $(\cdot)_{\rm h}$ denotes a state of the Hill's equations and $(\cdot)_{\rm cn}$ denotes a perturbation state. Eq. 2.4 can be rewritten as

$$\begin{aligned} \ddot{x}_{\rm cn} - 2n_{\rm ref}\dot{y}_{\rm cn} - 3n_{\rm ref}^2 x_{\rm cn} &= (1/2)(y_{\rm h}^2 + z_{\rm h}^2 - 2x_{\rm h}^2) \\ \ddot{y}_{\rm cn} + 2n_{\rm ref}\dot{x}_{\rm cn} &= x_{\rm h} y_{\rm h} \\ \ddot{z}_{\rm cn} + n_{\rm ref}^2 z_{\rm cn} &= x_{\rm h} z_{\rm h} \end{aligned} \tag{2.6}$$

The right hand side of Eq. 2.6 can be found by substituting in the Hill's solution from Eq. 2.2, yielding

$$\begin{aligned} \frac{y_{\rm h}^2 + z_{\rm h}^2 - 2x_{\rm h}^2}{2} &= \frac{1}{2}\left(-2\frac{\dot{x}(0)}{n_{\rm ref}} + 2\frac{\dot{x}(0)\cos(n_{\rm ref}t)}{n_{\rm ref}} + y(0) - 2x(0)\sin(n_{\rm ref}t)\right)^2 \\ &\quad + \frac{1}{2}\left(\frac{\dot{z}(0)\sin(n_{\rm ref}t)}{n_{\rm ref}} + z(0)\cos(n_{\rm ref}t)\right)^2 \\ &\quad - \left(\frac{\dot{x}(0)\sin(n_{\rm ref}t)}{n_{\rm ref}} + x(0)\cos(n_{\rm ref}t)\right)^2 \end{aligned} \tag{2.7}$$

$$\begin{aligned} x_{\rm h} y_{\rm h} &= \left(x(0)\cos(n_{\rm ref}t) + \frac{\dot{x}(0)\sin(n_{\rm ref}t)}{n_{\rm ref}}\right) \times \\ &\quad \left(-2\frac{\dot{x}(0)}{n_{\rm ref}} + 2\frac{\dot{x}(0)\cos(n_{\rm ref}t)}{n_{\rm ref}} + y(0) - 2x(0)\sin(nt)\right) \end{aligned} \tag{2.8}$$

$$\begin{aligned} x_{\rm h} z_{\rm h} &= \left(x(0)\cos(n_{\rm ref}t) + \frac{\dot{x}(0)\sin(n_{\rm ref}t)}{n_{\rm ref}}\right) \times \\ &\quad \left(z(0)\cos(n_{\rm ref}t) + \frac{\dot{z}(0)\sin(n_{\rm ref}t)}{n_{\rm ref}}\right) \end{aligned} \tag{2.9}$$

Treating the Hill's states as inputs, the perturbation states evolve as

$$\mathbf{X}_{\rm cn}(\mathrm{t}) = \Phi_{\rm h}(\mathrm{t})\mathbf{X}_{\rm cn}(0) + \int_0^{\mathrm{t}} \Phi_{\rm h}(\mathrm{t}-\tau)\mathrm{B}\mathbf{u}_{\rm h}(\tau)\mathrm{d}\tau \tag{2.10}$$

where[1]

$$\mathbf{X}_{\rm cn}(\mathrm{t}) = \left[x_{\rm cn}(t), y_{\rm cn}(t), z_{\rm cn}(t), \dot{x}_{\rm cn}(t), \dot{y}_{\rm cn}(t), \dot{z}_{\rm cn}(t)\right]^{\mathrm{T}}$$

[1]For brevity, n is used in place of $n_{\rm ref}$, c in place of $\cos(nt)$, and s in place of $\sin(nt)$.

$$\mathbf{u}_{\mathrm{h}}(\mathrm{t}) = \begin{bmatrix} \frac{y_{\mathrm{h}}^2+z_{\mathrm{h}}^2-2x_{\mathrm{h}}^2}{2} \\ x_{\mathrm{h}}y_{\mathrm{h}} \\ x_{\mathrm{h}}z_{\mathrm{h}} \end{bmatrix} \qquad B = \begin{bmatrix} 0 \\ I \end{bmatrix}$$

and

$$\Phi_{\mathrm{h}}(t) = \begin{bmatrix} 4-3c & 0 & 0 & \frac{s}{n} & \frac{2(1-c)}{n} & 0 \\ 6(s-nt) & 1 & 0 & \frac{2(1-c)}{n} & \frac{4s-3nt}{n} & 0 \\ 0 & 0 & c & 0 & 0 & \frac{s}{n} \\ 3ns & 0 & 0 & c & 2s & 0 \\ -6n(1-c) & 0 & 0 & -2s & 4c-3 & 0 \\ 0 & 0 & -ns & 0 & 0 & c \end{bmatrix}$$

Evaluating Eq. 2.10 symbolically yields the solutions in Eqs. 2.31–2.34 (see appendix to Chapter 2). These six equations show that, similar to the case for the standard Hill's solution, only the along-track position, $y(t)$, has secular drift terms. The secular drift can be eliminated from the solution if the coefficient of that term is set equal to zero, which From Eq. 2.31 gives

$$-\frac{1}{2n^3}\Big(12n^4x(0)_{\mathrm{cn}} + 6\dot{y}(0)_{\mathrm{cn}}n^3 - x(0)^2n^2 - 2\dot{x}(0)y(0)n \\ +\dot{x}(0)^2 + \dot{z}(0)^2 + 2y(0)^2n^2 + z(0)^2n^2\Big) = 0 \quad (2.11)$$

If $x(0)_{\mathrm{cn}}$ is set to zero, then the condition for drift-free second-order terms is

$$\dot{y}(0)_{\mathrm{cn}} = \frac{1}{6n^3}\Big(x(0)^2n^2 + 2\dot{x}(0)y(0)n - \dot{x}(0)^2 - \dot{z}(0)^2 - 2y(0)^2n^2 - z(0)^2n^2\Big) \quad (2.12)$$

The secular term cancelation now depends on all five initial conditions from the Hill's solution in Eq. 2.2. The value of $\dot{y}(0)_{\mathrm{cn}}$ is orders of magnitude larger than the Hill's initial conditions. This is reduced by $\epsilon \ll 1$ when recombined with the state (see Eq. 5).

Ref. [48] discusses techniques for combining the nonlinearity state vector with a state vector that is propagated using a model that includes the reference orbit eccentricity. The result is a solution that accounts for both eccentricity and second order nonlinearity effects,

$$X(t) = X_{\text{le}}(t) + \epsilon X_{\text{cn}}(t) \tag{2.13}$$

where $X_{\text{le}}(t)$ are the relative states given by a linear eccentric propagator (such as the one developed in Section 2.2) and $X_{\text{cn}}(t)$ are given by Eqs. 2.31–2.34. The new initial conditions for a formation in the Hill's frame are

$$\begin{aligned} X(0) &= X_{\text{le}}(0) + \epsilon X_{\text{cn}}(0) \\ &= X_{\text{le}}(0) + \epsilon \begin{bmatrix} 0 & 0 & 0 & 0 & \dot{y}(0)_{\text{cn}} & 0 \end{bmatrix}^{\text{T}} \end{aligned} \tag{2.14}$$

Note that Tillerson presents several approaches for finding optimal initial conditions for $X_{\text{le}}(0)$ for a given initial position [16]. The nonlinearity correction developed in this Section can be used to find initial conditions that substantially reduce secular drift for widely spaced formations, with the new capability to specify 5 of the 6 possible initial conditions. Additionally, the form in Eq. 2.13 can be used to propagate the relative orbits of the satellites of the formation. This approach has been used to create recurring tetrahedron formations with sides extending beyond 10 km, whereas previous approaches restricted formations to have inter-spacecraft separations of approximately 0.1 km.

2.1.1 Simulation Results

The initial condition correction for nonlinearity developed in Section 2.1 (called NL) was tested against initializing with eccentricity corrections (EC), initializing with both eccentricity and nonlinearity corrections (NLEC), and initializing ignoring all corrections (NO). In each case, a tetrahedron with 10 km sides was created in an orbit with a period of 0.0824 days and an eccentricity of 0.05. The simulation was

conducted with a fully nonlinear propagator, but without the presence of drag or J_2 disturbances. The quality factor Q_{GM}, was used to compare the approaches, where

$$Q_{GM} = \frac{\text{True Volume}}{\text{Ideal Volume}} + \frac{\text{True Surface}}{\text{Ideal Surface}} + 1 \tag{2.15}$$

where *True Volume* is the volume of the tetrahedron (in this case, formed by the four spacecraft), *Ideal Volume* is the volume of a regular tetrahedron based on the average side length of the tetrahedron, *True Surface* is the surface area of the tetrahedron, and *Ideal Surface* is the surface area of a regular tetrahedron based on the average side length of the tetrahedron [49,50]. Q_{GM} ranges between 3.0 (a regular tetrahedron) and 1.0 (a line). There are a variety of commonly used tetrahedron quality factors, but Q_{GM} was used because it is consistently capable of unambiguously identifying regular tetrahedrons [50]. The tetrahedron shape is designed to appear only at apogee, so measurements of Q_{GM} are made once per orbit at whatever point the shape is most regular.

Results for the four initialization cases are shown in Figure 2–2, which plots the Q_{GM} trend after each orbit. The results clearly show that the EC and NLEC initializations maintain their shapes much longer than the NO and NL. It is also clear that correctly accounting for the orbit eccentricity has a significant influence on the quality of the tetrahedron, confirming the analysis in [18] (NL $\Rightarrow$ EC). The improvement from the eccentricity corrected to the combined nonlinearity/eccentricity corrected initialization (EC $\Rightarrow$ NLEC) is smaller but still clearly important for reducing the shape deformation over time [48].

A second simulation was conducted with the same formation, but with a highly elliptical orbit (period of 1 day, $e = 0.82$). The results of that simulation are shown in Figure 2–3. The results in Figure 2–3 use $3 - Q_{GM}$ as a metric, because the tetrahedrons are very regular in this case. It can be seen that over 40 orbits, the quality of the tetrahedron in the formation decreases negligibly and at nearly the same rate for both the EC and NLEC initializations. Figure 2–4 compares the effects of using the EC and NLEC initializations at different separations in the same highly eccentric

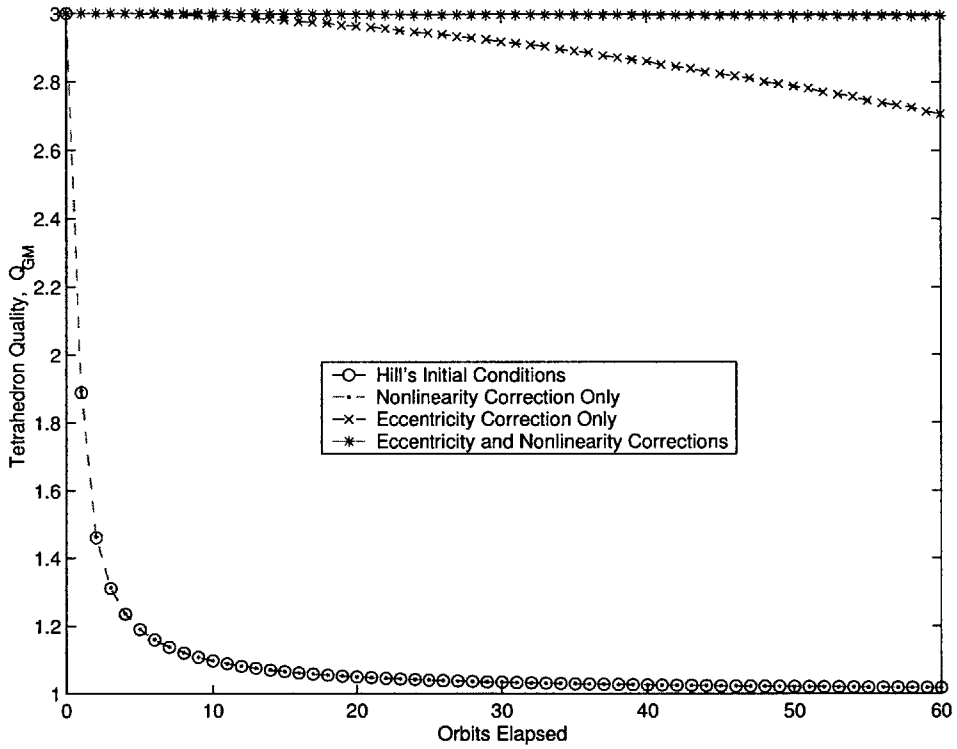

Fig. 2–2: Effect of Initial Conditions on Tetrahedron Quality in Low Earth Orbit ($e = 0.05$)

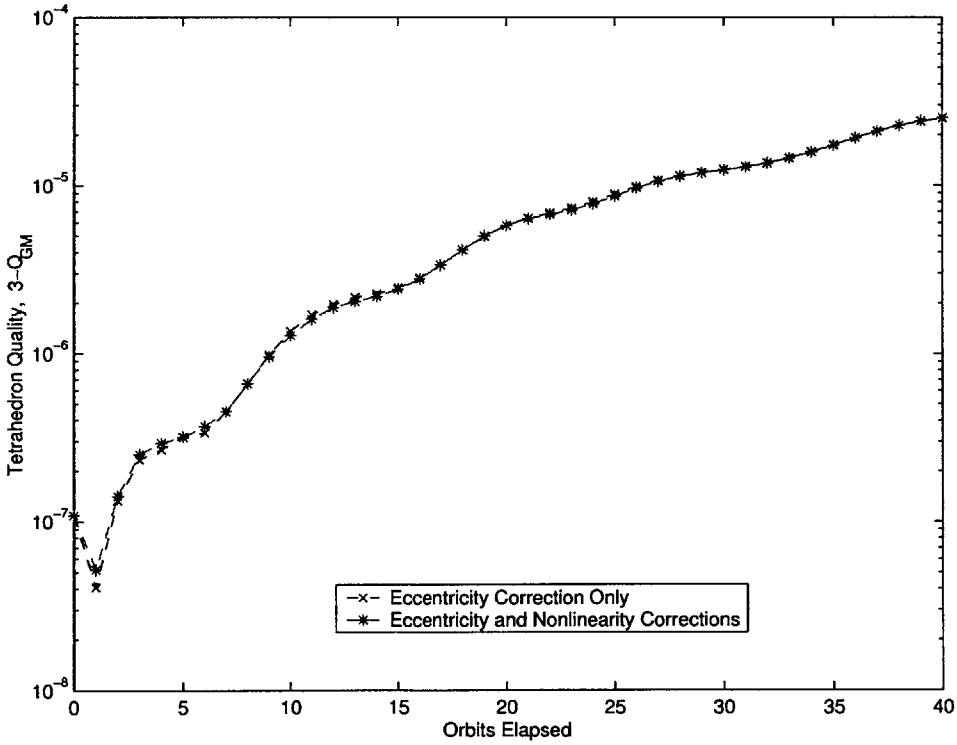

Fig. 2–3: Effect of Initial Conditions on Tetrahedron Quality in a Highly Eccentric Orbit ($e = 0.82$)

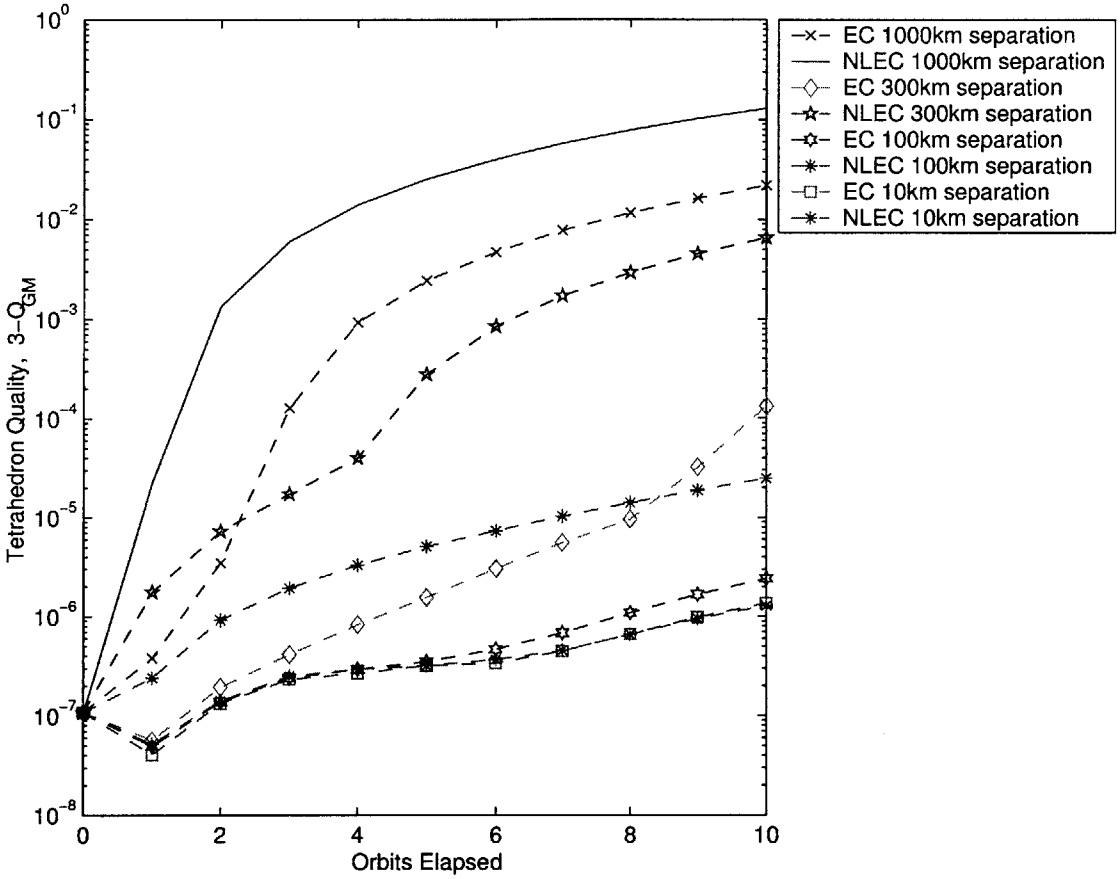

Fig. 2–4: The Effect of Initial Conditions and Interspacecraft Separation on Tetrahedron Quality in a Highly Eccentric Orbit

orbit. In each case, the NLEC initialization results in a decrease in tetrahedron quality. These results suggest that decoupling in Eq. 2.14 that is used in the initialization is invalid for large eccentricities, but further investigation is required.

2.2 Elliptical Time-varying Equations of Motion

The previous section presented a way to initialize spacecraft in drift-free formations. In practice, there are always differential disturbances acting upon spacecraft in a formation that will result in drift, even when it has been initialized correctly. As a result, feedback control will be required to maintain the formation geometry. A linear programming (LP) trajectory planning approach has been developed to design

fuel-optimized trajectories and station-keeping control inputs [30]. The basic form of the LP is

$$\min \|u\|_1 \quad \text{subject to} \quad \mathbf{A}u \leq \mathbf{b} \tag{2.16}$$

where u is the vector of fuel inputs (ΔV) at each time step and $\mathbf{A}, \mathbf{b}$ are functions of the linearized spacecraft dynamics, initial conditions, and final conditions. The LP determines the control inputs for a specified time interval that minimizes the fuel cost (the sum of the inputs) while satisfying the constraints on the trajectory. Constraints to the problem can include state constraints such as remaining within some tolerance of a specified point, maximum input values (actuator saturation), and terminal constraints. This approach can include differential disturbances such as drag and linearized forms of the differential J_2 effects [30]. To complete the low-level control design, the LP is also embedded within a real-time optimization control approach that monitors spacecraft relative positions and velocities, and then redesigns the control input sequence if the vehicle approaches the edge of the error box [30]. This control formulation will be used again, but with a different set of dynamics, in Chapter 3.

A mission with a highly elliptical orbit (*e.g.,* MMS) will require a propagator that accounts for eccentricity. Two common approaches to propagating relative states in eccentric orbits are Lawden's equations [10] and Melton's equations [35]. Melton's approach is in the time-domain, but is only valid for eccentricities up to 0.3, which is much less than that required for MMS [35]. Lawden's equations are valid for all eccentricities, but are written as a function of the true anomaly. Tillerson presented a relatively simple strategy of designing the trajectories as a function of the true anomaly, and then converting back to the time-domain for implementation. However, that is a complex process to perform in real-time and can introduce errors if the commands are not implemented in the correct way. The following presents a variation on Lawden's equations based on a derivation presented by Inalhan [18] that corrects this problem.

2.2.1 Derivation of Equations of Motion

Ref. [18] gives the following linearized equations of relative motion for an LVLH frame in an elliptical orbit,

$$\frac{d}{dt}\begin{bmatrix}\dot{x}\\ \dot{y}\\ \dot{z}\end{bmatrix}_j = -2\begin{bmatrix}0 & -\dot{f} & 0\\ \dot{f} & 0 & 0\\ 0 & 0 & 0\end{bmatrix}\begin{bmatrix}\dot{x}\\ \dot{y}\\ \dot{z}\end{bmatrix}_j - \begin{bmatrix}-\dot{f}^2 & 0 & 0\\ 0 & -\dot{f}^2 & 0\\ 0 & 0 & 0\end{bmatrix}\begin{bmatrix}x\\ y\\ z\end{bmatrix}_j - \begin{bmatrix}0 & -\ddot{f} & 0\\ \ddot{f} & 0 & 0\\ 0 & 0 & 0\end{bmatrix}\begin{bmatrix}x\\ y\\ z\end{bmatrix}_j + n^2\left(\frac{1+e\cos f}{1-e^2}\right)^3\begin{bmatrix}2x\\ -y\\ -z\end{bmatrix}_j + \begin{bmatrix}f_x\\ f_y\\ f_z\end{bmatrix}_j \quad (2.17)$$

where f is the true anomaly of the reference orbit, $\dot{f}$ and $\ddot{f}$ are the first and second differential of f with respect to time, and e is the eccentricity of the reference orbit. Also, f_x,f_y,and f_z are disturbance accelerations in radial, in-track, and cross-track directions of an LVLH frame. The subscript j denotes the j^{th} spacecraft in the formation. This equation may be rewritten in the matrix form

$$\frac{d}{dt}\begin{bmatrix}x\\ y\\ z\\ \dot{x}\\ \dot{y}\\ \dot{z}\end{bmatrix}_j = \begin{bmatrix}0 & 0 & 0 & 1 & 0 & 0\\ 0 & 0 & 0 & 0 & 1 & 0\\ 0 & 0 & 0 & 0 & 0 & 1\\ a_{41} & \ddot{f} & 0 & 0 & 2\dot{f} & 0\\ -\ddot{f} & a_{52} & 0 & -2\dot{f} & 0 & 0\\ 0 & 0 & a_{63} & 0 & 0 & 0\end{bmatrix}\begin{bmatrix}x\\ y\\ z\\ \dot{x}\\ \dot{y}\\ \dot{z}\end{bmatrix}_j + \begin{bmatrix}0 & 0 & 0\\ 0 & 0 & 0\\ 0 & 0 & 0\\ 1 & 0 & 0\\ 0 & 1 & 0\\ 0 & 0 & 1\end{bmatrix}\begin{bmatrix}f_x\\ f_y\\ f_z\end{bmatrix}_j \quad (2.18)$$

where

$$a_{41} = \dot{f}^2 + 2n^2\left(\frac{1+e\cos f}{1-e^2}\right)^3 \quad (2.19)$$

$$a_{52} = \dot{f}^2 - n^2\left(\frac{1+e\cos f}{1-e^2}\right)^3 \quad (2.20)$$

$$a_{63} = -n^2\left(\frac{1+e\cos f}{1-e^2}\right)^3 \quad (2.21)$$

Ref. [22] gives the following orbital dynamics relations for elliptical orbits,

$$\cos f = \frac{e - \cos E}{e\cos E - 1} \tag{2.22}$$

$$\frac{df}{dt} = \frac{\sin E}{\sin f}\cdot\frac{1 + e\cos f}{1 - e\cos E} = \frac{\sin E}{\sin f}\cdot\frac{p/r}{r/a} = \frac{a\sqrt{1-e^2}}{r}\cdot\frac{dE}{dt} \tag{2.23}$$

$$\sin f = \frac{a\sqrt{1-e^2}}{r}\sin E \tag{2.24}$$

$$r = a(1 - e\cos E) \tag{2.25}$$

where E is the eccentric anomaly of the reference orbit (radians), a is the semimajor axis (meters), and p is the latus rectum (meters). Ref. [34] gives

$$\frac{dE}{dt} = \frac{n}{1 - e\cos E} \tag{2.26}$$

Substituting Eq. 2.22 into Eq. 2.26 yields

$$\frac{dE}{dt} = \frac{n}{\frac{1-e^2}{1+e\cos f}} = \frac{(1 + e\cos f)n}{1 - e^2} \tag{2.27}$$

which is then differentiated with respect to time

$$\frac{d^2E}{dt^2} = \frac{-en\sin f}{1 - e^2}\cdot\frac{df}{dt} \tag{2.28}$$

Expanding terms in Eq. 2.23 results in the expression for $\dot{f}$ presented in [18],

$$\begin{aligned}
\frac{df}{dt} &= \frac{1 + \cos f}{1 - e^2}\sqrt{1-e^2} = \frac{1 + e\cos f}{\sqrt{1-e^2}}\frac{dE}{dt} \\
&= \frac{(1 + e\cos f)n}{(1 - e\cos E)\sqrt{1-e^2}} = \frac{(1 + e\cos f)n}{(1 - e\frac{e+\cos f}{1+e\cos f})\sqrt{1-e^2}} \\
&= \frac{(1 + e\cos f)n}{\frac{1+e\cos f - e^2 - e\cos f}{1+e\cos f}\sqrt{1-e^2}} = \frac{(1 + e\cos f)^2 n}{(1-e^2)^{3/2}} \\
&= \frac{n}{(1-e^2)^{3/2}}(e^2\cos^2 f + 2e\cos f + 1)
\end{aligned} \tag{2.29}$$

Differentiating again yields an expression for $\ddot{f}$ in terms of Keplerian elements

$$\begin{aligned}
\frac{d^2f}{dt^2} &= \frac{1+e\cos f}{\sqrt{1-e^2}} \cdot \frac{d^2E}{dt^2} - \frac{e\cos f}{\sqrt{1-e^2}} \cdot \frac{dE}{dt} \cdot \frac{df}{dt} \\
&= \frac{-n}{(1-e^2)^{3/2}}(2e^2 \cos f \sin f \dot{f} + 2e \sin f \dot{f}) \\
&= \frac{-2en \sin f \dot{f}}{(1-e^2)^{3/2}}(e\cos f + 1) \qquad (2.30)
\end{aligned}$$

This propagator is given as a function of the true anomaly, making it parameter varying. But using Kepler's equation, an accurate mapping between elapsed time and true anomaly of the reference orbit can easily be created [9]. If such a mapping is created before the planning step, then f will be a known function of time, and the equations can effectively be rewritten as being linear time-varying. This result is a simple way to propagate a system in a highly elliptical orbit using fixed time-steps. This enables the use of the time-varying discretized form of these dynamics with the LP optimization technique in Eq. 2.16 and thereby extends the range of applications where the planner developed in Ref. [30] can be used effectively. Furthermore, the need for a real-time domain conversion while executing the resulting plan is eliminated, instead shifting added computation to the pre-planning phase, before any optimization takes place.

2.3 Closed-Loop Demonstrations

The linear time-varying equations of motions in Eq. 2.18 have been used in the model predictive planner developed in [30]. This application extends previous work by enabling the problem to be formulated using constant time-step planning without additional steps for frame rotation. The LVLH-based planner was previously restricted to orbits with very low eccentricities where Hill's equations were valid. The new propagator/controller combination was used in a *closed-loop* two week simulation of four satellites, which included fully nonlinear propagation, differential drag, and GPS-like

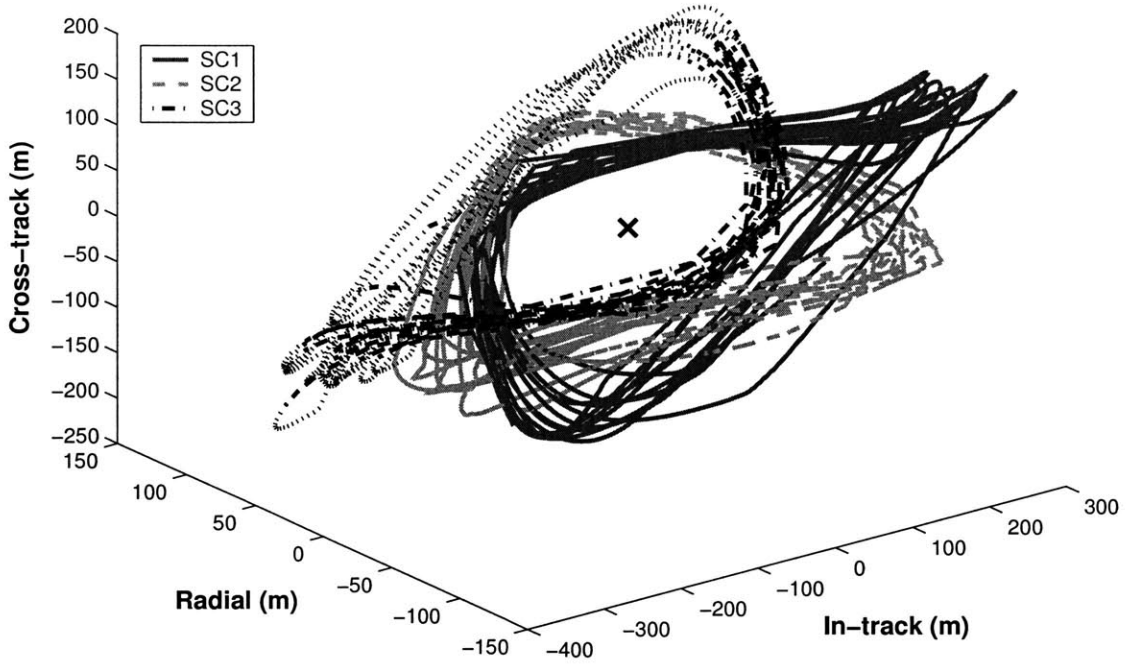

Fig. 2–5: Error box motion of three-spacecraft in a controlled passive aperture formation

sensing noise. The spacecraft orbits are all highly eccentric ($e \approx 0.8$) and the formation baseline is 100 m. The robustness approach introduced in [32] is used to reduce the controller's sensitivity to sensing noise. Figure 2–5 shows an initial set of closed-loop results, with each line-style indicating the motion of a different spacecraft with respect to its desired position.

The online planner used in the simulations could be used in a real-time control system. Although an optimization problem is solved at each time-step, this is not an impediment to timely implementation. Using LTI dynamics, forming the optimization problem (a linear program) requires a fraction of a second. The time required to form the linear program (LP) with LTV dynamics varies depending on the discretization time-step and the number of state space constraints being imposed. For this simulation, the time step was 84.4 seconds (chosen to create 1000 steps in an orbit) and error box constraints were imposed every 20^{th} step, requiring approximately twenty seconds to form the matrix and vector inputs of a standard LP. The LP itself requires less than 0.2 seconds to solve regardless of the type of dynamics used. Simulations were run on a 1 GHz computer.

2.4 Chapter Summary

New technologies have been developed to support emerging formation flying missions. An initialization scheme for creating widely-separated formations was extended to a more general case that allows for any three-dimensional drift-free geometry (*i.e.*, a tetrahedron). This approach works well for low eccentricity orbits, but is less useful for the highly eccentric orbits planned for the MMS mission. A new linear relative orbit propagator was also presented, which is useful for real-time planning for missions in highly eccentric orbits. It is valid for any eccentricity, but it does require a mapping between the times considered for thruster firings and the true anomaly of the reference orbit at those times. The primary advantage of this approach is that it shifts this conversion to the pre-planning phase, before any optimization takes place. This should reduce the real-time processor load.

Appendix

$$
\begin{aligned}
x_{cn}(t) &= \frac{1}{12n^4}\Big(48x(0)_{cn}n^4 - 36x(0)_{cn}n^4\cos(nt) + 12\sin(nt)vx(0)_{cn}n^3 + 24\dot{y}(0)_{cn}n^3 \\
&\quad -24\dot{y}(0)_{cn}n^3\cos(nt) + 3z(0)^2n^2 - 6x(0)^2n^2 + 4x(0)\dot{x}(0)\sin(2nt)n + \cos(2nt)\dot{z}(0)^2 \\
&\quad -2\cos(2nt)\dot{x}(0)^2 + 6y(0)^2n^2 + 8\dot{x}(0)^2\cos(nt) - \cos(2nt)z(0)^2n^2 + 2\cos(2nt)x(0)^2n^2 \\
&\quad -2\sin(2nt)n\dot{z}(0)z(0) - 8x(0)\sin(nt)n\dot{x}(0) - 4\cos(nt)\dot{z}(0)^2 + 4n\sin(nt)\dot{z}(0)z(0) \\
&\quad +4\cos(nt)x(0)^2n^2 - 6\cos(nt)y(0)^2n^2 - 2\cos(nt)z(0)^2n^2 + 3\dot{z}(0)^2 - 6\dot{x}(0)^2\Big) \\
y_{cn}(t) &= x(0)_{cn}[-6nt + 6\sin(nt)] + y(0)_{cn} + \frac{\dot{x}(0)_{cn}}{n}[-2 + 2\cos(nt)] + \frac{\dot{y}(0)_{cn}}{n}[4\sin(nt) - 3nt] \\
&\quad -\frac{1}{n^4}\Big(\frac{2}{3}\sin(nt)x(0)^2n^2 - \frac{1}{3}\sin(nt)z(0)^2n^2 - \sin(nt)y(0)^2n^2 - x(0)n^2y(0) + \frac{1}{2}x(0)n\dot{x}(0) \\
&\quad +\frac{1}{2}n\dot{z}(0)z(0) - \frac{1}{12}\sin(2nt)x(0)^2n^2 - \frac{1}{12}\sin(2nt)z(0)^2n^2 - \frac{2}{3}\dot{x}(0)^2\sin(nt) - \frac{2}{3}\sin(nt)\dot{z}(0)^2 \\
&\quad -\frac{2}{3}n\cos(nt)\dot{z}(0)z(0) + x(0)\cos(nt)n^2y(0) - \frac{2}{3}x(0)\cos(nt)n\dot{x}(0) + \dot{x}(0)\sin(nt)y(0)n \\
&\quad +\frac{1}{6}\cos(2nt)nx(0)\dot{x}(0) + \frac{1}{6}\cos(2nt)n\dot{z}(0)z(0) - \frac{1}{2}n^3tx(0)^2 - t\dot{x}(0)y(0)n^2 + \frac{1}{2}t\dot{x}(0)^2n \\
&\quad +\frac{1}{2}nt\dot{z}(0)^2 + n^3ty(0)^2 + \frac{1}{2}n^3tz(0)^2 + \frac{1}{12}\sin(2nt)\dot{x}(0)^2 + \frac{1}{12}\sin(2nt)\dot{z}(0)^2\Big)
\end{aligned}
$$

$$
\begin{aligned}
z_{cn}(t) &= z(0)_{\mathrm{cn}}\cos(nt) + \frac{\dot{z}(0)_{\mathrm{cn}}}{n}\sin(nt) + \frac{1}{n^4}\Big(\frac{1}{2}x(0)z(0)n^2 - \frac{1}{6}\sin(2nt)nx(0)\dot{z}(0) \\
&\quad -\frac{1}{6}\sin(2nt)n\dot{x}(0)z(0) + \frac{1}{2}\dot{x}(0)\dot{z}(0) - \frac{1}{6}\cos(2nt)x(0)z(0)n^2 + \frac{1}{6}\cos(2nt)\dot{x}(0)\dot{z}(0) \\
&\quad +\frac{1}{3}x(0)\sin(nt)n\dot{z}(0) + \frac{1}{3}n\sin(nt)\dot{x}(0)z(0) - \frac{1}{3}x(0)\cos(nt)z(0)n^2 - \frac{2}{3}\cos(nt)\dot{x}(0)\dot{z}(0)\Big)
\end{aligned} \tag{2.31}
$$

$$
\begin{aligned}
\dot{x}_{cn}(t) &= 3n\sin(nt)x(0)_{\mathrm{cn}} + \cos(nt)\dot{x}(0)_{\mathrm{cn}} + 2\sin(nt)\dot{y}(0)_{\mathrm{cn}} + \frac{1}{3n^3}\Big(2\cos(2nt)nx(0)\dot{x}(0) \\
&\quad -2x(0)\cos(nt)n\dot{x}(0) - \cos(2nt)n\dot{z}(0)z(0) + \frac{1}{2}\sin(2nt)z(0)^2n^2 - \sin(2nt)x(0)^2n^2 \\
&\quad -\frac{1}{2}\sin(2nt)\dot{z}(0)^2 + \sin(2nt)\dot{x}(0)^2 - 2\dot{x}(0)^2\sin(nt) + n\cos(nt)\dot{z}(0)z(0) \\
&\quad +\frac{1}{2}\sin(nt)z(0)^2n^2 - \sin(nt)x(0)^2n^2 + \frac{3}{2}\sin(nt)y(0)^2n^2 + \sin(nt)\dot{z}(0)^2\Big)
\end{aligned} \tag{2.32}
$$

$$
\begin{aligned}
\dot{y}_{cn}(t) &= (-6n + 6n\cos(nt))x(0)_{\mathrm{cn}} - 2\sin(nt)\dot{x}(0)_{\mathrm{cn}} + \frac{1}{n^3}\Big(-3 + 4\cos(nt)\dot{y}(0)_{\mathrm{cn}} \\
&\quad +(-\frac{1}{2}z(0)^2n^2 + \frac{1}{2}x(0)^2n^2 - y(0)^2n^2 + \dot{x}(0)y(0)n - \frac{1}{2}\dot{z}(0)^2 - \frac{1}{2}\dot{x}(0)^2 \\
&\quad -\cos(nt)\dot{x}(0)y(0)n + \frac{1}{3}\sin(2nt)n\dot{z}(0)z(0) + x(0)\sin(nt)n^2y(0) \\
&\quad -\frac{2}{3}x(0)\sin(nt)n\dot{x}(0) + \frac{1}{3}x(0)\dot{x}(0)\sin(2nt)n + \frac{2}{3}\dot{x}(0)^2\cos(nt) \\
&\quad -\frac{1}{6}\cos(2nt)\dot{z}(0)^2 - \frac{1}{6}\cos(2nt)\dot{x}(0)^2 + \frac{1}{6}\cos(2nt)z(0)^2n^2 \\
&\quad +\frac{1}{6}\cos(2nt)x(0)^2n^2 - \frac{2}{3}n\sin(nt)\dot{z}(0)z(0) - \frac{2}{3}\cos(nt)x(0)^2n^2 \\
&\quad +\cos(nt)y(0)^2n^2 + \frac{1}{3}\cos(nt)z(0)^2n^2 + \frac{2}{3}\cos(nt)\dot{z}(0)^2\Big)
\end{aligned} \tag{2.33}
$$

$$
\begin{aligned}
\dot{z}_{cn}(t) &= -n\sin(nt)z(0)_{\mathrm{cn}} + \cos(nt)\dot{z}(0)_{\mathrm{cn}} - \frac{1}{n^3}\Big(-\frac{1}{3}\sin(2nt)x(0)z(0)n^2 \\
&\quad +\frac{1}{3}\sin(2nt)\dot{x}(0)\dot{z}(0) + \frac{1}{3}\cos(2nt)nx(0)\dot{z}(0) + \frac{1}{3}\cos(2nt)n\dot{x}(0)z(0) \\
&\quad -\frac{1}{3}\sin(nt)x(0)z(0)n^2 - \frac{2}{3}\sin(nt)\dot{x}(0)\dot{z}(0) - \frac{1}{3}n\cos(nt)x(0)\dot{z}(0) \\
&\quad -\frac{1}{3}n\cos(nt)\dot{x}(0)z(0)\Big)
\end{aligned} \tag{2.34}
$$

Chapter 3

Planning Using Gauss' Variational Equations

In a spacecraft formation flying mission design, it is generally of greater importance to control the relative states of spacecraft than their absolute states. In addition, knowledge of the relative states of spacecraft in a formation is often far more accurate than knowledge of the formation's absolute state. For these reasons, formation control objectives are typically focused on controlling the satellites' relative states. In Chapter 2, variants of Hill's and Lawden's equations of relative motion were used for online planning. Both of these approaches linearize the nonlinear dynamics of orbital motion about a reference orbit. However, the linearization approach taken in those cases restricts the separation distances of the satellites in the formation. As the separation distance is increased, the equations of motion can no longer be used to cancel relative drift rates (initialization) or to accurately predict the effect of inputs (control). In the case of the MMS mission, four spacecraft will be placed in a tetrahedron-shaped relative configuration that will have sides ranging between 10–1000 km. These distances far exceed the distances for which Hill's and Lawden's models are valid, even with the correction terms introduced in Section 2.1.

Another approach that often appears in the literature is formation control using Gauss' Variational Equations (GVEs) [37,44,38,39]. GVEs have been used for many years to account for perturbations in orbits arising from drag and Earth oblateness

effects, as well as to design Lyapunov and fixed impulse control systems [46]. GVEs are convenient for specifying and controlling widely separated formations because they are linearized about orbital elements, which are expressed in a curvilinear frame in which large rectilinear distances can be captured by small element perturbations. In addition, the GVEs provide a computationally simple way (no frame rotations are required) to obtain linearized dynamics about the orbits of each spacecraft in the formation. This bypasses the linearization error created by representing the entire formation in a single rectilinear frame, which was the approach used in Refs. [26,30]. The use of GVE dynamics as opposed to Hill's dynamics incurs the cost of additional computation associated with the use of time-varying equations of motion. Likewise, the use of a separate set of time-varying linearized dynamics for each spacecraft in a formation requires further computation. Specifying formation relative geometry in terms of differential orbital elements is an exact approach that does not degrade for large spacecraft separations. The approaches for specifying drift-free formations in an LVLH frame presented in Refs. [8,18] both degrade with separation. However, the advantage of using GVEs for control could be reproduced by using a separate Lawden's frame for each spacecraft in the formation while still using orbital element differences to represent the formation relative geometry. Given that a nonlinear transformation and rotation is required to switch between a Lawden's frame and orbital element differences, and that GVEs are already linearized in an orbital element frame, it is both simpler and computationally more efficient to use orbital elements differences to specify the formation configuration and GVEs for control.

Several research groups have proposed control laws for formation-flying spacecraft that use GVEs to design impulsive thrusting maneuvers for orbit correction. For example, Ref. [44] proposes an general orbit correction scheme that uses GVEs to develop four impulsive thrusts that are applied at fixed points in an orbit. This four-impulse method is not guaranteed to be fuel-optimal and the approach presented in this chapter consistently produces trajectories that require less fuel to accomplish identical goals. A method of producing optimized four-impulse plans for very-low eccentricity orbits is presented in Ref. [41], but this approach does not extend to the

higher eccentricities required for MMS missions. Another method based on GVEs [39] allows optimized planning for low Earth orbits, but only permits optimization over a single impulsive thrust, guaranteeing that the solution will be sub-optimal in many cases. In addition, this approach is only derived for correcting errors in semimajor axis, eccentricity, and inclination. Another approach to using GVEs for formation control is to derive a continuous proportional-derivative controller satisfying the Lyapunov equation [37, 40, 43, 38].

This chapter presents a formation flying spacecraft control approach using GVEs as the dynamics in a model predictive control system. The novel aspect of this approach is the use of the GVEs for optimized planning. The advantage of this approach is the ability to design optimized plans for spacecraft in widely-separated, highly elliptic orbits. The combined GVE/planning system is demonstrated to be more fuel-efficient than both the four-impulse method in Ref. [44] and the single-impulse optimized method in Ref. [39]. In addition control optimized online has the advantage of being capable of handling many types of constraints, such as limited thrust capability, sensor noise robustness, and error box maintenance [30].

Gauss' Variational Equations (GVEs) are derived in Ref. [46] and are reproduced here for reference

$$\frac{d}{dt}\begin{pmatrix} a \\ e \\ i \\ \Omega \\ \omega \\ M_0 \end{pmatrix} = \begin{pmatrix} 0 \\ 0 \\ 0 \\ 0 \\ 0 \\ n \end{pmatrix} + \begin{pmatrix} \frac{2a^2 e \sin f}{h} & \frac{2a^2 e \sin f}{h} & 0 \\ \frac{p \sin f}{h} & \frac{(p+r)\cos f + re}{h} & 0 \\ 0 & 0 & \frac{r\cos\theta}{h} \\ 0 & 0 & \frac{r\sin\theta}{h\sin i} \\ -\frac{p\cos f}{he} & \frac{(p+r)\sin f}{he} & \frac{r\sin\theta\cos i}{h\sin i} \\ \frac{b(p\cos f - 2re)}{ahe} & -\frac{b(p+r)\sin f}{ahe} & 0 \end{pmatrix} \begin{pmatrix} \mathbf{u_r} \\ \mathbf{u_\theta} \\ \mathbf{u_h} \end{pmatrix} \tag{3.1}$$

where the state vector elements are a (semimajor axis), e (eccentricity), i (inclination), Ω (right ascension of the ascending node), ω (argument of periapse), and M_0 (mean motion). The other terms in the variational expression are p (semi-latus rectum), b (semiminor axis), h (angular momentum), θ (argument of latitude), r (magnitude of radius vector), and n (mean motion). All units are in radians, except for semi-

major axis and radius (meters), angular momentum (kilogram · meters^2 per second), mean motion (1/seconds), and eccentricity (dimensionless). The input acceleration components $\mathbf{u_r}$, $\mathbf{u_\theta}$, and $\mathbf{u_h}$ are in the radial, in-track, and cross-track directions, respectively, of an LVLH frame centered on the satellite and have units of meters per second^2. The form of the GVEs can be more compactly expressed as

$$\dot{\mathbf{e}} = A(\mathbf{e}) + B(\mathbf{e})\mathbf{u} \tag{3.2}$$

where $\mathbf{e}$ is the state vector in Eq. 3.1, $B(\mathbf{e})$ is the input effect matrix, $\mathbf{u}$ is the vector of thrust inputs in the radial, in-track, and cross-track directions, and

$$A(\mathbf{e}) = \begin{pmatrix} 0 & 0 & 0 & 0 & 0 & \sqrt{\mu/a^3} \end{pmatrix}^T \tag{3.3}$$

where μ is the gravitational parameter.

3.1 Previous Approaches to Control Using GVEs

A common approach when basing control on GVE dynamics is to use a nonlinear PD-based Lyapunov regulator of the form

$$\mathbf{u} = -KB(\mathbf{e})^T\zeta \tag{3.4}$$

where ζ is the current orbital element offset from the reference orbit $\mathbf{e}$ and K is a constant positive definite matrix [37, 40, 43, 38]. Control algorithms of this type have been shown to be asymptotically stable in most cases [40], but belong to a class of control systems that fire continuously. Continuous firing is generally not desirable for space missions because it is often disruptive to the science mission, it typically must be coupled with attitude maneuvers, and it expends fuel (nonreplenishable aboard a spacecraft) continuously.

Another approach to differential element control is presented in Ref. [44]. In that approach, it is observed that the GVEs decouple at several points during an orbit. By

exploiting the decoupling points, an algorithm requiring a maximum of four impulsive thrusts is proposed. This approach is simple in an algorithmic sense, but requires a fixed time period (*i.e.*, one orbit) to correct state errors and is not guaranteed to be fuel-optimal (or even near-fuel-optimal). Ref. [39] presents another method of formation control based on GVEs that uses a single corrective thrust that is optimized nonlinearly. Although this method is guaranteed to find the optimal single-thrust correction for an arbitrary time period, it is not guaranteed (or likely) to find the optimal multiple-thrust correction. In addition, this approach is restricted to use in low Earth orbits and is only designed to correct errors in semimajor axis, eccentricity, and inclination. An approach presented in Ref. [45] uses a pseudo-inverse to the GVE control effect matrix to calculate a single corrective impulse. This approach is not guaranteed to be fuel-optimal for any cases and is not accurate for correcting position errors.

In contrast, this chapter describes a control law that generally does not fire continuously and makes explicit its objective to minimize fuel use. The control approach utilizes the linearized relative dynamics of Gauss' Variation Equations to optimize the effects of arbitrarily many inputs over a chosen planning horizon. The next section examines the validity of using a linearized relative form of the equations of satellite motion based on GVEs.

3.2 Relative Orbital Elements and Linearization Validity

In a formation, the orbital element state of the ith satellite is denoted $\mathbf{e}_i$. The states of the vehicles in the formation can be specified by relative orbital elements by subtracting the state of an arbitrarily chosen spacecraft in the formation ($\mathbf{e}_1$)

$$\delta\mathbf{e}_i = \mathbf{e}_i - \mathbf{e}_1 \tag{3.5}$$

For a desired orbit geometry, a set of desired relative elements, $\delta\mathbf{e}_{di}$ will specify the desired state $\mathbf{e}_{di}$ of each spacecraft in the formation

$$\mathbf{e}_{di} = \mathbf{e}_1 + \delta\mathbf{e}_{di} \tag{3.6}$$

The state error, ζ_i for the ith spacecraft in the formation is then defined as

$$\zeta_i = \mathbf{e}_i - \mathbf{e}_{di} = \delta\mathbf{e}_i - \delta\mathbf{e}_{di} \tag{3.7}$$

The form of Gauss' Variational Equations in Eq. 3.1 is for perturbations of orbital elements. To reformulate these equations for perturbations of relative orbital elements [43], the GVEs for $\mathbf{e}_i$ and $\mathbf{e}_{di}$ are placed together

$$\dot{\zeta}_i = \dot{\mathbf{e}}_i - \dot{\mathbf{e}}_{di} = A(\mathbf{e}_i) - A(\mathbf{e}_{di}) + B(\mathbf{e}_i)\mathbf{u}_i \tag{3.8}$$

where the term $B(\mathbf{e}_{di})\mathbf{u}_{di}$ has been excluded because thrusting only occurs at the point of the spacecraft, not at its desired state, which is assumed to be a constant Keplerian orbit. The unforced dynamics can be linearized by introducing the first order approximation

$$A(\mathbf{e}_i) - A(\mathbf{e}_{di}) \simeq \left.\frac{\partial A}{\partial \mathbf{e}}\right|_{\mathbf{e}_{di}} (\mathbf{e}_i - \mathbf{e}_{di}) = \left.\frac{\partial A}{\partial \mathbf{e}}\right|_{\mathbf{e}_{di}} \zeta_i \equiv A^*(\mathbf{e}_{di})\zeta_i \tag{3.9}$$

where the matrix $A^*(\mathbf{e}_{di})$ is all zeros except for the lower-leftmost element, which is $-3n/2a$. With this approximation, the differential GVE expression can be rewritten as

$$\dot{\zeta}_i = A^*(\mathbf{e}_{di})\zeta_i + B(\mathbf{e}_i)\mathbf{u}_i = A^*(\mathbf{e}_{di})\zeta_i + B(\mathbf{e}_{di} + \zeta_i)\mathbf{u}_i \tag{3.10}$$

In this case the control of the relative error state, ζ_i, is nonlinear, because the control effect matrix B is a function of the state. Ref. [43] accounts for this nonlinearity in a continuous nonlinear control law that was proven to be asymptotically stable. The control approach developed in this chapter uses linearized dynamics to predict the

effect of future control inputs. Linearizing the matrix B in Eq. 3.10 yields

$$\dot{\zeta}_i \simeq A^*(\mathbf{e}_{di})\zeta_i + \left(B(\mathbf{e}_{di}) + \left.\frac{\partial B}{\partial \mathbf{e}}\right|_{\mathbf{e}_{di}} \zeta_i \right) \mathbf{u}_i \tag{3.11}$$

$$= A^*(\mathbf{e}_{di})\zeta_i + B(\mathbf{e}_{di})\mathbf{u}_i + [B^*(\mathbf{e}_{di})]\zeta_i \mathbf{u}_i \tag{3.12}$$

where the term $B^*(\mathbf{e}_{di})$ is a third rank tensor and the quantity $B^*(\mathbf{e}_{di})\zeta_i$ is a matrix with the same dimensions as $B(\mathbf{e}_{di})$. For convenience, define

$$\Delta B = B^*(\mathbf{e}_{di})\zeta_i \tag{3.13}$$

resulting in the new state equation

$$\dot{\zeta}_i = A^*(\mathbf{e}_{di})\zeta_i + (B(\mathbf{e}_{di}) + \Delta B)\,\mathbf{u}_i \tag{3.14}$$

Note that if ΔB is much smaller than $B(\mathbf{e}_{di})$, then the first order term can safely be ignored, yielding the linearized system

$$\dot{\zeta}_i = A^*(\mathbf{e}_{di})\zeta_i + B(\mathbf{e}_{di})\mathbf{u}_i \tag{3.15}$$

which can be controlled using any one of a variety of linear control techniques, including the model predictive controller discussed in Section 3.3.

The critical requirement for linear control and planning is that the term ΔB holds much less influence on the state than the term $B(\mathbf{e}_{di})$. However, ΔB is a linear function of the state error ζ_i, which can be arbitrarily large. The amount of acceptable error due to linearization will be a function of the mission scenario, but the linearization assumption will typically only be valid for small values of the state error. A bound on the magnitude of this error can be developed by comparing the induced norm of the difference between the control influence matrix at its desired state, $B(\mathbf{e}_{di})$ and at the actual position of the spacecraft, $B(\mathbf{e}_i)$. In Eq. 3.13, the first order approximation of this term was defined as ΔB. In the following examples,

ΔB_{true}, which is defined as

$$\Delta B_{\text{true}} = B(\mathbf{e}_i) - B(\mathbf{e}_{di}) \tag{3.16}$$

and will be calculated numerically. The cutoff point of acceptable linearization error is when the norm of ΔB exceeds some (mission dependent) fraction of the norm of $B(\mathbf{e}_{di})$.

To investigate this cutoff point, the following examples consider many random values of ζ_i in the set $\|\zeta_i\|_2 = r$ and calculate ΔB_{true}. The ΔB_{true} with the largest 2-norm will be used to test the validity of the linearization for a given r. This procedure is repeated for multiple r to find the largest $\|\zeta\|_2$ for which the linearization is considered valid.

Example: Low Earth Orbit – An example low Earth orbit is

$$\mathbf{e}_{di} = \begin{pmatrix} 1.08182072 \\ 0.005000000 \\ 0.610865238 \\ 6.28318530 \\ 3.14159265 \\ 3.82376588 \end{pmatrix} \tag{3.17}$$

where the first element, the semimajor axis, is given normalized by the Earth's radius, making the entire orbital element vector dimensionless. The matrix corresponding

$B(\mathbf{e}_{di})$ is

$$B(\mathbf{e}_{di}) = \begin{pmatrix} -5.67944780 & 1808.60113 & 0 \\ -0.0000823087799 & -0.000205025722 & 0 \\ 0 & 0 & 0.000103044042 \\ 0 & 0 & 0.000144062928 \\ 0.0205284192 & -0.0329879762 & -0.00000310525295 \\ -0.0207923257 & 0.0329875639 & 0 \end{pmatrix} \tag{3.18}$$

where $\|B(\mathbf{e}_{di})\|_2 = 1808.61$. The effect of perturbing $\mathbf{e}_{di}$ for a given norm bound on ζ_i is shown in Figure 3–1. The figure shows that for a linearization validity cutoff of 0.1, where $\|\Delta B(\mathbf{e}_{di}, \zeta)_{\text{true}}\|_2 \leq 0.1\|B(\mathbf{e}_{di})_{\text{true}}\|_2$, can be achieved by observing the bound $\|\zeta\|_2 \leq 0.09$. This choice of bound allows for orbital element perturbations that equate to rectilinear distances on the order of 330 kilometers and velocities on the order of 34 meter per second. Since typical error box sizes for LEO formation flying missions are between 10–1000 meters in size, the linearization should be a valid approximation for most missions of interest.

Example: Highly Elliptical Earth Orbit – One motivation for using GVEs as the linearized dynamics in a planner is recent interest in widely spaced, highly elliptical orbits[51]. An orbit of this type is

$$\mathbf{e}_{di} = \begin{pmatrix} 6.59989032 \\ 0.818181000 \\ 0.174532925 \\ 6.28318530 \\ 0 \\ 3.14159265 \end{pmatrix} \tag{3.19}$$

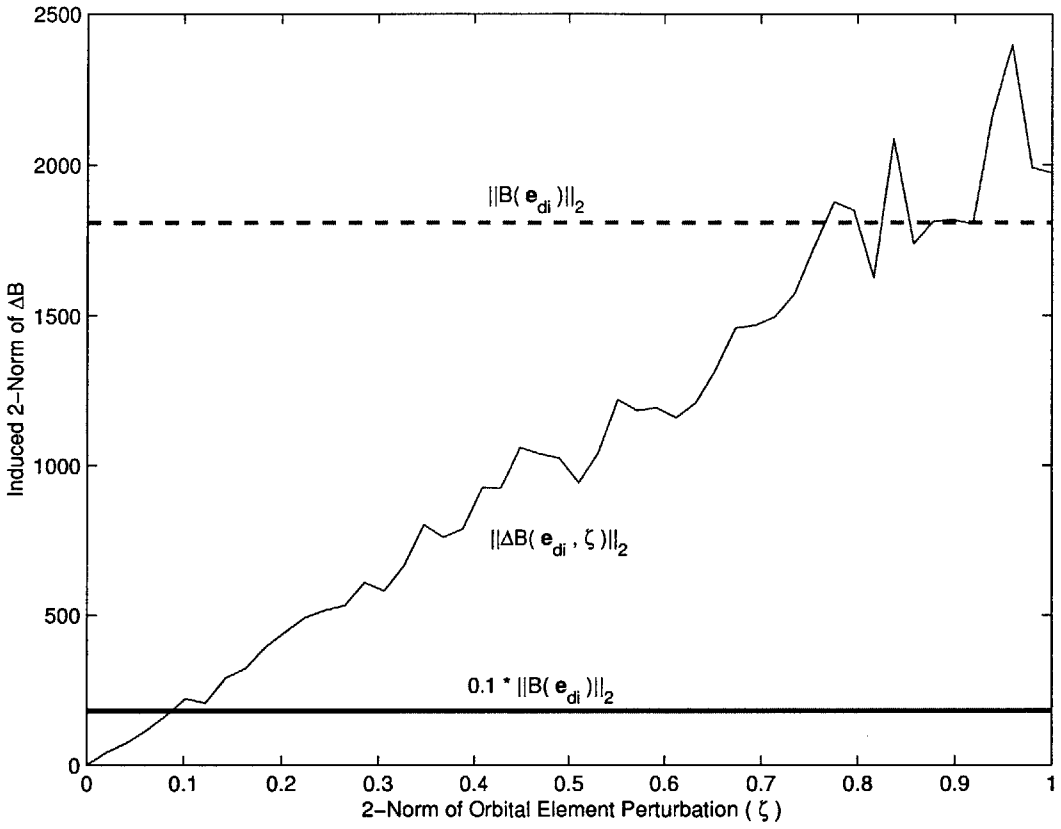

Fig. 3–1: Effect of Orbital Element Perturbations on the ΔB_{true} Matrix for a LEO Orbit

with

$$B(\mathbf{e}_{di}) = \begin{pmatrix} 4.767920 \times 10^{-12} & 8651.830 & 0 \\ 2.288208 \times 10^{-20} & -0.0003736926 & 0 \\ 0 & 0 & -0.001027650 \\ 0 & 0 & 7.247461 \times 10^{-19} \\ 0.0002283680 & 1.817849 \times 10^{-19} & -1.629943 \times 10^{-22} \\ -0.001313020 & -1.45192 \times 10^{-19} & 0 \end{pmatrix} \tag{3.20}$$

Repeating the same procedure used for the LEO case, it is determined from Figure 3–2 that for a 10% linearization validity cutoff, the bound which must be observed is $\|\zeta\|_2 \leq 0.04$. In this case, the bound on $\|\zeta\|_2$ corresponds to rectilinear distances

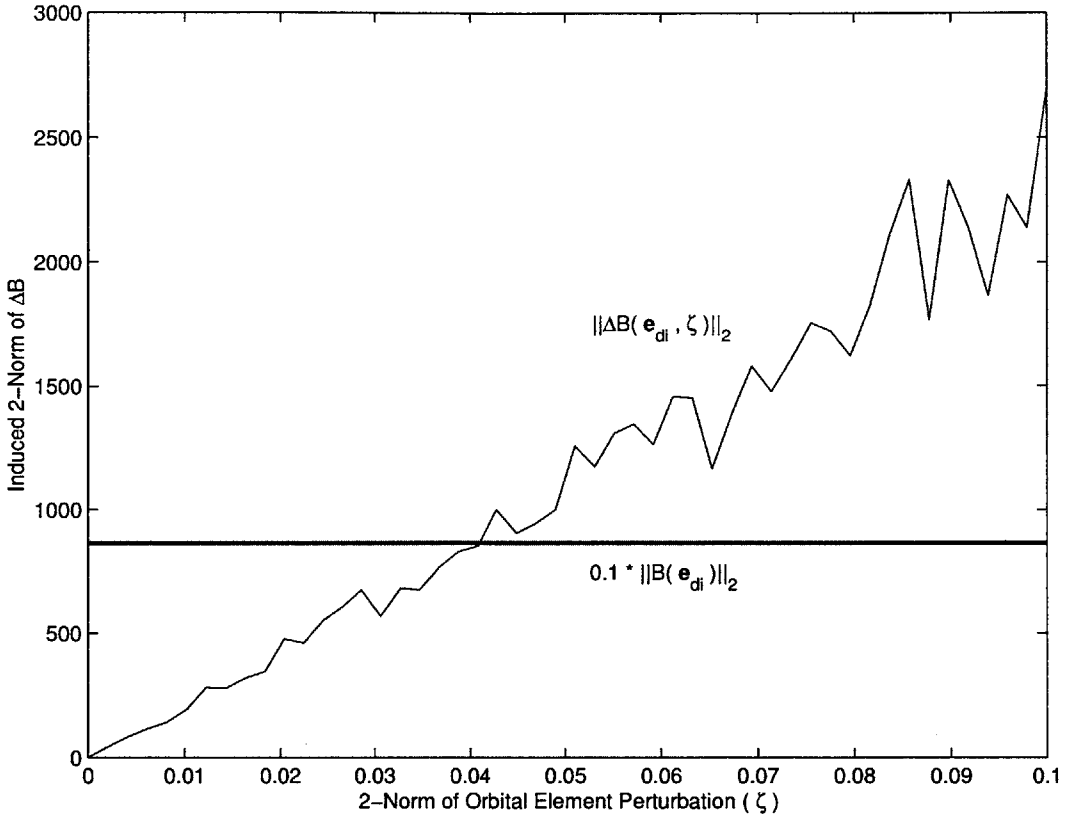

Fig. 3–2: Effect of Orbital Element Perturbations on the ΔB_{true} Matrix for a HEO Orbit

of approximately 470 kilometers and velocities of 24 meters per second. As in the LEO case, these distances are far larger than expected error box sizes (*i.e.*, expected distances over which control would be planned). Unlike the LEO case, error boxes for widely-separated missions, such as MMS, may be much larger than 10 meters to a side, even approaching 10's of kilometers. However, the 10% cutoff ensures that error boxes of up to half the baseline are acceptable. In an actual mission, it is unlikely that error boxes would be large enough to impact the linearization validity, because it would allow the regularity of the tetrahedron geometry (*i.e.*, the quality of the science data) to be significantly diminished.

3.3 Model Predictive Control Using GVEs

Reference [30] showed that given a valid set of linearized dynamics and a desired trajectory, a model predictive controller for a spacecraft formation can be designed that allows for arbitrarily many convex terminal and intermediate state conditions, as well as sensor noise robustness requirements. This controller is implemented on each spacecraft in the formation and it is using a linear programming formulation. The general form of the optimization performed by the controller is reviewed in Section 2.2. In order to use the linearized GVE-based dynamics dynamics developed in Eq. 3.15 in the MPC formulation, the dynamics are discretized using a zero order hold assumption according to the procedure described in [25] yielding the discrete form

$$\zeta_i(k+1) = A_d^*(\mathbf{e}_{di})\zeta_i(k) + B_d(\mathbf{e}_{di})\mathbf{u}_i(k) \tag{3.21}$$

where k is the current time step, $A_d^*(\mathbf{e}_{di})$ is the system's parameter-varying state transition matrix, and $B_d(\mathbf{e}_{di})$ is the discretized form of the linearized GVE control input matrix $B(\mathbf{e}_{di})$.

3.4 Comparison to Another GVE-based Impulsive Control Scheme

Section 3.1 describes a GVE-based impulse control scheme was described, which uses four impulses over the course of an orbit. This section will compare that approach to the MPC-based approach presented in Section 3.3. Both approaches are designed to drive the elements of a state error ζ_i to zero over a fixed time interval. The four-impulse approach has not been presented in the context of performance criteria (*e.g.,* trajectory or terminal error boxes, robustness to disturbances) or constraints (*e.g.,* maximum thrust level), so the comparisons in this section will use an MPC controller formulation that minimizes fuel use while driving the error state to zero in a fixed time and has no other constraints.

The 4-impulse approach developed in [44] can be summarized in four steps to be taken over the course of an orbit. When the angle of latitude, θ, is 0 or π radians, implement a velocity change (impulsive thrust), Δv_{h_i} in the cross-track direction of an LVLH frame centered on the spacecraft to cancel the inclination error component of ζ_i

$$\Delta v_{h_i} = \frac{h}{r\cos\theta}\Delta i \tag{3.22}$$

When the angle of latitude, θ, is $\pi/2$ radians, implement a velocity change, Δv_{h_Ω} in the cross-track direction to cancel the ascending node error

$$\Delta v_{h_\Omega} = \frac{h\sin i}{r\sin\theta}\Delta\Omega \tag{3.23}$$

At perigee and apogee, implement Δv_{r_p} and Δv_{r_a}, respectively, in the radial direction to cancel the argument of perigee and mean anomaly errors

$$\Delta v_{r_p} = -\frac{na}{4}\left(\frac{(1+e)^2}{\eta}(\Delta\omega + \Delta\Omega\cos i) + \Delta M\right) \tag{3.24}$$

$$\Delta v_{r_a} = \frac{na}{4}\left(\frac{(1-e)^2}{\eta}(\Delta\omega + \Delta\Omega\cos i) + \Delta M\right) \tag{3.25}$$

Also at perigee implement Δv_{θ_p} and at apogee implement Δv_{θ_a} in the in-track direction, to cancel the semimajor axis and eccentricity errors

$$\Delta v_{\theta_p} = \frac{na\eta}{4}\left(\frac{\Delta a}{a} + \frac{\Delta e}{1+e}\right) \tag{3.26}$$

$$\Delta v_{\theta_a} = \frac{na\eta}{4}\left(\frac{\Delta a}{a} - \frac{\Delta e}{1-e}\right) \tag{3.27}$$

Using the notation and the HEO reference orbit from Section 3.2, the following example compares the MPC method with the control approach reviewed in this section. For the state error

$$\zeta_1 = \begin{pmatrix} 10^{-9} & 10^{-7} & 10^{-7} & 10^{-7} & 10^{-7} & 10^{-7} \end{pmatrix}^T \tag{3.28}$$

the 4-impulse method requires 2.29 mm/s of fuel to correct the state error over the

course of an orbit and the MPC method requires 0.0422 mm/s of fuel. For this example, the model predictive controller was given a full orbit time horizon. However, the same control objective could have been achieved in less time, but using more fuel.

A series of 1000 orbital element state error vectors, ζ_i, were generated, in which each perturbed element was a random number between $\pm 10^{-6}$. For each of the error vectors, both control methods were used to generate plans for eliminating the error. The average MPC maneuver required 47% of the average fuel required by the 4-impulse maneuver.

3.5 General Drift-free Tetrahedron Initial Conditions

The MMS mission, depicted in Figure 1, will require spacecraft to form very large tetrahedron shapes, while simultaneously not drifting with respect to one another. Drift-free designs based on Hill's and Lawden's equations are valid only for formations with short baselines, because of the linearization assumptions inherent in the specification of the frames in the derivation of the dynamics. For any group of spacecraft, a no-drift requirement is equivalent to requiring that all spacecraft have the same orbital energy, which is also equivalent to stating that all spacecraft have the same semimajor axis. For a formation specified in differential orbital elements, this is the same as requiring that the desired differential semimajor axes for all spacecraft in the formation be zero. Thus, in differential orbital elements it is trivial to design a drift-free formation, however, the curvilinear nature of the elements makes describing and manipulating general tetrahedron shapes complicated.

One approach is to begin with tetrahedron coordinates in a rectilinear frame (such as LVLH or ECEF) and then convert those coordinates into orbital element perturbations. However, producing the desired orbital element differences for a tetrahedron requires knowledge of the full relative state in a rectilinear frame, including both position and velocity. If the only constraint on the formation geometry is that the

satellite positions form a tetrahedron shape, then the velocity must be selected based on additional criteria.

A regular tetrahedron can be described in a rectilinear frame using the coordinates given in Eq. 2.3. If the rectilinear frame is LVLH, the coordinates can be transformed into differential orbital elements using the first order approximation

$$\delta\mathbf{e}_{di} = M(\mathbf{e}_1)\mathbf{x}_{di} \tag{3.29}$$

where $\mathbf{e}_1$ is the reference orbit that the differential elements of the vector $\delta\mathbf{e}_{di}$ are described with respect to, and $\mathbf{x}_{di}$ is a relative state vector in the LVLH frame centered on the absolute orbit $\mathbf{e}_1$. The elements of the 6×6 rotation matrix $M(\mathbf{e}_1)$ are known analytically and can be found in Appendix G of Ref. [43].

The desired LVLH state of satellite i can be expressed as the concatenation of a position vector $\mathbf{p}_i$ and a velocity vector $\mathbf{v}_i$, each with states in the x, y, and z directions.

$$\mathbf{x}_i = \begin{pmatrix} \mathbf{p}_i^T & \mathbf{v}_i^T \end{pmatrix}^T = \begin{pmatrix} x_i & y_i & z_i & v_{x_i} & v_{y_i} & v_{z_i} \end{pmatrix}^T \tag{3.30}$$

To find velocity vectors that satisfy the no-drift requirement, the system

$$\delta\mathbf{e}_{di} = M(\mathbf{e}_1)\begin{pmatrix} \mathbf{p}_{di} \\ \mathbf{v}_{di} \end{pmatrix} \quad \forall \; i = 1 \ldots n \tag{3.31}$$

must be solved with the additional constraint that the semimajor axis element of $\delta\mathbf{e}_{di}$ be equal to zero for all spacecraft in the formation ($n = 4$ for a tetrahedron formation). In this system, the elements of $\delta\mathbf{e}_{di}$ and $\mathbf{v}_i$ are allowed to vary, while the matrix M and the vectors $\mathbf{x}_i$ are determined by the reference orbit and the tetrahedron geometry, respectively. The system has $9n$ variables and $7n$ constraints and will, therefore, have many possible solutions. In Ref. [49], the velocity magnitude is chosen to achieve the no-drift condition and the ECI velocity direction of each spacecraft in the formation is chosen to match the direction of reference orbit's velocity vector. This method will succeed in creating a drift-free formation, however it does not take into account the states of the spacecraft in the formation immediately prior to initialization.

The approach presented here minimizes the size of the maneuvers that would be required to create the desired formation. The approach selects initial conditions, $\delta\mathbf{e}_{di}$, that are closest to the current differential states, $\delta\mathbf{e}_i$, of the spacecraft in the formation and that will minimize the state error, ζ_i, across the formation at the start of the initialization. For the entire formation, this criterion becomes

$$\min_{\delta\mathbf{e}_{di},\mathbf{v}_{di}\ \forall i=1\ldots n} \sum_{i=1}^{n} \|W_i(\delta\mathbf{e}_{di} - \delta\mathbf{e}_i)\|_1 \tag{3.32}$$

where W_i are weighting matrices that represent the expected fuel-cost of changing orbital elements (obtainable from the GVEs). Allowing different W_i for each spacecraft enables the formation design to take into account factors such as fuel-weighting to extend overall mission duration, similar to the approach used in choosing the *virtual center* in Section 3.7. The use of a 1-norm is appropriate in this case, because the distance that a given element must be changed is the absolute value of the difference between that element's current and desired state. This approach is similar to the optimization used in Ref. [18], in which drift-free, minimum maneuver constants of integration were found for Lawden's Equations. Next, the optimization is expanded by exploiting specific aspects of the MMS mission science goals.

The *quality* of the shape of the regular tetrahedron[1] largely determines the value of the science data recovered by a mission such as MMS [50]. In choosing the initial conditions for a regular tetrahedron-shaped formation, certain quantities that do not affect shape quality such as the scale, position, and orientation of the tetrahedron can be considered degrees of freedom in the optimization described by Eqs. 3.31 and 3.32. By optimizing the additional degrees of freedom, tetrahedron-shaped initial conditions can be found that require smaller maneuvers to achieve from the current formation state. Scaling the tetrahedron shape equally in three dimensions introduces a single scalar variable s and allowing translation in each orthogonal direction of the LVLH

[1]Tetrahedron quality is discussed in Section 2.1.1

frame introduces the variables t_x, t_y, and t_z. The new constraint set is

$$\delta \mathbf{e}_{di} = M(\mathbf{e}_1) \left[\begin{pmatrix} {}^{s}\mathbf{p}_{di} \\ \mathbf{v}_{di} \end{pmatrix} + \mathbf{t} \right] \quad \forall \ i = 1 \ldots n \tag{3.33}$$
$$\begin{pmatrix} 1 & 0 & 0 & 0 & 0 & 0 \end{pmatrix} \delta \mathbf{e}_{di} = 0$$

where $\mathbf{t} = \begin{pmatrix} t_x & t_y & t_z & 0 & 0 & 0 \end{pmatrix}^T$ and the second constraint forces a no-drift condition by ensuring that the relative semimajor axes, the first element of each $\delta \mathbf{e}_{di}$ vector, are zero. These constraints can be combined with the objective in Eq. 3.32 and formulated as a linear program. In addition to the geometric and no-drift constraints, additional limits on the desired differential angle state variables are required to ensure that they remain within $\pm\pi$ and on eccentricity and semimajor axis to ensure that the spacecraft remain in Earth orbit.

For elliptical orbits, it is not possible to maintain constant relative geometry between satellites for all points in the orbit. Instead, a single position in the orbit must be chosen for the satellites to form a tetrahedron. The mean anomaly at the time of the tetrahedron geometry will be M_t. When formulating the optimization in Eqs. 3.32 and 3.33, the current differential element vectors ζ_i must be propagated forward using the A^* matrix in Eq. 3.10 to the mean anomaly M_t. In addition, the reference orbit used to compute the matrix $M(\mathbf{e}_1)$ should have a mean anomaly set to M_t.

There are several limitations to this optimization approach. First, it does not optimally assign spacecraft to positions in the tetrahedron (a formulation that does this is possible using mixed integer linear programming or network LP [53, 30]). Second, the optimization posed here does not optimally orient the tetrahedron in three space. Introducing a rotation matrix dependent on three Euler parameters would create a nonlinear optimization. This limitation could be bypassed by creating a spherical lattice about the orbit and optimizing the formation rotated once for each point on the lattice. After performing all the optimizations, the desired state corresponding to the rotation with the lowest cost would be chosen. Although this approach requires a

preset number of optimizations (possibly many depending upon the degree of rotation resolution desired), the optimizations are small linear programs, which complete in a fraction of a second.

An alternative form of Eq. 3.33 can be written to allow for small rotations using the linearized form of a three-dimensional rotation matrix [47]

$$\mathbf{x}' = \begin{pmatrix} 1 & \theta_z & -\theta_y \\ -\theta_z & 1 & \theta_x \\ \theta_y & -\theta_x & 1 \end{pmatrix} \mathbf{x} \equiv \mathbf{R}\mathbf{x} \tag{3.34}$$

where θ_x is the rotation about the x axis, θ_y is the rotation about the y axis, θ_z is the rotation about the z axis, $\mathbf{x}$ is an arbitrary LVLH position vector, and $\mathbf{x}'$ is the vector $\mathbf{x}$ after having been rotated. Using Eq. 3.34 in Eq. 3.33 yields

$$\begin{gathered} \delta\mathbf{e}_{di} = M(\mathbf{e}_1)\left[\begin{pmatrix} \mathbf{R} & \mathbf{0}_3 \\ \mathbf{0}_3 & \mathbf{I}_3 \end{pmatrix}\begin{pmatrix} \mathbf{p}_{di} \\ \mathbf{v}_{di} \end{pmatrix} + \mathbf{t}\right] \quad \forall \ i = 1 \ldots n \\ \begin{pmatrix} 1 & 0 & 0 & 0 & 0 & 0 \end{pmatrix} \delta\mathbf{e}_{di} = 0 \end{gathered} \tag{3.35}$$

where $\mathbf{R}$ is the rotation matrix defined in Eq. 3.34, $\mathbf{0}_3$ is a 3×3 matrix of zeros, and $\mathbf{I}_3$ is a 3×3 identity matrix. The variables being chosen in the new optimization are the vectors $\delta\mathbf{e}_{di}$, the rotations θ_x, θ_y, and θ_z (contained in $\mathbf{R}$), the velocities $\mathbf{v}_{di}$, and the translations $\mathbf{t}$. The optimization can perform small rotations (θ_x, θ_y, and θ_z will have constrained limits), but can no longer optimize the tetrahedron scale and still retain linearity.

Example: Fuel Expenditure for Rotation Approach – Using the highly elliptical orbit from the example in Section 3.2, the initial conditions for a tetrahedron with 1000 kilometer sides were found using the optimization criterion in Eq. 3.32 and the constraints in Eq. 3.35 and Eq. 3.33. It was assumed that the four satellites began

Table 3.1: Maneuver Cost: Tetrahedron Initial Condition Optimization

DOF	SC 1	SC 2	SC 3	SC 4	Initialization Total
No Rotation No Translation	50.6[2]	221	271	6.487×10^6	6.487×10^6
No Rotation Translation: ± 1 km	127	303	190	388	1007
No Rotation Scaling: $\pm 5\%$ Translation: ± 1 km	101	537	0.430	247	885
Rotation: ± 0.1 radians No Translation	9.11	8.58	5.97	1.27	24.93
Rotation: ± 0.1 radians Translation: ± 1 km	1.46	3.24	0.82	0.81	6.33

from the near-tetrahedron configuration

$$\begin{pmatrix} \delta\mathbf{e}_1^T \\ \delta\mathbf{e}_2^T \\ \delta\mathbf{e}_3^T \\ \delta\mathbf{e}_4^T \end{pmatrix}^T = \begin{pmatrix} 0.00000051246464 & 0.000000037450312 & 0.00000055474668 & 0.00000071331420 \\ 0.000013574046 & -0.000014775678 & 0.0000023691051 & 0.019396998 \\ 0.00000069359286 & 0.00000096599445 & 0.00000031827579 & 0.00000025502725 \\ 0.043440693 & -0.021683522 & -0.021758507 & -0.000062072563 \\ 0.00000046215002 & 0.00000015393732 & 0.00000045211263 & 0.00000013838810 \\ -0.24535033 & -6.1230191 & -6.1975472 & -6.2827584 \end{pmatrix} \tag{3.36}$$

When computing the objective function for this example, the spacecraft state errors and individual elements were weighted equally. Table 3.1 shows the results of several optimizations, each with different degrees of freedom enabled. The table shows that the most significant fuel advantage is achieved through the combination of rotation and translation. In the rotation/translation combination, the optimization created

[2]Fuel use indicated in mm/s

the desired differential elements

$$\begin{pmatrix} \delta\mathbf{e}_{d1}^T \\ \delta\mathbf{e}_{d2}^T \\ \delta\mathbf{e}_{d3}^T \\ \delta\mathbf{e}_{d4}^T \end{pmatrix}^T = \begin{pmatrix} 0 & 0 & 0 & 0 \\ 0.0000023691051 & 0.0000023691050 & 0.0000023691051 & 0.019410037 \\ 0.00000069359286 & 0.00000096599445 & 0.00000031827579 & 0.00000025502725 \\ 0.043440693 & -0.021758507 & -0.021758507 & -0.000025440407 \\ 0.00000046217628 & 0.00000015485741 & 0.00000045197460 & 0.00000013818768 \\ -0.24525410 & -6.1225395 & -6.1975472 & -6.2829781 \end{pmatrix} \tag{3.37}$$

where the limits of the translation variables are ± 1 km and the limits of the three rotation variables were each ±0.1 radians. Within those limits, the optimal translation and rotation vectors were found to be

$$\mathbf{t} = \begin{pmatrix} 20.034 & 74.627 & -6.344 \end{pmatrix}^T \tag{3.38}$$

$$\begin{pmatrix} \theta_x & \theta_y & \theta_z \end{pmatrix}^T = \begin{pmatrix} -0.000998 & -0.000995 & -0.000710 \end{pmatrix}^T \tag{3.39}$$

in meters and radians. The planner described in Section 3.3 was used to create the formation geometries specified in Eq. 3.37 from the initial conditions specified in Eq. 3.36. The total maneuver fuel cost to create the formation (*i.e.*, the sum of the costs for each spacecraft) was 6.33 mm/s.

3.6 Error-Box Constraints Using Relative Orbital Elements

Several approaches have been developed to specify formation-flying mission performance constraints. Generally, the goal of formation-flying control is to keep the formation from "drifting apart" and to maintain some relative geometry. This requirement has been translated into maintaining orbits that have the same period and specifying desired relative points for spacecraft to follow. Both goals can be accomplished simultaneously by specifying relative desired points that have identical periodicity. To ensure that the spacecraft do not drift and that the formation

geometry is maintained adequately, the control objective is to keep the spacecraft within some region around its desired point. This region is defined as a dead-band in Ref. [78] and similarly as an error box in Refs. [30, 29].

Maintaining a spacecraft within an error box has several advantages over tracking a desired point: it is more fuel efficient, better captures the mission constraints, and allows "breathing room" for the controller to account for modeling errors. In addition, the method of planning based on GVEs proposed in Section 3.3 relies on the validity of the linearization analyzed in Section 3.2, which degrades as the difference between the actual orbital element state and the orbital element state that has been linearized increases. Keeping this distance small through the use of an error box should improve the accuracy with which planned trajectories are followed.

Several approaches can be taken to create an error box. In Ref. [30], position error boxes are demonstrated, but formulations for semimajor axis error boxes and velocity error boxes are also presented. Position is a convenient bounding mechanism for a formation flying mission, because it coincides well with science requirements on the accuracy of the formation geometry shape. When the formation geometry is specified in orbital elements, it is most convenient to use a six dimensional error box with bounds on each of the state elements. This approach, while simple and convenient for enforcing acceptable relative drift levels, does not map well into the position error box constraints typical of previous performance specifications. However, it is possible to enforce relative position and relative velocity error box constraints using the $M(\mathbf{e}_1)$ matrix in Eq. 3.29 by formulating the optimization problem in Eq. 2.16 with intermediate constraints at every step k where it is desired that the spacecraft remain inside an error box about the full state

$$\mathbf{x}_{\min} \leq M^{-1}(\mathbf{e}_{di})\zeta_i \leq \mathbf{x}_{\max} \tag{3.40}$$

where $\mathbf{x}_{\max}$ is one corner of the error box and $\mathbf{x}_{\min}$ is the opposing corner. Definitions for $\mathbf{e}_{di}$, the desired state, and ζ_i, the state error, are given in Section 3.2. To exclusively enforce a partial state error box (*e.g.*, a position box), an additional matrix H can be

premultiplied by $M(\mathbf{e}_1)$ in both constraints to only retain the desired components.

3.7 Formation Flying: Coordination Using GVEs

The model predictive controller described in Section 3.3 is designed to be decentralized, with a fully independent controller being run on each spacecraft. The controller designs trajectories that will keep a spacecraft i inside an error box centered about the spacecraft's desired orbit, $\mathbf{e}_{di}$. In Section 3.2, the desired orbits are defined with respect to the actual orbit of an arbitrary satellite in the formation, $\mathbf{e}_1$, using differential orbital element vectors, $\delta\mathbf{e}_{di}$, in the same manner used in Ref. [43]. Section 3.5 presented an approach to choosing initial conditions that minimized the weighted state error across the formation. In a system where initial conditions are chosen infrequently, it may be desirable to introduce additional coordination into the formation. When spacecraft each track desired states with no coordination, the control task is referred to as *formation-keeping* [30]. Alternately, *formation-flying* occurs when the spacecraft controllers collaborate to achieve formation-wide fuel minimization. This coordination can be achieved by calculating a central point that minimizes the overall weighted state error of each spacecraft in the formation. Approaches to implementing closed-loop coordination of this type are presented in Refs. [54,55]. The *virtual center* approach in Ref. [55] is a centralized calculation of the error-minimizing center based on fuel-weighting and derived from measurements available through carrier-phase differential GPS (CDGPS) relative navigation of the type described in Refs. [56, 57]. An equivalent approach can be used to find an error-minimizing reference orbit for a formation described in differential orbital elements.

Measurements from a CDGPS relative navigation system are assumed to be in the form of relative LVLH states [56, 57], $\mathbf{x}_i$, for each satellite in the formation. The measurements will be relative to an arbitrary absolute satellite state, $\mathbf{e}_1$, in the formation, which is assumed to be at the origin of the LVLH frame. In addition to relative states, the GPS sensors on each satellite can be expected to compute a less accurate estimate of the spacecraft's absolute state. Given an estimate of the

absolute state in Earth Centered Inertial (ECI) coordinates, $\mathbf{X}_{\mathrm{ECI}_1}$ and the relative states $\mathbf{x}_i$, the differential states $\delta\mathbf{e}_i$ in Eq. 3.5 can be computed in several ways. The matrix $M(\mathbf{e}_1)$ from Eq. 3.29 could be computed and used to create a first order approximation of the relative differential element states. However, an exact conversion can be calculated by forming estimates of the absolute states of each of the satellites based on their relative measurements

$$\mathbf{X}_{\mathrm{ECI}_i} = \mathbf{X}_{\mathrm{ECI}_1} + \mathbf{x}_i \tag{3.41}$$

The absolute states $\mathbf{X}_{\mathrm{ECI}_i}$ can be converted to Keplerian orbital elements, $\mathbf{e}_i$, of each satellite using a well-known procedure described in Ref. [9]. The relative measurements are then recovered in terms of differential orbital elements, $\delta\mathbf{e}_i$, using Eq. 3.5. Desired relative differential elements, $\delta\mathbf{e}_{dci}$, are then specified with respect to an unknown virtual center state, $\delta\mathbf{e}_c$, which will be specified with respect to the absolute state $\mathbf{e}_1$. Using the procedure described in Ref. [55], the error of an individual spacecraft with respect to the virtual center, ζ_{ci} is given by

$$\mathbf{e}_i - \delta\mathbf{e}_{dci} - \delta\mathbf{e}_c = \zeta_{ci} \tag{3.42}$$

which can be placed in the standard least squares form

$$b_i - A_i\delta\mathbf{e}_c = \zeta_{ci} \tag{3.43}$$

where $b_i = \mathbf{e}_i - \delta\mathbf{e}_{dci}$, A_i is a 6×6 identity matrix, and $\delta\mathbf{e}_c$ denotes the location of the virtual center with respect to $\mathbf{e}_1$ in differential orbital elements. By concatenating the b_i, A_i, and ζ_{ci} vectors for each spacecraft, the statement of error for the entire formation is written

$$b - A\delta\mathbf{e}_c = \zeta \tag{3.44}$$

where $b = \begin{pmatrix} b_1 & \dots & b_n \end{pmatrix}^T$, $A = \begin{pmatrix} A_1 & \dots & A_n \end{pmatrix}^T$, and $\zeta = \begin{pmatrix} \zeta_{c1} & \dots & \zeta_{cn} \end{pmatrix}^T$. The solution that minimizes the error vectors globally in a weighted least squares

sense is

$$\delta \mathbf{e}_c = (A^T W A)^{-1} A^T W b \tag{3.45}$$

where W is a weighting matrix that can be used to bias the center location according to the fuel-use rates of different satellites in the formation, as well as to weight orbital elements individually based upon the amount of control required to alter them (obtainable from the GVEs for $\mathbf{e}_1$).

3.7.1 Decentralization of Virtual Center Scheme

The virtual center calculation in Eq. 3.45 is the well-known closed-form solution to a least squares problem. The solution to the decentralized least-squares problem is also readily available in the literature and is given for spacecraft i as

$$\delta \mathbf{e}_{c_i} = \delta \mathbf{e}_{c_{i-1}} + (A^T \bar{W}_i A)^{-1} A_i^T W_i (b_i - A_i \delta \mathbf{e}_{c_{i-1}}) \ \ \forall \ \ i = 1 \ldots n \tag{3.46}$$

where $A = \begin{pmatrix} A_1 & \ldots & A_i \end{pmatrix}^T$ and $\bar{W}_i = \text{diag}\,(W_1, \ldots, W_i)$. This decentralized procedure would begin with an initial estimate $\delta \mathbf{e}_{c_1} = b_1$ and spacecraft i would pass both $\bar{W}_i$ and $\delta \mathbf{e}_{c_i}$ on to the next spacecraft $(i+1)$ in the formation. The estimate of the virtual center, $\delta \mathbf{e}_n$ will then be equal to the fully centralized solution, which could be broadcast back to the entire formation.

The decentralized calculation can be simplified using several reasonable assumptions. First, assume that the relative weighting between differential orbital elements is the same for all spacecraft and is calculated to be $W_\mathbf{e}$ based on the absolute orbit $\mathbf{e}_1$, which is known by all spacecraft in the formation. Next, let the fuel-based weighting for each spacecraft be represented by a scalar, w_i. Now, the total weighting matrix, W_i, for each spacecraft is given by

$$W_i = w_i W_\mathbf{e} \ \ \forall \ \ i = 1 \ldots n \tag{3.47}$$

Also assume that the variable being solved for is always the exact virtual center, $\delta \mathbf{e}_c$, making the A_i matrix for each satellite a 6×6 identity matrix. Now, for the ith

satellite,

$$W = \text{diag}\,(w_1 W_e, \ldots, w_i W_e) \tag{3.48}$$

and A is a column of i concatenated 6×6 identity matrices. The decentralized solution for the ith satellite becomes

$$\begin{aligned}
\delta\mathbf{e}_{c_i} &= \delta\mathbf{e}_{c_{i-1}} + (A^T W A)^{-1} A_i^T W_i (b_i - A_i \delta\mathbf{e}_{c_{i-1}}) \qquad (3.49)\\
&= \delta\mathbf{e}_{c_{i-1}} + w_i \left(\begin{bmatrix} I & \ldots & I \end{bmatrix} \begin{bmatrix} w_1 W_e & 0 & \ldots & 0 \\ 0 & w_2 W_e & \ldots & 0 \\ \vdots & 0 & \ddots & 0 \\ 0 & 0 & \ldots & w_i W_e \end{bmatrix} \begin{bmatrix} I \\ I \\ \vdots \\ I \end{bmatrix} \right)^{-1} W_e (b_i - \delta\mathbf{e}_{c_{i-1}})
\end{aligned}$$

which can be further simplified to

$$\begin{aligned}
\delta\mathbf{e}_{c_i} &= \delta\mathbf{e}_{c_{i-1}} + w_i [(w_1 + \ldots + w_i) W_e]^{-1} W_e (b_i - \delta\mathbf{e}_{c_{i-1}}) \qquad (3.50)\\
&= \delta\mathbf{e}_{c_{i-1}} + \frac{w_i}{w_1 + \ldots + w_i} (b_i - \delta\mathbf{e}_{c_{i-1}}) \qquad (3.51)
\end{aligned}$$

Introducing $\bar{w}_i$, which is the sum of all previous scalar weights,

$$\bar{w}_i = \sum_{k=1}^{i} w_k \tag{3.52}$$

then the new recursion becomes

$$\delta\mathbf{e}_{c_i} = \delta\mathbf{e}_{c_{i-1}} + \frac{w_i}{\bar{w}_{i-1} + w_i} (b_i - \delta\mathbf{e}_{c_{i-1}}) \tag{3.53}$$

and the only information that needs to be passed to the next spacecraft to form $\delta\mathbf{e}_{c_{i+1}}$ is the current virtual center estimate, $\delta\mathbf{e}_{c_i}$, and the scalar $\bar{w}_i$.

3.8 Formation Maintenance on MMS-like Mission

The control system developed in Chapter 3 was demonstrated on a segment of the MMS mission. The MMS mission is comprised of four spacecraft that create regular

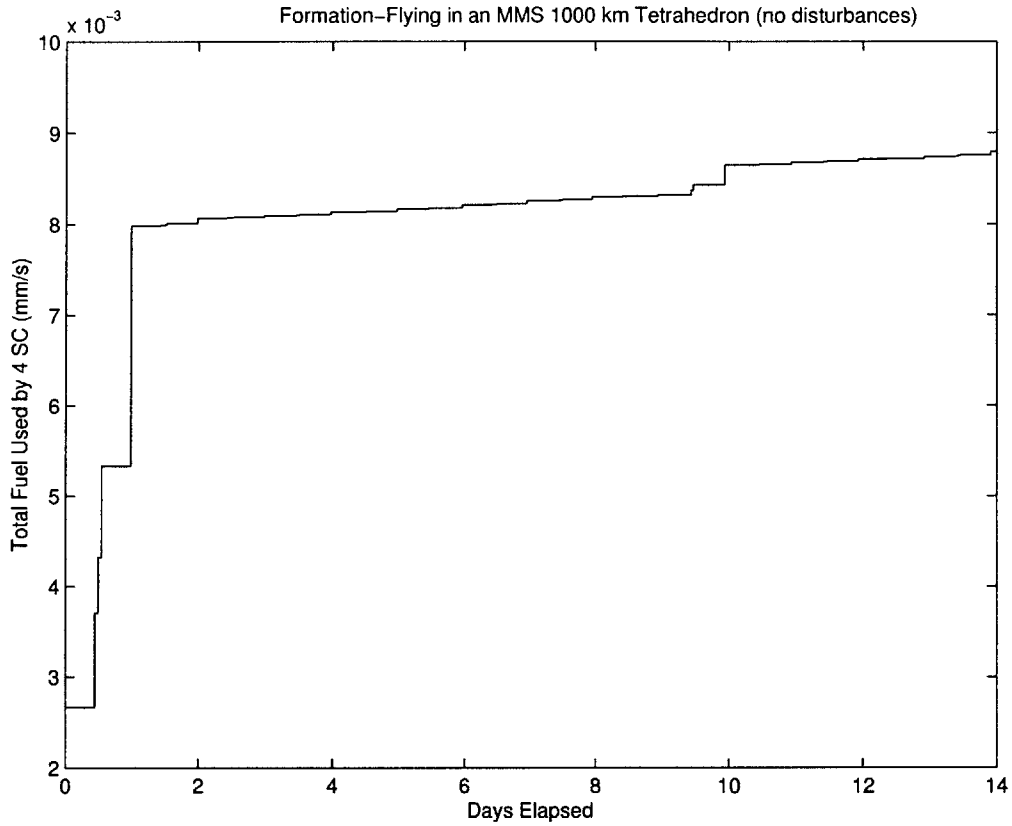

Fig. 3–3: Fuel cost for maintaining a 1000 km tetrahedron formation in a highly eccentric orbit

tetrahedron geometries once per orbit. The orbits of the four spacecraft are widely separated and highly elliptical, presenting a challenge for many optimal formation specification and control approaches in the literature [15, 16]. Using the tetrahedron initial-condition optimization approach in Section 3.5 and the model predictive approach in Section 3.3, the four spacecraft were controlled in a fully nonlinear simulation (unmodeled oblateness and drag disturbances were not used) using a commercial orbit propagator. Figure 3–3 shows the rate at which fuel was used over the course of two weeks of formation flying. After an initial transient period, the formation fuel use rate converges to approximately 2.1 mm/s per day ($\approx$ 1 orbit) for each satellite.

3.9 Chapter Summary

Gauss' Variational Equations have been used to derive a set of linearized relative dynamics of orbital motion. The linearization assumptions for the new set of dynamics were shown to be valid for typical spacecraft error box sizes. The linearized GVE-based dynamics were used in a model predictive controller of the form described in [30] and the combination is shown to be more fuel-efficient than another GVE-based technique. A method of specifying formation geometry through differential orbital elements was reviewed. By combining differential element orbit specification and dynamics linearized about each of the spacecraft in the formation, the problems of long-baseline initialization and control discussed in Chapter 2 can be bypassed. A method of specifying differential orbital elements for a desired formation geometry was introduced which optimizes degrees of freedom in the problem of initial condition selection to minimize the fuel required to maneuver into the new formation. This method was applied to a regular tetrahedron-shaped orbit of the type used in the MMS mission. A method of applying rectilinear error box constraints to a formation specified in differential orbital elements was presented. Also, a virtual center approach to coordinating spacecraft formations of the type introduced in [42] was derived in terms of the differential orbital element formation specification and decentralized. A demonstration of the GVE-based dynamics/MPC controller being used with differential orbital element formation specification was created in a tetrahedron-shaped formation in an MMS-like orbit was controlled for a period of two weeks.

Chapter 4

Analytic Prediction of Spacecraft Performance Using Robust MPC in the Presence of Sensor Noise

Reference [32] showed that sensor noise in a spacecraft formation flying mission using carrier-phase differential GPS (CDGPS) will be a dominant disturbance. It presented an approach to mitigating the effects of sensor noise on a model predictive control scheme of the type discussed in Section 3.3. This robustness was achieved by designing trajectories that would meet performance criteria for a set of possible initial conditions. The size of this set was determined by the expected sensor noise. The approach taken in that paper is characterized as "open-loop," because it generates a trajectory which is feasible for all initial conditions, without requiring replanning. An alternate approach is to design a thrusting plan which will be guaranteed to produce a feasible state and a new feasible plan at the next time step. This approach is considered "closed-loop," because each plan explicitly considers future feedback action in response to as-yet unknown information [65].

In references [67,66] it was shown that the fuel use of the robust model predictive control scheme presented in Ref. [59] can be predicted for bounded process noise and sensor noise disturbance models. This chapter will apply the robustly-feasible MPC scheme to the problem of controlling spacecraft relative motion. Hill's equations of relative motion in a circular orbit are used to model a formation flying control

problem in which a spacecraft is constrained to remain inside an error box. Some assumptions about the noise source and the error box are made when using the predictive method and validated by simulation. The analytical prediction method is then used to examine a wide range of missions in order to identify trends, sensitivities, and optimal regions in the space of controller parameters, such as error box size, sensor noise, fuel use, replan frequency and the planning horizon length. The validity of these relations is verified by simulation and their application to designing future spacecraft formation flying missions is demonstrated using relevant parameter ranges. A number of realistic and desirable parameter combinations are identified, indicating the value of future research to extend and refine the analysis tool.

To demonstrate the viability of the robust model predictive scheme to actual spacecraft formation flight, a demonstration is conducted in which a multiple spacecraft are controlled over an extended period using a nonlinear propagator with a realistic disturbance model. A formulation is developed that simultaneously incorporates bounds on state error, process noise, sensor noise, and thrust availability. Simulations demonstrate the effectiveness of both the bounded models and of closed-loop robustness technique applied to a realistic spacecraft formation control problem. Terminal conditions presented in [66] and others suggested in [60] were evaluated.

4.1 Overview of Robust MPC Scheme

For the spacecraft formation flying problem with sensor noise, robust feasibility guarantees that, provided the initial optimization is feasible and the noise is bounded, all subsequent optimizations are feasible and constraints are satisfied, *e.g.,* the spacecraft remains inside the specified error box. This guarantee holds despite the plans being based on inaccurate information. Ref. [67, 60] proves that the formulation reviewed in this section guarantees both robust feasibility and constraint satisfaction. Ref. [59] reviews an approach to transform the dynamics of the *true* state $\mathbf{x}$ to those of the *estimated* state $\hat{\mathbf{x}}$. Robust feasibility depends on the estimate, since that is the initial

condition parameter of the optimization. The dynamics of the true state are

$$\mathbf{x}(k+1) = \mathbf{A}\mathbf{x}(k) + \mathbf{B}\mathbf{u}(k) \tag{4.1}$$

and the estimation error is an additive term, applied at each time step

$$\hat{\mathbf{x}}(k) = \mathbf{x}(k) + \mathbf{n}(k) \tag{4.2}$$

$$\hat{\mathbf{x}}(k+1) = \mathbf{x}(k+1) + \mathbf{n}(k+1) \tag{4.3}$$

where $\mathbf{n}(k)$ is the estimation error at time k, which is assumed to lie in a bounded set $\mathcal{N}$. Substituting (4.2) and (4.3) into (4.29) gives the dynamics of the estimate

$$\begin{aligned} \hat{\mathbf{x}}(k+1) &= \mathbf{A}\hat{\mathbf{x}}(k) + \mathbf{B}\mathbf{u}(k) + \mathbf{n}(k+1) - \mathbf{A}\mathbf{n}(k) \\ &= \mathbf{A}\hat{\mathbf{x}}(k) + \mathbf{B}\mathbf{u}(k) + \begin{bmatrix} -\mathbf{A} & \mathbf{I} \end{bmatrix} \begin{pmatrix} \mathbf{n}(k) \\ \mathbf{n}(k+1) \end{pmatrix} \end{aligned} \tag{4.4}$$

With the dynamics now involving an affine disturbance, the formulation of [59] can be employed to synthesize a robustly feasible MPC scheme. The disturbance vector is bounded using

$$\mathbf{w}(k) = \begin{bmatrix} -\mathbf{A} & \mathbf{I} \end{bmatrix} \begin{pmatrix} \mathbf{n}(k) \\ \mathbf{n}(k+1) \end{pmatrix} \in \mathcal{W} \quad \forall k \tag{4.5}$$

If $\mathcal{N}$ is polyhedral, the set $\mathcal{W}$ is polyhedral and can therefore be generated using a polyhedral mapping routine of the form in Ref. [62]. Output constraints take the form

$$\mathbf{y}(k) = \mathbf{C}\hat{\mathbf{x}}(k) + \mathbf{D}\mathbf{u}(k) \in \mathcal{Y} \quad \forall k \tag{4.6}$$

where $\mathcal{Y}$ is a bounded set which can incorporate error box and thrust constraints.

The MPC optimization is performed over a horizon of N steps and uses an arbitrary nilpotent linear control law $\mathbf{u}(j) = \mathbf{K}_{NP}\mathbf{x}(j)$ $j \in \{0 \ldots N-1\}$. Define $\mathbf{L}(j)$ as

the state transition matrix for the closed-loop system under this control law

$$\mathbf{L}(0) = \mathbf{I} \tag{4.7}$$

$$\mathbf{L}(j+1) = (\mathbf{A} + \mathbf{B}\mathbf{K}_{NP})\,\mathbf{L}(j) \quad \forall j \in \{0 \dots N\} \tag{4.8}$$

Then the nilpotency requirement for $\mathbf{K}_{NP}$ implies

$$\mathbf{L}(N) = \mathbf{0} \tag{4.9}$$

Define the MPC optimization problem $\mathsf{P}(\hat{\mathbf{x}}(k))$

$$J^*(\hat{\mathbf{x}}(k)) = \min_{\mathbf{u},\mathbf{x},\mathbf{y}} \sum_{j=0}^{N} \ell\left(\mathbf{u}(k+j|k), \mathbf{x}(k+j|k)\right) \tag{4.10}$$

subject to

$$\forall j \in \{0 \dots N\}$$

$$\mathbf{x}(k+j+1|k) = \mathbf{A}\mathbf{x}(k+j|k) + \mathbf{B}\mathbf{u}(k+j|k) \tag{4.11}$$

$$\mathbf{y}(k+j|k) = \mathbf{C}\mathbf{x}(k+j|k) + \mathbf{D}\mathbf{u}(k+j|k) \tag{4.12}$$

$$\mathbf{x}(k|k) = \hat{\mathbf{x}}(k) \tag{4.13}$$

$$\mathbf{x}(k+N+1|k) \in \mathcal{X}_F \tag{4.14}$$

$$\mathbf{y}(k+j|k) \in \mathcal{Y}(j) \tag{4.15}$$

where the double subscript notation $(k+j|k)$ denotes the prediction made at time k of a value at time $k+j$. The constraint sets are chosen according to the recursion

$$\mathcal{Y}(0) = \mathcal{Y} \tag{4.16}$$

$$\mathcal{Y}(j+1) = \mathcal{Y}(j) \sim (\mathbf{C} + \mathbf{D}\mathbf{K}_{NP})\,\mathbf{L}(j)\mathcal{W} \quad \forall j \in \{0 \dots N\} \tag{4.17}$$

where $\sim$ denotes the Pontryagin difference operation [64], defined by

$$\mathcal{X} \sim \mathcal{Y} \triangleq \{\mathbf{z} \mid \mathbf{z} + \mathbf{y} \in \mathcal{X} \ \forall \mathbf{y} \in \mathcal{Y}\} \tag{4.18}$$

and the matrix mapping of a set is defined such that

$$\mathbf{A}\mathcal{X} \triangleq \{\mathbf{z} \mid \exists \mathbf{x} \in \mathcal{X} : \mathbf{z} = \mathbf{A}\mathbf{x}\} \tag{4.19}$$

A MATLAB toolbox for performing these operations on polyhedral sets is available in Ref. [62].

The terminal constraint $\mathcal{X}_F$ is problem-specific. It must be a control invariant admissible set [63], *i.e.* there exists a control law $\kappa(\mathbf{x})$ satisfying the following

$$\begin{aligned} &\forall \mathbf{x} \in \mathcal{X}_F \\ \mathbf{A}\mathbf{x} + \mathbf{B}\kappa(\mathbf{x}) &\in \mathcal{X}_F \qquad (4.20) \\ \mathbf{C}\mathbf{x} + \mathbf{D}\kappa(\mathbf{x}) &\in \mathcal{Y}(N) \qquad (4.21) \end{aligned}$$

The origin $\mathcal{X}_F = \{\mathbf{0}\}$ is a straightforward choice of terminal set, and when conducting performance analyses in Section 4.3. However, any nominally invariant set is valid for $\mathcal{X}_F$. Section 4.5.2 demonstrates that the origin is an overly restrictive terminal condition for spacecraft formation flight control.

4.2 Overview of Analytic Performance Prediction

Reference [67] describes an approach for analytically predicting the value of a performance criterion for the type of model predictive control system described in Section 4.1. The prediction method is based on similarities between optimal solution to the LQR problem and the solution to the closed loop MPC problem when several restrictions are introduced

1. The performance index is a quadratic function of the control input, $\ell(\mathbf{u}, \mathbf{x}) = \mathbf{u}^T\mathbf{Q}\mathbf{u}$ where $\mathbf{Q}$ is positive definite.

2. The terminal constraint is the origin, $\mathcal{X}_F = \{\mathbf{0}\}$ (note that this trivially satisfies the invariancy requirement with $\kappa(\mathbf{x}) = \mathbf{0}$).

3. The estimation uncertainty is of the form $\mathbf{n}(k) = \mathbf{e}\tilde{n}(k)$ where $\tilde{n}(k)$ is uniformly distributed over a bounded set

$$-\bar{N} \leq \tilde{n}(k) \leq \bar{N} \tag{4.22}$$

and uncorrelated, giving $E\{\tilde{n}(k)\tilde{n}(k+j)\} = \frac{\bar{N}^2}{3}\Delta(j)$ [67]

4. There is only one constraint, $y(k) = \mathbf{c}^T\hat{\mathbf{x}}(k) + \mathbf{d}^T\mathbf{u}(k) \in \mathcal{Y}$

Section 4.4 will show that this restrictive form can still capture the dominant behavior of a spacecraft system.

The dynamics in Eq. 4.30 are augmented with additional states $\mathbf{z}$ to create a system driven by a single noise signal

$$\left[\begin{array}{c} \hat{\mathbf{x}}(k+1) \\ \mathbf{z}(k+1) \end{array}\right] = \left[\begin{array}{c|c} \mathbf{A} & -\mathbf{A} \\ \hline \mathbf{0} & \mathbf{0} \end{array}\right] \left[\begin{array}{c} \hat{\mathbf{x}}(k) \\ \mathbf{z}(k) \end{array}\right] + \left[\begin{array}{c} \mathbf{B} \\ \hline \mathbf{0} \end{array}\right] \mathbf{u}(k) + \left[\begin{array}{c} \mathbf{e} \\ \mathbf{e} \end{array}\right] \tilde{n}(k+1) \tag{4.23}$$

If the control law is a constant matrix state feedback, $\mathbf{K}$, operating on the known state estimate

$$\mathbf{u}(k) = \mathbf{K}\hat{\mathbf{x}}(k) \tag{4.24}$$

then the system (4.23) becomes the following

$$\left[\begin{array}{c} \hat{\mathbf{x}}(k+1) \\ \mathbf{z}(k+1) \end{array}\right] = \left[\begin{array}{c|c} \mathbf{A}+\mathbf{B}\mathbf{K} & -\mathbf{A} \\ \hline \mathbf{0} & \mathbf{0} \end{array}\right] \left[\begin{array}{c} \hat{\mathbf{x}}(k) \\ \mathbf{z}(k) \end{array}\right] + \left[\begin{array}{c} \mathbf{e} \\ \mathbf{e} \end{array}\right] \tilde{n}(k+1) \tag{4.25}$$

In the examples provided in Section 4.4, the performance metric is the control effort, so the following performance output equation is used

$$\mathbf{u}(k) = \left[\begin{array}{c|c} \mathbf{K} & \mathbf{0} \end{array}\right] \left[\begin{array}{c} \hat{\mathbf{x}}(k) \\ \mathbf{z}(k) \end{array}\right] \tag{4.26}$$

To summarize, the prediction method reviewed in this section makes use of the observation that the model predictive control system described in Section 4.1 using a terminal set that include only the origin, behaves like an LQR control at low disturbance levels and like a nilpotent controller at high disturbance levels.

4.3 Spacecraft Formation Flight Application

This section describes the application of the analysis method developed in Section 4.2 to the spacecraft formation flying control problem. The specific application examined is relative motion in a circular orbit using the radial/in-track plane in Hill's equations. The prediction method assumes only a single noise source and a single constraint. For the spacecraft formation control problem, the performance is dominated by the effects of the in-track velocity estimation error and the in-track position constraint [32], hence the conjecture is that the single-constraint model can still capture the behavior of the system. Simulation results will investigate the validity of these assumptions.

The system used for analysis will use impulsive velocity changes in both the in-track and radial directions as control inputs. The system is driven by the in-track velocity noise, with $\mathbf{e} = [\ 0 \quad 0 \quad 0 \quad 1\ ]^{\mathrm{T}}$ and assumes perfect knowledge of the other states. The in-track direction will be constrained, so $\mathbf{c} = [\ 0 \quad 1 \quad 0 \quad 0\ ]$ and $\mathbf{d} = [\ 0 \quad 0\ ]$. A constant K_{NP} can be found that drives a state in the radial/in-track plane of the Hill's frame to the origin in 4 steps (which restricts the horizon length to $N > 4$). This example will use an orbit with frequency $n = 0.001$ and with a discretization $T \approx 314s$ (twenty steps per orbit). The MPC controller is implemented with $N = 5$ predictive steps and a ± 5 meter error box is placed around the origin in the in-track direction.

A typical trajectory for spacecraft relative motion using the MPC controller with the system is shown in Figure 4–1. Although the radial position is left unconstrained in the control formulation, the coupling between the radial and in-track directions causes a constraint on one axis to act on the other axis as well. The motion approximately forms a 6x3 ellipse, which is to be expected, because the harmonic terms

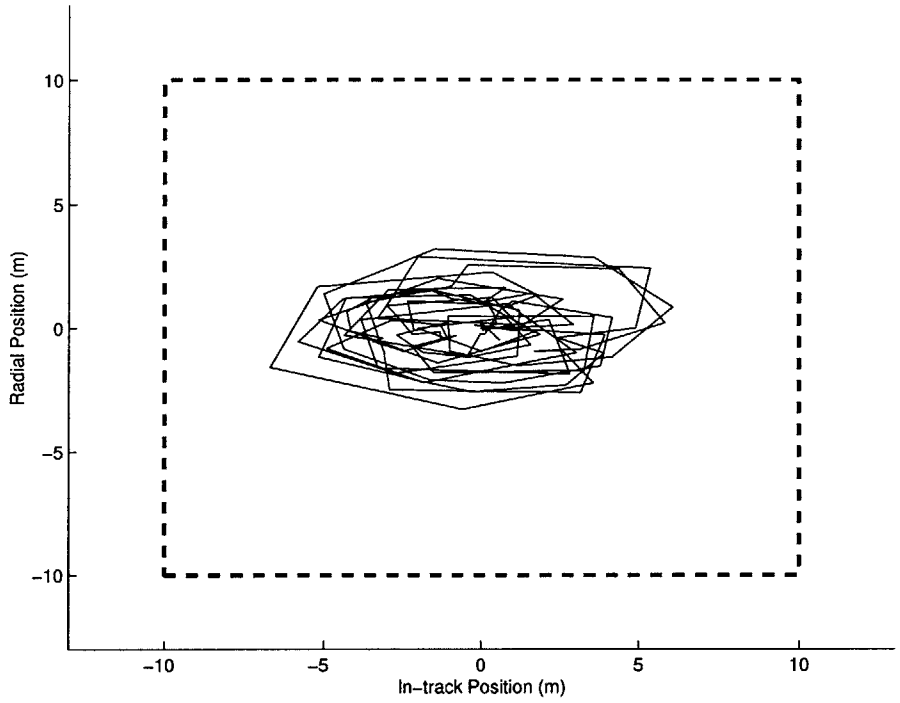

Fig. 4–1: Simulation trajectory using MPC controller (6 orbits shown)

in the in-track direction are twice the harmonic terms in the radial direction. In addition, the radial position is constrained to stay near the origin by the terminal condition that the spacecraft arrive at the origin after N steps. Figure 4–2 is a plot of required control energy versus sensor noise. The solid line shows the predicted fuel use using the assumptions of bounded in-track position error and velocity noise solely in the in-track direction. The asterisks indicate the values from simulations including the assumptions used for analytic prediction. The dots show the simulated fuel use requirements for the complete problem, including bounded position in the radial and in-track directions and velocity noise in both the radial and in-track directions. The simulation results and the predicted values show close agreement for both the simulation based on the prediction assumptions and the simulation using the complete problem formulation. To account for the addition of a second noise source, the noise values for the full simulation have been scaled by a factor of $\sqrt{2}$. Having demonstrated the relevance of the prediction method, that method can be used to

predict the effects of wide ranges of parameter variations.

Figure 4–3 shows predictions of the effect of varying the horizon length and replan-frequency for a constant ten meter square error box using the analytical prediction method. Generally, increasing the horizon length and lowering the replan frequency (increasing discretization time-step) both reduce the expected control cost. There is a limit to how far the replan frequency can be lowered before the problem becomes infeasible. For fixed time-steps, there appears to be a critical plan length at approximately 0.8 orbits. The horizontal line corresponds to the division (separating dark and light areas in Figure 4–3(b)) between the high- and low-disturbance regimes. Conceptually, the preferred planning horizon length is that at which the unconstrained LQR solution just begins to interact with the error box constraints. The prediction method suggests a globally preferential combination of time-step and plan length at the intersection of the dashed lines in the figure. The combination lies in the region of the quadratic approximation, which is the subject of ongoing research. For further verification, several vertical cross sections (constant time-step) of Figure 4–3(a) have been compared to simulation data in Figure 4–4.

Recreating the same contour plot for a different orbit ($n = 0.0005$) results in a graph (shown in Figure 4–5) with many of the same characteristics as the $n = 0.001$ graph, where n is the frequency of the circular reference orbit. The preferred plan length (indicated by a horizontal line) has become slightly longer in relative orbits, while the preferred time-step is now significantly longer.

4.4 Analytical Predictions

The analytical prediction method enables the rapid optimization of control parameters for a variety of different trades relevant to planning a formation flying mission. GPS is a commonly examined method of sensing relative state and is known to produce estimates of velocity with sensing error between 0.5 mm/s and 2 mm/s [70]. Figure 4–6 shows contours of constant expected fuel use for the relation between error box size and noise level. Consider a scenario in which the noise is known to be 3 mm/s,

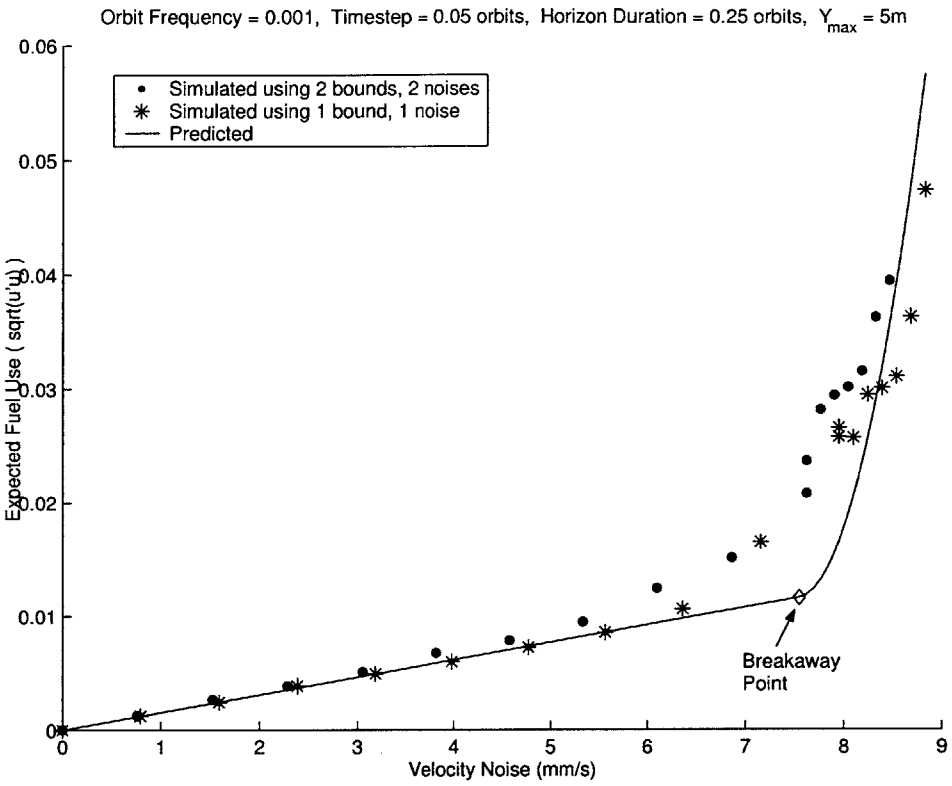

Fig. 4–2: Comparison of Prediction Assumptions

slightly higher than a realistic GPS estimate. Setting the error box size to 1 meter gives an infeasible problem. If the error box size is increased to 3 meters, the problem becomes feasible. Further increases give a significant decrease in fuel use, up to a size of about 10 meters. This lies on the line of transition between constrained and unconstrained operation, beyond which there is no fuel-use gain for enlarging the error box. Therefore, like the choice of planning horizon, the ideal design is at the point where the constraints become active.

Another trade relevant to control system design is the relationship between error box size and planning horizon length. Figure 4–7 shows this trade for the example system. The fuel use numbers are low relative to those in the literature [30], because the problem being examined has perfectly linear dynamics and no process noise – including these effects in the analysis are the subjects of the ongoing research. The figure shows that fuel use is very high regardless of horizon length for error boxes smaller than $\sim$2.5 meters. For each error box larger than $\sim$2.5 meters, there is a

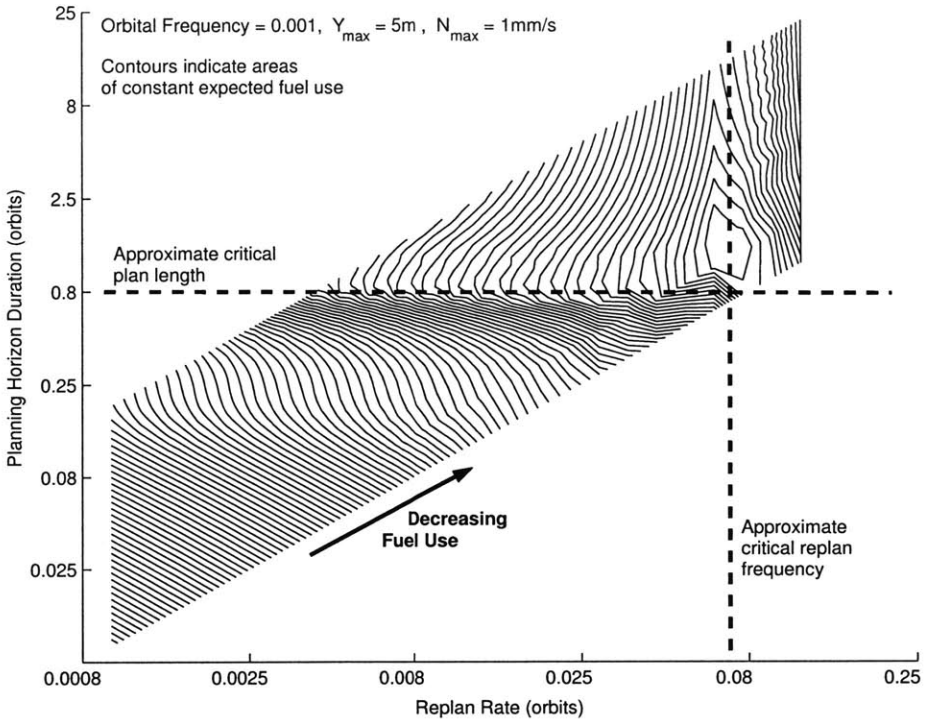

(a) Contour plot shows fuel use decreases as prediction horizon is extended

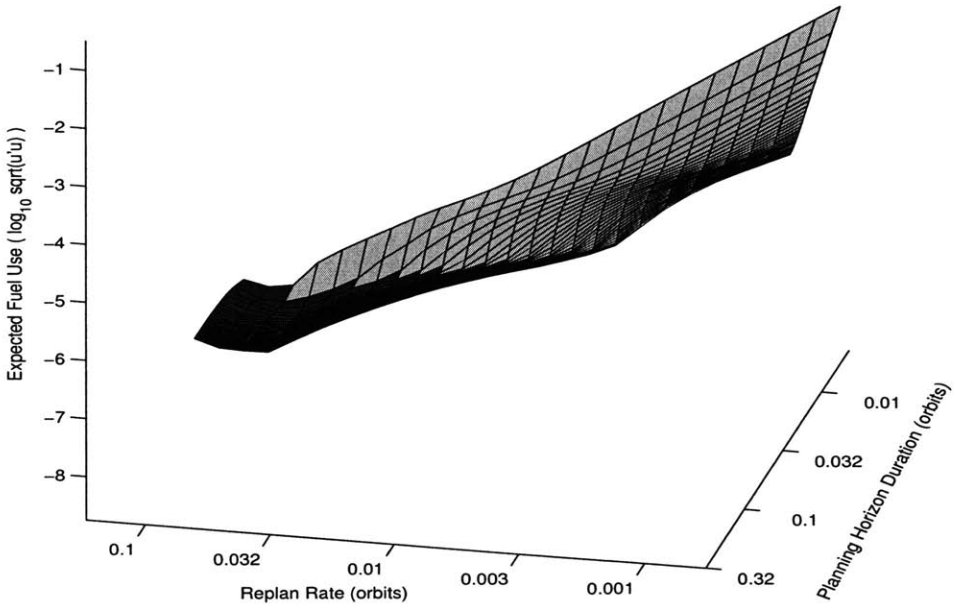

(b) Surface showing interaction between low and high noise regime models (note axes reversed from Fig. 4–3(a))

Fig. 4–3: Effect of Plan Length and Replan Frequency on Fuel Use

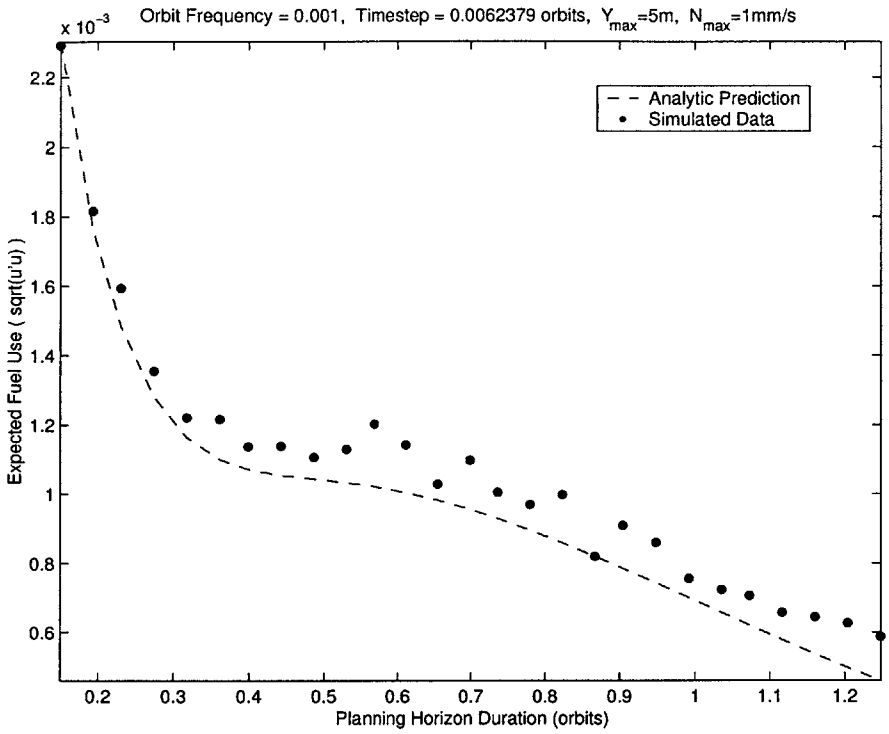

(a) Cross section at time-step = 0.0062 orbits

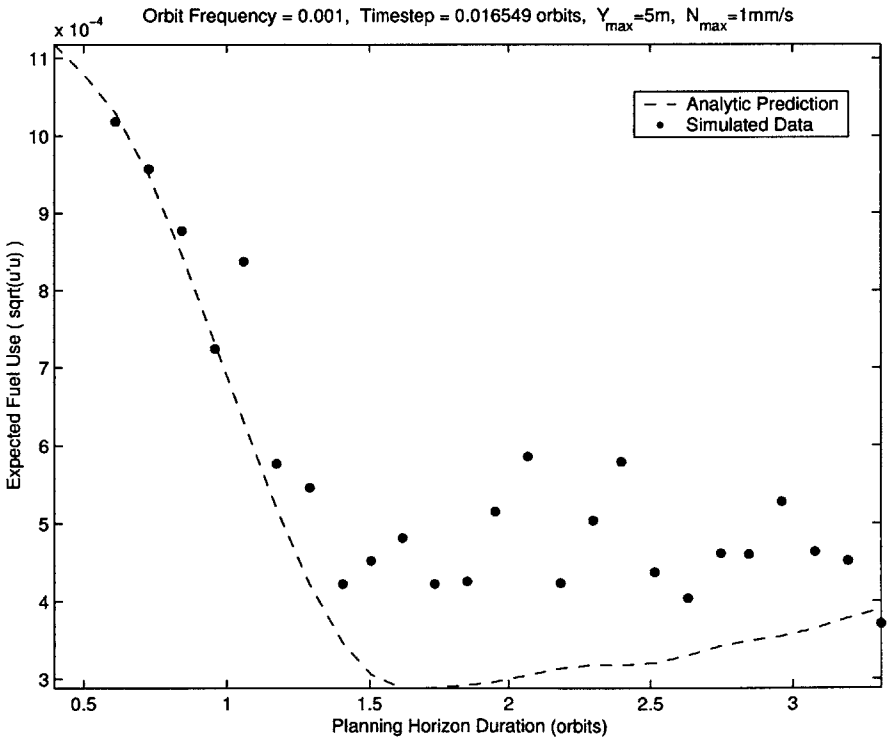

(b) Cross section at time-step = 0.016 orbits

Fig. 4–4: Effect of Plan Length and Replan Frequency on Fuel Use

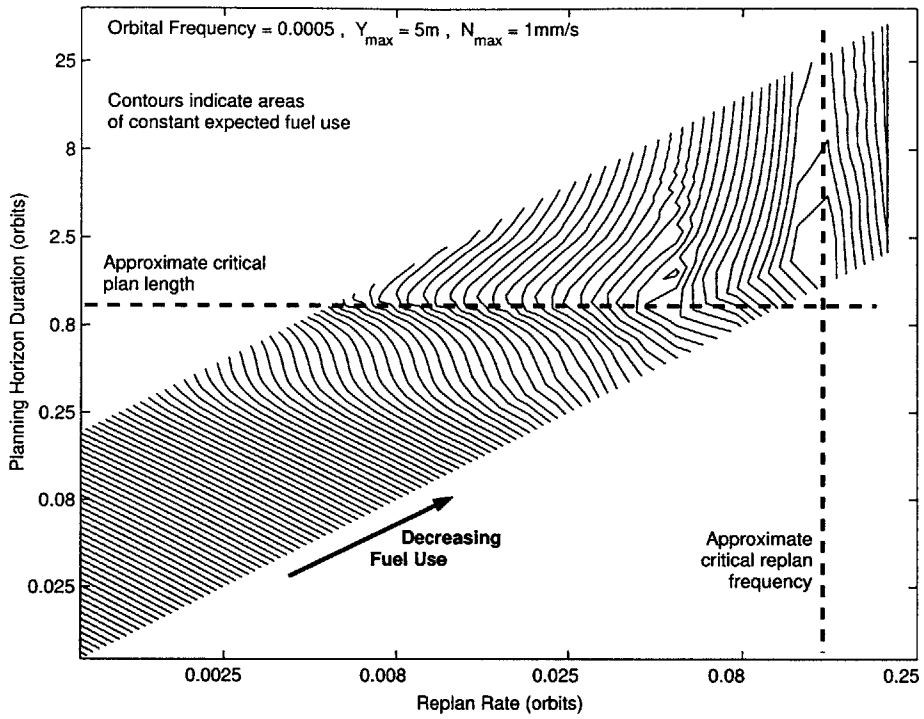

Fig. 4–5: Effect of Plan Length and Replan Frequency on Fuel Use ($n = 0.0005$)

particular planning horizon length that gives the minimum expected fuel use. As in Figure 4–6, the expected fuel use is insensitive to error box size in many regions of the plot.

4.5 Simulation Results

This section describes a series of more realistic simulations utilizing the robust MPC approach described in Section 4.1. To work in a realistic environment, the controller must be posed using many constraints and an additional disturbance model, neither of which were considered in the analytical predictions of Section 4.4. Simulations were run in FreeFlyer^{TM}, a commercial nonlinear orbit propagator [24], to demonstrate that the closed-loop robustness scheme presented in Ref. [59] could be applied to a realistic spacecraft formation flying mission. In addition to sensor noise, a high fidelity disturbance model was used, which includes Earth oblateness effects (J_2), aerodynamic disturbances, solar pressure, and third body effects from the sun and

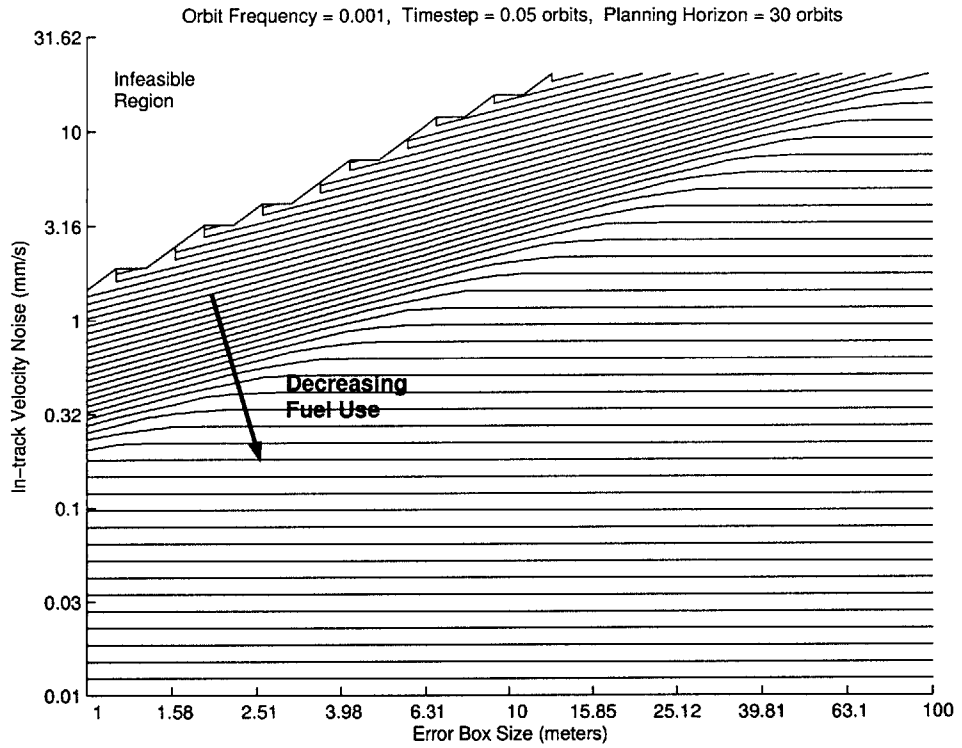

Fig. 4–6: Effect of Velocity Noise and Error Box Size on Fuel Use

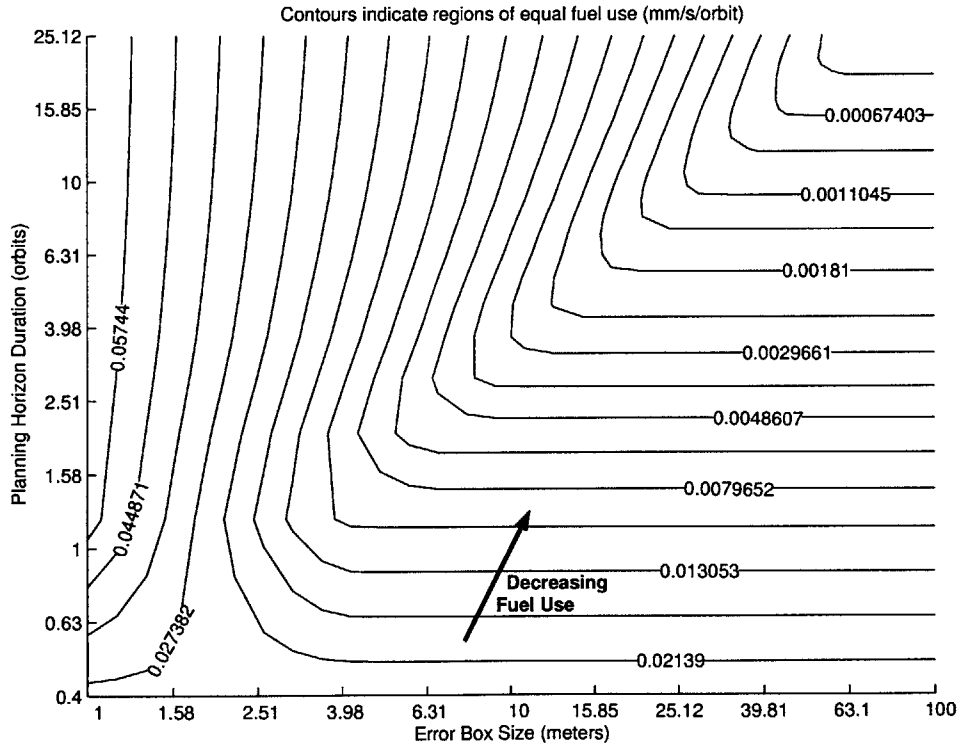

Fig. 4–7: Effect of Plan Length and Error Box Size on Fuel Use

the moon. In addition, normally distributed sensor noise with standard deviations of 2 cm for relative position and 0.5 mm/s was added to the state to simulate the CDGPS measurement errors. In order to guarantee that the optimizations for the closed-loop robustness are feasible, all disturbances on the system must be bounded. Bounds were determined numerically using a procedure described in Section 4.5.1 and the results of the closed-loop robustness demonstrations are compared for several different terminal sets and with results obtained using a different form of robust MPC. The reference orbit used for this example is

$$\mathbf{e}_{\text{ref}} = \begin{pmatrix} 1.08182072 & 0.0 & 0.610865238 & 0.0 & 0.0 & \pi \end{pmatrix}^T \tag{4.27}$$

4.5.1 Bounding the Process Noise

Reference [68] describes an open-loop approach to accounting for disturbances in a model predictive control scheme. This approach uses analytic models of J_2 and drag to predict time-varying disturbances which are then added to the LP formulation in Eq. 2.16. The closed-loop approach in Refs. [59, 67, 66] uses constant dynamics and a bounded disturbance model. To develop polytopic bounds on the disturbance set, two spacecraft were simulated in close proximity to one another and propagated using both the high fidelity nonlinear integration-based propagator (NLP) and Hill's equations. The NLP used for the bounding process included the perturbations due to J_2, drag, third body effects, and solar pressure. At each time step in the simulation, the previous state of the NLP was propagated forward using both a Hill's propagator and the NLP. The difference between the two states was found and the magnitudes of each of its position and velocity states were stored. Similar simulations were run using different initial starting states of the second satellite within an error box ($5 \times 10 \times 5$ meters in the radial, in-track, and cross-track directions, respectively) centered about the first satellite. The maximum absolute value of the differences between the nonlinear and linear propagated states from all of simulations were calculated. These maxima were then chosen as the maximum perturbations for position and velocity, respectively.

For the orbit $\mathbf{e}_{\text{ref}}$ in Eq. 4.27, the disturbance sets for a 100 second propagation time step were found to be

$$\begin{pmatrix} p_x \\ p_y \\ p_z \end{pmatrix} \leq \begin{pmatrix} 85.5 \\ 30.3 \\ 0.0168 \end{pmatrix} \qquad \begin{pmatrix} v_x \\ v_y \\ v_z \end{pmatrix} \leq \begin{pmatrix} 0.635 \\ 0.323 \\ 0.00334 \end{pmatrix} \tag{4.28}$$

in units of centimeters and millimeters per second, respectively. These numbers are roughly on the same order of magnitude as the sensing noise, which is expected, given the large integration time-step and the presence of many disturbances not modeled by Hill's equations. Another approach to developing a disturbance model of this type would be to use analytical models of the effects of J_2, drag, and nonlinearities to due separation distance and eccentricity. For a given reference orbit, the maximum perturbation predicted by each model would be combined to give the largest possible unmodeled disturbance on Hill's equations.

4.5.2 Demonstration Results

To use the model predictive control formulation reviewed in Section. 4.1, the system described in Eq. 4.29 is augmented with an additive disturbance, $\mathbf{q}(k)$, which will be used to represent process noise. The system in Eq. (4.29) then becomes

$$\mathbf{x}(k+1) = \mathbf{A}\mathbf{x}(k) + \mathbf{B}\mathbf{u}(k) + \mathbf{q}(k) \tag{4.29}$$

where $\mathbf{q}(k)$ in a vector belonging to a bounded polyhedral set $\mathcal{Q}$. Likewise, the estimated state with sensing noise in Eq. 4.30 becomes

$$\hat{\mathbf{x}}(k+1) = \mathbf{A}\hat{\mathbf{x}}(k) + \mathbf{B}\mathbf{u}(k) + \begin{bmatrix} -\mathbf{A} & \mathbf{I} & \mathbf{I} \end{bmatrix} \begin{pmatrix} \mathbf{n}(k) \\ \mathbf{n}(k+1) \\ \mathbf{q}(k) \end{pmatrix} \tag{4.30}$$

This altered formulation yields the new bounded disturbance set $\mathcal{W}$

$$\mathbf{w}(k) = \begin{bmatrix} -\mathbf{A} & \mathbf{I} & \mathbf{I} \end{bmatrix} \begin{pmatrix} \mathbf{n}(k) \\ \mathbf{n}(k+1) \\ \mathbf{q}(k) \end{pmatrix} \in \mathcal{W} \quad \forall k \tag{4.31}$$

The robust formulation in Section 4.1 can accommodate a disturbance set of this form, but its implementation is complicated by the high dimensionality of the uncertainty set and constraints. In particular, the calculation of the Pontryagin difference is the subject of on-going work. Therefore, an approximation similar to that made in Equation 4.22 is used, whereby two scalar noise inputs capture the dominant sensing uncertainty. This approximation is extended to represent sensing noise uncertainty in all states and a term is added to the to represent the process noise. Equation 4.22 states that the bounds on a single sensor noise $\mathbf{n}(k)$ are $\pm\mathbf{e}\bar{N}$. This constraint is unchanged if a new vector, $\mathbf{e}_{\text{sn}}$ is defined as

$$\mathbf{e}_{\text{sn}} = \bar{N}\mathbf{e} \tag{4.32}$$

and $\bar{n}(k)$ is now distributed over the bounded set

$$-1 \leq \bar{n}(k) \leq 1 \tag{4.33}$$

For the examples in this section, $\mathbf{e}_{\text{sn}}$ is defined to be the expected noise on relative spacecraft states in a CDGPS system: 0.02 meters for position sensing and 0.0005 meters/second for velocity sensing.

A vector, $\mathbf{e}_{\text{pn}}$, describing the maximum process noise magnitude on each state (taken directly from Eq. 4.28) is introduced to form an approximation for the total possible state perturbation due to noise at any step k. The disturbance vector $\mathbf{w}(k)$ is now defined to be

$$\mathbf{w}(k) = \begin{bmatrix} (\mathbf{e}_{\text{pn}} - \mathbf{A}\mathbf{e}_{\text{sn}}) & \mathbf{e}_{\text{sn}} \end{bmatrix} \begin{pmatrix} \bar{n}(k) \\ \bar{n}(k+1) \end{pmatrix} \in \bar{\mathcal{W}} \quad \forall\, k \tag{4.34}$$

The new set $\bar{\mathcal{W}}$ attempts to capture the uncertainty present in the formation flying demonstrations conducted in this section. Current research is investigating computationally efficient methods of accurately bounding the actual $\mathcal{W}$.

The output constraints will be both on the spacecraft state and on the input magnitude. The spacecraft state will be constrained to error box of dimensions (in meters) of $5 \times 10 \times 5$ in the radial, in-track, and cross-track directions, respectively, of an LVLH frame. In addition, the spacecraft will be constrained to have a maximum acceleration in each direction of 0.003 m/s^2. The cost function will be the one-norm of the thrust inputs over the planning horizon. The controller's cost function and constraints are both linear, so the controller optimizations are formulated as linear programs. A two week simulation of four spacecraft on an equally spaced passive aperture formation is shown in Figure 4–8. The passive aperture formation is a drift-free in-track–cross-track projected circle with a 100 meter radius and in-track–radial 400×200 meter ellipse. A fuel-weighted virtual center method, described in Ref. [42], is used to minimize state error and equalize fuel use across the formation. Spacecraft error box motion throughout the duration of the simulation is shown in Figure 4–11. It can be observed from the figures that no spacecraft exceeds its state constraints at any time in the simulation. However, the trajectories of the spacecraft remained close to the center of their respective error boxes, likely a result of the requirement that the each spacecraft arrive at the origin at the end of its plan. On average over the course of the simulation, each spacecraft used 14.5 mm/s of fuel per orbit, significantly more than 2.46 mm/s per orbit, the figure reported for a similar simulation in Ref. [42].

To reduce fuel expenditures, an alternate terminal constraint set was used, in which the spacecraft is restricted to lying on a closed ellipse in the LVLH frame at the end of the plan [60]. This requirement is enforced through two conditions:

1. The spacecraft must remain inside the error box at every time step for a full orbit after the plan ends.
2. The spacecraft state at the end of the plan is restricted to be the same as the state a full orbit after the end of the plan

The origin terminal condition is a subset of the closed form ellipse terminal condi-

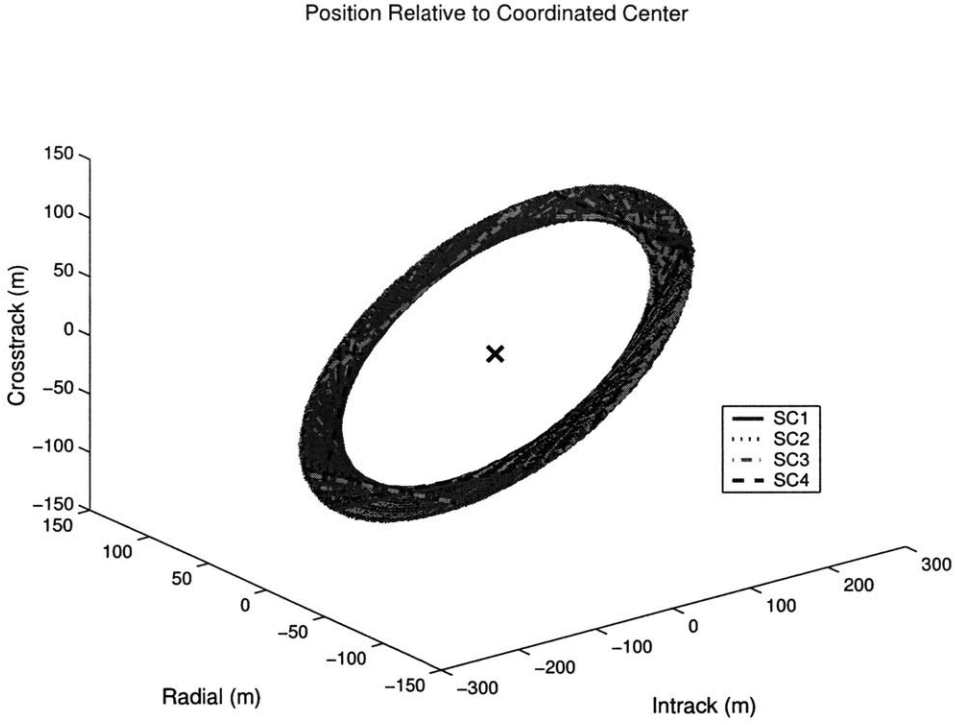

Fig. 4–8: Formation Relative to the Virtual Center

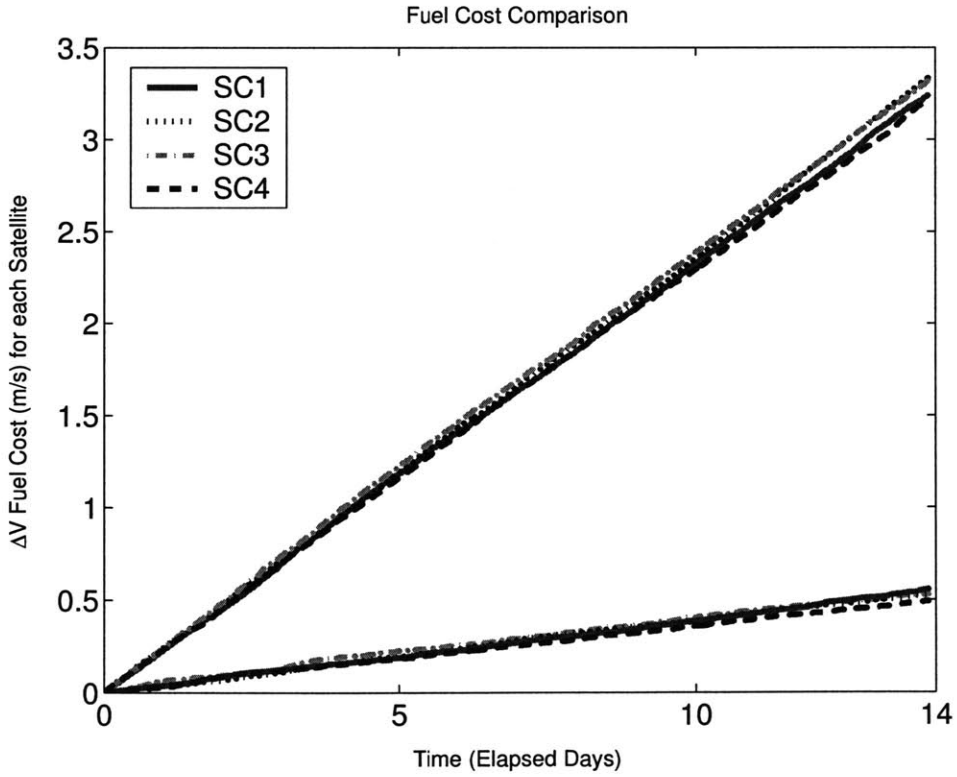

Fig. 4–9: Effect of Terminal Condition on Fuel Use Rates

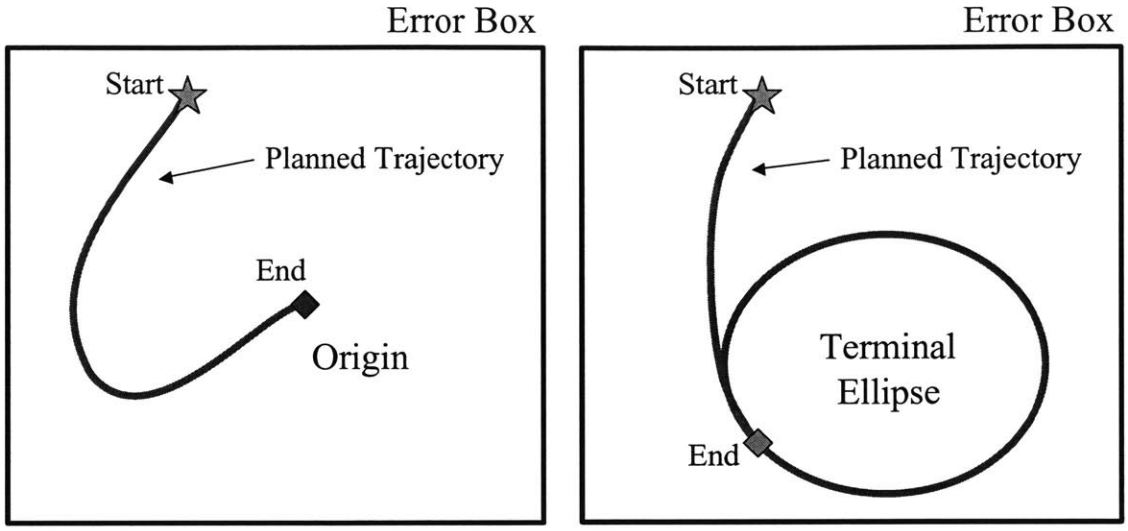

(a) Origin

(b) Closed Ellipse

Fig. 4–10: Terminal conditions examined for closed loop MPC

tion, because Hill's equations state that a spacecraft at the origin of an LVLH frame (*i.e.,* zero position and zero velocity) will remain motionless in that frame. This motionless trajectory is a closed form ellipse with major and minor radii of zero meters. The difference between the terminal conditions is illustrated in Figure 4–10.

Figure 4–12 shows error box motion during a two week simulation using the closed ellipse terminal conditions. It is clear that the spacecraft motion occupies a much larger region of the error box and appears to take on the shape of an ellipse in the in-track–radial plane. As expected, the less restrictive terminal conditions led to significantly lower average fuel usage: 2.22 mm/s per orbit, which is a slight improvement over the results in Ref. [42]. Unlike the approach used previously, the closed-loop robust method replans at all times, effectively guaranteeing that the spacecraft never drifts out of the error box. Furthermore, the spacecraft never enters an area of the error box that would be costly, from a fuel-use perspective, to prevent a constraint violation. The tradeoff for using the closed-loop method is that known time-varying disturbances must now be modeled as bounded polytopes, which does not allow the controller to exploit well-known orbital dynamics. It is likely that performance can

be further improved by using the LTV relative dynamics used for planning in Ref. [68] (excluding cross disturbances) to capture J_2 effects and creating a new bounded process noise model. By including some of the effects of J_2 in the state transition matrix, the system should be better able to exploit natural dynamics and be capable of operating with less conservative process noise bounds. Both of these improvements should reduce overall use.

4.6 Chapter Summary

A form of MPC previously introduced in Ref. [66], has been shown to be valid for spacecraft and has been used to explore the parameter space of spacecraft formation flying problems in general. For a particular problem, preferred settings of replan frequency and planning horizon length were suggested. An optimal relation of error box size to sensing noise was determined. It was also shown that for a given error box size there is a particular planning horizon length that gives the minimum fuel use. Trends and optimums were identified without recourse to numerical simulation.

Spacecraft formation flying simulations using the closed loop MPC controller were conducted using a nonlinear orbit propagator with a realistic disturbance and sensor noise models and constraints on state error and thrust magnitude. These simulations were done using two alternate terminal conditions. The first, restricted the spacecraft to end each plan at the origin. The other was less restrictive and only required each plan to terminate on a closed ellipse. The simulations demonstrated that the closed-loop method of uncertainty robustness is viable (succeeds in satisfying constraints while consuming fuel at comparable or lower rates than other methods) for realistic applications and that the closed ellipse terminal condition is much more fuel-efficient than the origin terminal condition.

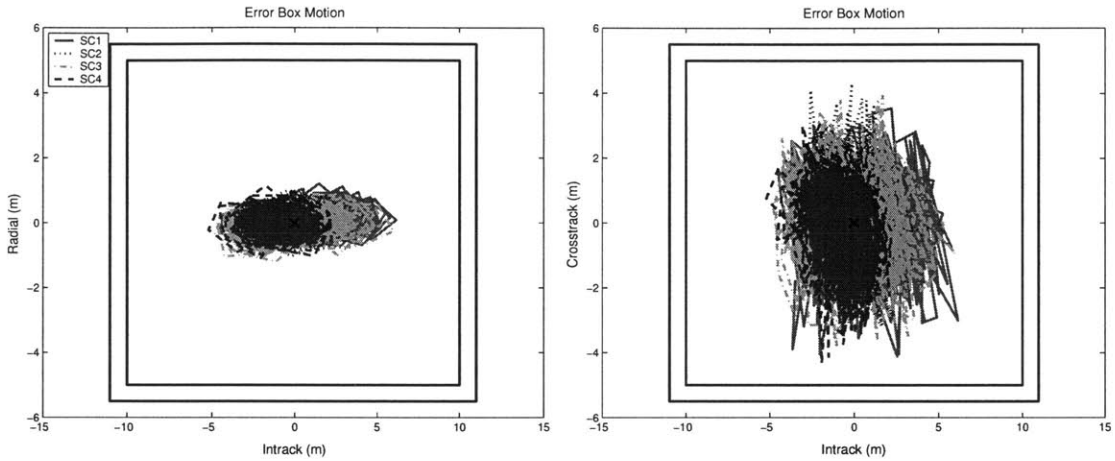

(a) Radial–In-track Error Box

(b) Cross-track–In-track

Fig. 4–11: Error box motion using Origin terminal constraint

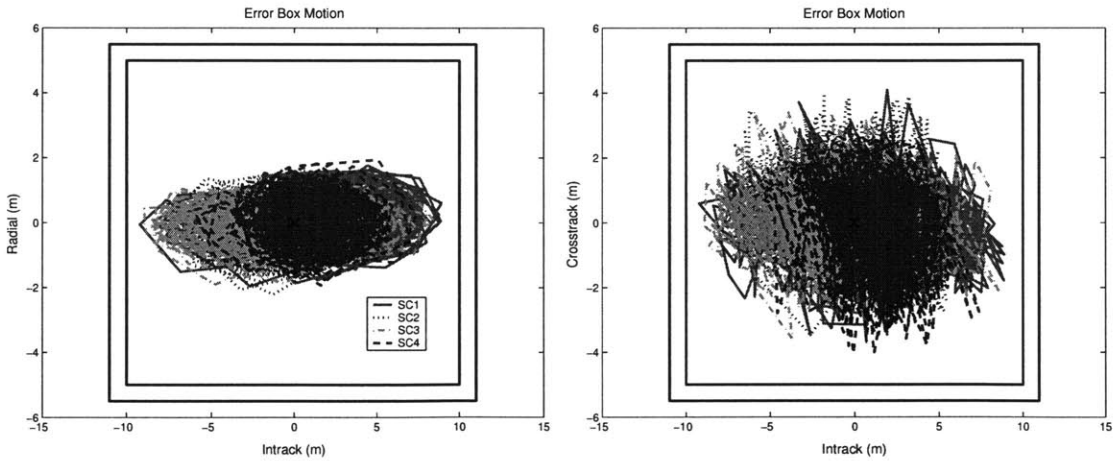

(a) Radial–In-track Error Box

(b) Cross-track–In-track

Fig. 4–12: Error box motion using Closed Ellipse terminal constraint

Chapter 5

Hardware Testbed Development

In order to evaluate the control approaches presented in Chapters 2, 3, and 4 in an environment with realistic output feedback, communication, and synchronization constraints, the control algorithms were integrated with flight-ready GPS receivers at the Goddard Space Flight Center (GSFC) Formation Flying Testbed (FFTB). The integrated hardware setup employed a Spirent GPS signal generator [79] to create realistic GPS signals, which were provided to GPS receivers and used for real-time absolute and relative state estimation, described in detail in Ref. [69]. The estimated state was used by the controller, which then closed the loop. A photograph of the test setup is shown in Figure 5–1.

5.1 Formation Flying Testbed at GSFC

In 2002, Busse used the Spirent Signal Generator at GSFC to evaluate an adaptive Carrier-Phase Differential GPS (CDGPS) estimator [70]. In the work conducted in July and August 2003, a decentralized form of the same adaptive estimator was re-evaluated using Orion and Architect GPS receivers, leading to a new hardware-in-the-loop formation flying testbed [69]. This chapter describes the expansion of the off-line Signal Generator/GPS Receiver system into a real-time closed-loop testbed using distributed computation and GPS hardware. To create the testbed, all relative navigation and control implementations were decentralized and distributed across the

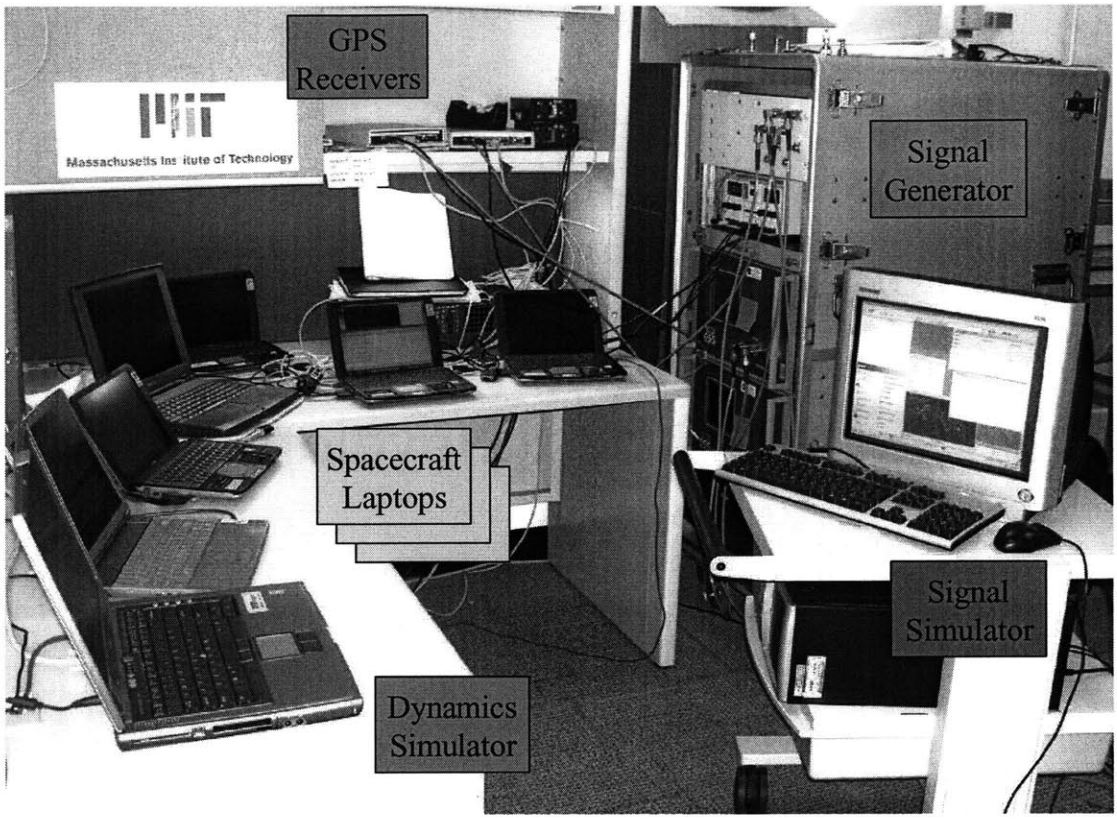

Fig. 5–1: GSFC Formation Flying Testbed

multiple vehicles in the fleet (typically 4). Separate computers were used to implement the algorithms for each spacecraft, ensuring that all communication and synchronization issues likely to occur in a real formation flying mission were addressed. In addition, software was developed to provide dynamics to the Spirent Signal Generator in real-time at a rate of 10 Hz, while maintaining synchronization across the entire testbed to within a hundredth of a second using a global clock pulse. The resulting system was shown to be capable of closed-loop operation.

Figures 5–1 and 5–2 show the specific hardware used to simulate a three-spacecraft formation at NASA GSFC. The testbed uses multiple laptops to run controllers and estimators for each spacecraft, and an additional laptop simulates the vehicle dynamics. The motions of the spacecraft were simulated using FreeFlyer^{TM}, a fully nonlinear orbit propagator with many realistic disturbances including J_2 and third body effects. Communications between the "spacecraft" were sent via TCP/IP on a local network,

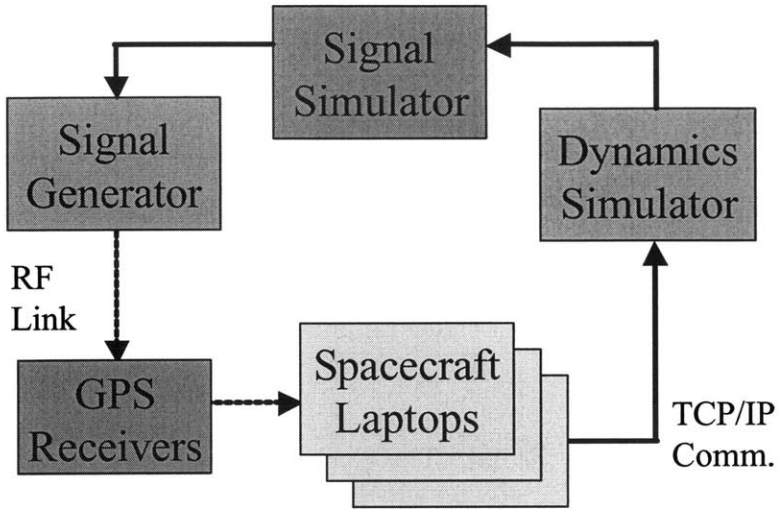

Fig. 5–2: Information Flow Through Hardware

as was communication between the dynamics simulator, the spacecraft, and the signal generation computer. Communication from the signal generators to the GPS receivers was through a RF link, which connected directly to the antenna port of the receiver. Simulating dynamics in real-time was a key challenge with five Windows-networked computers, online linear programming optimization, and MATLAB-based algorithm implementations. The receiver/estimator/controller portion of the testbed was operated on a slower time step, typically in the range of 4–10 seconds. Figure 5–2 shows the flow of information through the testbed.

For a fleet of n spacecraft, the testbed requires a total of $3+n$ computers – one for each spacecraft to run the controller and estimator, and then a total of 3 for the Dynamics Simulator, Signal Simulator, and the Operator. The Dynamics Simulator runs the orbit propagation software and an instance of MATLAB, which is used to communicate with the other computers in the testbed. The Signal Simulator computer runs SimGen^{TM} software, which receives state information for each spacecraft and drives the Signal Generator (Spirent 4760) via a data cable. The Operator computer can be used to enable/disable the controllers in the fleet. A BNC cable connected both the Dynamics Simulator and the Signal Simulator to the Signal Generator, which

Table 5.1: Communication Channels in Testbed

Number of Channels	Channel Description
1	Dynamics Simulator / Signal Simulator
n	Dynamics Simulator / Controllers
n	Controllers / Estimators
n	Controllers / Operator
n-1	Leader Controller / Follower Controllers
n-1	Leader Estimator / Follower Estimators

provided a clock pulse every second. The clock pulse was used to correct for clock drift between the computers in the system, which enabled time-synchronization to be maintained across the testbed for a 0.1 second time step. For the demonstrations described in this section, the controllers were both placed on a single computer and the estimators were placed on separate computers. This configuration eased software development, because the controller software and estimator software were maintained by different researchers.

5.2 Testbed Initialization and Operation

A precisely-timed and sequenced initialization procedure is required to begin testbed operation. To operate, the testbed requires a total of $1 + 3n + 2(n - 1)$ TCP/IP communication channels to be opened. A description the channel allocation is listed in Table 5.1. Before simulation begins, the communication channels connecting the controllers to the Dynamics Simulator and the Dynamics Simulator to the Signal Simulator must be established. The remaining communication channels must be established before estimation and control begin.

After having established the Dynamics Simulator communication channels, the simulation itself is begun using the procedure described in Algorithm 5.1. After this procedure is carried out, the Dynamics Simulator/Signal Simulator/Signal Generator portion of the testbed is ready to begin regular operation. The procedure for ongoing dynamics propagation and signal generation is described in Algorithm 5.2, which

Algorithm 5.1: Dynamics Simulator Initialization Procedure

Connect Dynamics Simulator to Signal Simulator;
for all Spacecraft i **do**
  Send initialization state for spacecraft i to Signal Simulator;
end for
for all Spacecraft i **do**
  Send state at time 0.0 seconds spacecraft i to Signal Simulator;
end for
Send "Run" command to Signal Simulator;
Wait for timing pulse from Spirent Signal Generator;
t:=time of simulated GPS signal = 0.0 seconds;
t_{dyn}:= 0 = seconds elapsed on Dynamics Simulator since timer reset;
t_{off}:= 0 = seconds of error between Dynamics Engine timer and Signal Simulator clock;
t_{sim}:= 0.3 = time of current dynamics simulation state in seconds elapsed;
Reset timer on Dynamics Simulator;
for all Spacecraft i **do**
  Send initial state with time tag 0.3 (seconds) for spacecraft i to Signal Simulator;
end for

Algorithm 5.2: Testbed Steady-State Procedure

t:=current GPS signal generator time;
for all Spacecraft i; **do**
  Propagate spacecraft i state to time t+0.3 seconds;
end for
t_{sim} = t+0.3;
Pause while $t_{dyn} + t_{off} < t_{sim}$ - 0.15;
for all Spacecraft i; **do**
  Send spacecraft i state to Signal Simulator;
end for
if $0.9 < t_{sim}$ - floor(t_{sim}) < 1.1 **then**
  t_{off} = round(t_{dyn}) - t_{dyn}; Update synchronization
end if
for all Spacecraft i; **do**
  Check if spacecraft i has sent a thrust command;
end for
if t_{sim} - floor(t_{sim}) = 0.0 **then**
  for all Spacecraft i; **do**
    Implement thrust command for spacecraft i if one was sent in the last second;
  end for
end if

includes details on both communication and time synchronization. During regular operation, the simulation engine stays two 0.1 second time steps ahead of the actual GPS simulation time, creating an inherent delay in the control system. If a communication between the Dynamics Simulator and the Signal Simulator arrives late, the Signal Simulator will stop operating and the simulation will halt. This portion of the testbed can operate independently of the control and estimation.

Before estimation and control can begin, the GPS receivers connected to the Signal Generator must be successfully tracking a sufficient number (8–12) GPS satellites. Once a sufficient number of satellites are being tracked, the communication channels between the estimators and controllers are established and estimation is begun. The controllers are initially in a sleeping mode, in which they send zero thrust commands. After a brief period of time (typically fifteen to twenty minutes) when it has been manually determined that the estimators converged, a command is sent from the Operator computer to the controllers indicating that they should begin to control the formation. Thus, control cannot begin for at least twenty minutes after estimation begins. Estimation cannot begin until the receivers are tracking a sufficient number of satellites (which often takes ten minutes). For this reason, the formation must be initialized in a stable configuration that does not drift significantly over the course of twenty minutes.

5.3 Closed-Loop Operation

The closed loop operation of the testbed involves regular coordinated communications between the estimators, the controllers, and the Dynamics Simulator. Although the dynamics simulation is run using a 0.1 second time step, the control/estimation loop is operated more slowly in order to facilitate the more complex sequence of communications which must occur. This slower rate is referred to as the Control time step and lies in the 4–10 second range for simulations described in this Chapter. Each of the estimators and controllers runs in a separate MATLAB instance and all communication occurs through TCP/IP sockets. In order to maintain synchronization

between many separate components, algorithms were developed for the controllers and estimators describing the order in which communications should arrive. Also described are actions which should be taken in the event of late message arrivals in order to prevent the system from losing synchronization. The estimator communication algorithms are described in [69]. This section describes the controller algorithms using a state machine model.

After the estimators have converged and control has been enabled, the control / estimation / Dynamics Simulator system enters into a regular pattern of estimate and control input exchange. Once enabled, the controller on the Leader spacecraft follows the logic described by the state transition diagram in Fig. 5–3. The Leader spacecraft controller begins in the **Waiting for Data** state, in which it is waiting for an absolute state estimate from its controller and relative state estimates from the Follower spacecraft. When all data has been received, a transition is made to the **Calculate Virtual Center** state, where the fuel-weighted average of the formation is computed according to the procedure described in Ref. [42]. After the virtual center is computed, the state immediately transitions to **Distribute Virtual Center**, in the location of the center state is sent to the Follower spacecraft. If the spacecraft is in either the **Calculate Virtual Center** or the **Distribute Virtual Center** state and a more recent relative state arrives from one of the Follower spacecraft or a more recent absolute state arrives from the Leader spacecraft estimator, the new state is kept and all old state information is abandoned. The spacecraft would then transition back to the **Waiting for Data** state. Alternately, after broadcasting the virtual center state, the leader computes its control commands in the **Compute Control** state and transmits it in the **Transmit Thrusts** state. If the control computation takes longer than a Control time step, then the resulting control command is set to zero in the **Null Thrusts** before transmitting. After transmitting the thrusts, the controller returns to the initial waiting state.

The Follower controller state transition diagram is in Figure 5–4 and is similar to the diagram for the Leader. The Follower spacecraft also begins in a **Waiting for Data** state, but does not transition out of it until it has received a relative state from

State Transition Diagram: Leader Control Logic

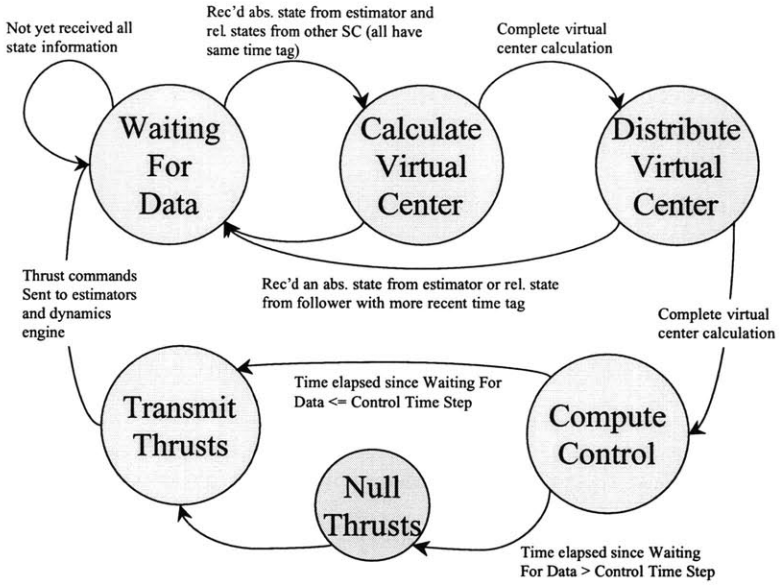

Fig. 5–3: Control Logic: Leader

State Transition Diagram: Follower Control Logic

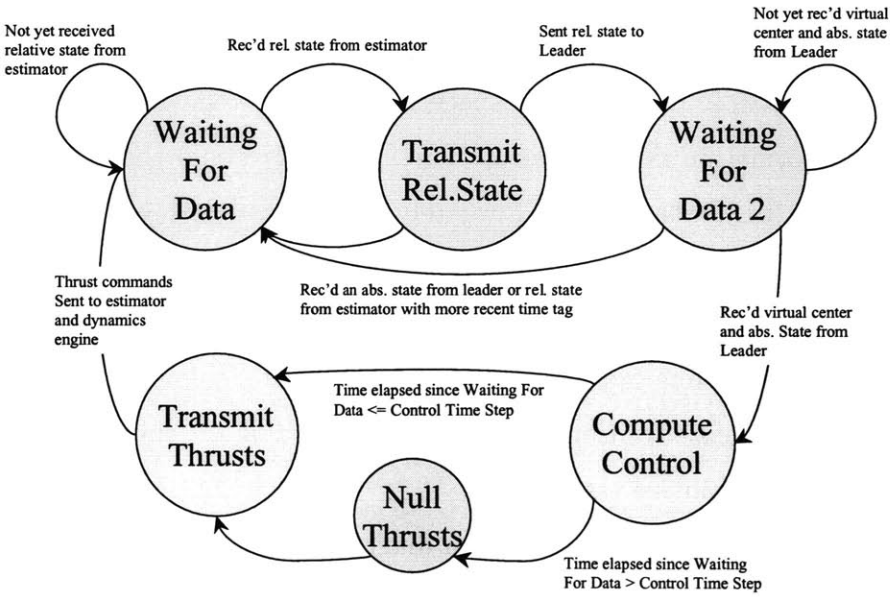

Fig. 5–4: Control Logic: Follower

its estimator. After receiving a relative state estimate, the Follower will transition to a **Transmit Relative State** state, in which it sends its relative state to the Leader controller and then transitions to the **Waiting for Data 2**, where no computations are performed. From either the **Transmit Relative State** state or the **Waiting for Data 2** state, if the Follower receives a more recent relative state from its estimator or an absolute state from the Leader that is more recent than its current relative state, it will transition back to the initial waiting for data state, retaining only the most recent data. If the follower is in the second waiting state and receives (or has already received) an absolute state estimate whose time matches the time of the relative state estimate, it will transition to the **Compute Control** state. The rest of the Follower logic is the same as the logic of the Leader.

5.4 Results

Several basic simulations were conducted using the new testbed. The initial simulations involved no control and were used to demonstrate online estimation using trajectory data generated by the Dynamics Simulator and streamed in real-time through the Signal Generator by way of the Signal Simulator. Subsequent simulations were conducted with controllers in the system, but with their control set to zero. Estimation results from these simulations can be found in Ref. [69].

Figure 5–5 shows results of a full hardware simulation in which control was enabled after approximately thirty minutes of estimation had elapsed. The spacecraft in the simulation were separated by twenty meters in the in-track direction of a LVLH frame centered on one of the spacecraft. The controller used in this example was a LQR with a very high control weighting. It was determined through experimentation that high bandwidth control caused the receivers to lose lock on satellites and the resulting decrease in estimator performance led to unstable behavior. The control objective in the figure is to cause the two satellites to rendezvous, and after the control is enabled, the satellite separation begins to decrease steadily. While these initial results may appear simple, this closed-loop behavior is the result of many different

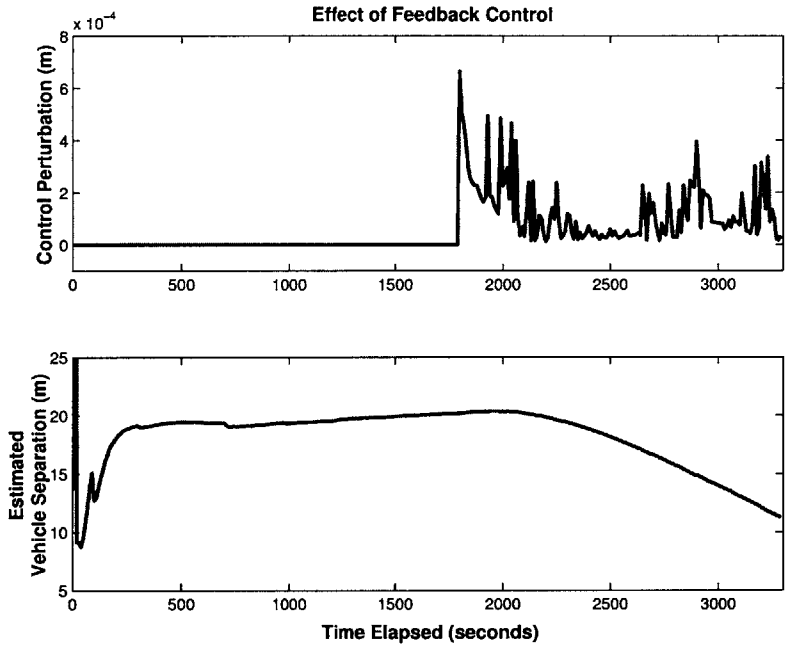

Fig. 5–5: Effect of Closed Loop Feedback Control

interconnecting, tightly-synchronized software and hardware components working in a coordinated fashion to simulate, estimate, and control a spacecraft formation flying mission.

5.5 Chapter Summary

An hardware-in-the-loop testbed was created at Goddard Space Flight Center using Orion GPS receivers, a Spirent GPS Signal Generator, a network of laptops across which computation was distributed. The system was driven with a nonlinear orbit propagator using a realistic disturbance model and was operated at a rate of 10 Hz with a real-time deadline. It was demonstrated that online estimation of the type described in Ref. [69] could converge correctly in the system with no control present. It was also shown that control could be introduced and utilized successfully at low bandwidth. The testbed has been used for an initial series of closed-loop tests, and it should be a valuable asset for future validation of combined control and estimation systems in realistic environments.

Chapter 6

Conclusions

This thesis addressed several problems associated with controlling formation flying spacecraft. This includes developing new initialization techniques for formations with large separations in highly elliptical orbits were developed. In addition, methods of predicting and mitigating the effects of CDGPS sensor noise were applied to the spacecraft formation flying problem in Low Earth Orbit. A new hardware-in-the-loop testbed was created to evaluate the combined estimation and spacecraft control in closed-loop with real-time constraints. This chapter presents a summary of the principal contributions of the thesis and concludes with a discussion of possible extensions to the work presented.

6.1 Thesis Contributions

Technical contributions were made to the areas of formation initialization, relative dynamics propagation, performance prediction, and sensor noise robustness.

Generalized Long-baseline Initializations: The approach to form large passive apertures in Ref. [48] was extended to allow formations with an arbitrary geometry, such as a tetrahedron. This approach was applied to both LEO and HEO mission scenarios, but was shown to lose effectiveness for highly eccentric orbits.

Time-varying Relative Dynamics Propagation: A set of relative equations of motion, similar to Lawden's equations, was derived that can be used in a time-varying sense in an LVLH frame. The equations of motion are written as explicit functions of the orbital elements of the reference orbit and are intended to be used in a discrete time controller (such as the MPC controller developed Ref. [30]) after having been numerically discretized. These equations of motion allow for simpler online planning than Lawden's equations, because they shift the creation of the mapping between time and true anomaly to the controller formulation stage, rather than the time-critical thrust implementation stage, and also bypass the need to rotate thrust inputs out of Lawden's frame. Control using these equations of motion was demonstrated for a tetrahedron-shaped formation in a highly elliptical orbit over a period of two weeks.

Planning Based on GVEs: Derived a linearized form of the relative dynamics from Gauss' Variational Equations that can be used in an optimized planning controller. The combined system of dynamics/model predictive controller was demonstrated to be more efficient than an impulsive approach from the literature and had the added advantage of being able to incorporate linear, convex performance constraints. Also presented a method for optimizing a formation geometry (specified in differential orbital elements) by minimizing the fuel required for the fleet to perform the necessary maneuvers. The approach exploits the various degrees of freedom in the problem, such as the velocity of the spacecraft and the orientation, translation, and scaling of the formation. The virtual center [68] developed to coordinate the formation flying controllers on each spacecraft was re-derived using differential orbital elements. It was also demonstrated that the virtual center could be computed using a decentralized calculation.

Formation Flying MPC Performance Prediction: Validated the assumptions required to use the Robust MPC performance prediction method introduced in [59]. Examined several case studies to demonstrate the viability of formation flying performance prediction. A complete MPC controller using closed-loop robustness and

thrust constraints was formulated and used in a realistic simulation and disturbance environment to control a formation of four satellites for two weeks. This demonstrated the validity of a bounded noise model for LEO and the ability of the closed-loop robust MPC approach to be used for a realistic spacecraft formation flying mission. Longer planning horizons enabled the use of more general optimization terminal conditions than were possible using the open-loop method. The closed-loop method using more general terminal conditions guarantees the robustness of the planning system to both process and sensing noise and is demonstrated to use fuel at rates similar to those of the open-loop method.

Formation Flying Testbed: A hardware-in-the-loop formation flying testbed was created using GPS receivers and a GPS signal generator at the Goddard Space Flight Center. The orbital dynamics used in the testbed were generated by a nonlinear orbit propagator with a realistic disturbance model and provided to the signal generator at a rate of 10 Hz with a real-time deadline. The testbed was composed of multiple computers (representing individual spacecraft) which necessitated that attention be paid to communication and coordination requirements of the decentralized controller/estimator system. The testbed was demonstrated operating in a closed-loop simulation.

6.2 Areas of Future Work

Although work must and should be frequently published and shared with the research community, it is the conviction of this researcher that no topic is ever fully exhausted. In this spirit, experience suggests several improvements and investigations related to the work herein may prove fruitful.

On the topic of drift-free initialization, the approaches presented in Chapters 2 and 3 to create drift-free formations of arbitrary geometry have only been posed in the context of specifying a geometry at a single point in an orbit. A useful extension of this work would allow constraints to be placed on other individual times or on all times

in the orbit. An example of such a constraint would be the passive aperture, in which the formation creates a projected circle continuously throughout the orbit. Another example would be for collision avoidance, whereby it could be specified that the initial conditions on a formation create orbits that do not come within a certain distance of one another at any time. Chapter 3 presents two methods of formation coordination: optimized initial conditions which consider minimization of error across the formation and the decentralized fuel-weighted virtual center. In the work presented in this thesis, initial conditions were chosen once, at the start of each simulation. Another approach would be to optimize the initial conditions at every time-step, which is feasible for LP optimization. The correct frequency of re-optimizing the desired initial conditions versus shifting the center of the formation remains to be determined.

In Chapter 4, a method of closed-loop robust MPC is reviewed and applied to the spacecraft formation flying problem. Presently, this MPC method has not been developed for time-varying dynamics, the class of dynamics into which most non-circular orbits fall. Hence, to be applied to MMS-like missions, the the closed-loop robust method must be derived and shown to be robustly feasible for the type of periodic time-varying dynamics present in Lawden's equations and GVEs. The nature of the formulation suggests that this may be possible for planning horizon lengths that are greater than the period of the dynamics (typically the period of an orbit). Planning horizons are already normally as long or longer than an orbit so as to capture all possible advantageous dynamics in the system, hence a restriction of this type would likely pose no obstacle to use the use of the closed-loop robustness method.

The formation flying testbed described in Chapter 5 holds a great deal of potential for future hardware-in-the-loop demonstrations of Matlab-based control and estimation algorithms. Future improvements to this testbed should include increased robustness to missed communications between control and estimation implementations, additional means of real-time monitoring and control of the testbed as a whole, and method of "fast-starting" the GPS receivers and estimators in order to decrease the time between simulations. Also, many of the algorithms running on the dynamics simulator should be ported to a compiled language in order to add timing margin

(through increased execution speed) to the only critically real-time portion of the testbed.

6.3 Final Comments

The field of spacecraft formation flying control has provided a wealth of opportunities for the application of cutting-edge controls and dynamics techniques. It is the sincere hope of this researcher that the field continues to develop and that some portion of the research contained herein may someday be used as the basis for future work or in an actual spacecraft formation flying mission.

Bibliography

[1] F. Bauer, K. Hartman, J. Bristow, D. Weidow, J. How, F. Busse, "Enabling Spacecraft Formation Flying Through Spaceborne GPS and Enhanced Autonomy Technologies," *ION-GPS '99*, Proceedings of the 12th International Technical Meeting of the Satellite Division of the Institute of Navigation, Nashville, TN, Sept. 14-17, 1999 (A01-27218 06-32), Alexandria, VA, Institute of Navigation, 1999, p.369-383.

[2] A. Das, R. Cobb, "TechSat 21 - Space Missions Using Collaborating Constellations of Satellites," *Proceedings of AIAA/USU Annual Conference on Small Satellites*, 12th, Utah State University, Logan, Aug. 31-Sept. 3, 1998, Proceedings (A99-10826 01-20), Logan, UT, Utah State University, 1998.

[3] C. Beichman, "The Terrestrial Planet Finder - The search for life-bearing planets around other stars," *Proceedings of Astronomical Interferometry Meeting*, Kona, HI, Mar. 20-24, 1998. Pt. 2 (A98-40801 11-35), Bellingham, WA, Society of Photo-Optical Instrumentation Engineers (SPIE Proceedings. Vol. 3350), 1998, p. 719-723.

[4] F. Bauer, J. Bristow, D. Folta, K. Hartman, D. Quinn, J. How, "Satellite Formation Flying Using an Innovative Autonomous Control System (AutoCon) Environment," *Proceedings of AIAA Guidance, Navigation, and Control Conference*, New Orleans, LA, Aug. 11-13, 1997, Collection of Technical Papers. Pt. 2 (A97-37001 10-63), Reston, VA, American Institute of Aeronautics and Astronautics, 1997, p. 657–666.

[5] J. How, R. Twiggs, D. Weidow, K. Hartman, F. Bauer, "Orion - A low-cost demonstration of formation flying in space using GPS," *Proceedings of AIAA/AAS Astrodynamics Specialist Conference and Exhibit*, Boston, MA, Aug. 10-12, 1998, Collection of Technical Papers (A98-37348 10-13), Reston, VA, American Institute of Aeronautics and Astronautics, 1998, p. 276-286.

[6] J. Leitner, F. Bauer, D. Folta, M. Moreau, R. Carpenter, J. How, "Distributed Spacecraft Systems Develop New GPS Capabilities," in *GPS World: Formation Flight in Space* Feb. 2002.

[7] R. Sedwick, D. Miller, E. Kong, "Mitigation of Differential Perturbations in Clusters of Formation Flying Satellites," *Proceedings of the AAS/AIAA Space Flight Mechanics Meeting*, Breckenridge, CO, Feb. 7-10, 1999. Pt. 1 (A99-39751 10-12), San Diego, CA, Univelt, Inc. (Advances in the Astronautical Sciences. Vol. 102, pt.1), 1999, p. 323-342.

[8] M. Kaplan. *Modern Spacecraft Dynamics and Control.* Wiley, 1976.

[9] D. Vallado. *Fundamentals of Astrodynamics and Applications.* McGraw-Hill, 1997.

[10] D. Lawden, *Optimal Trajectories for Space Navigation,* Butterworths, London, 1963.

[11] T. Carter, M. Humi, "Fuel-Optimal Rendezvous Near a Point in General Keplerian Orbit," AIAA Journal of Guidance, Control, and Dynamics , vol. 10, Nov.-Dec. 1987, p. 567-573.

[12] T. Carter, "New Form for the Optimal Rendezvous Equations Near a Keplerian Orbit," AIAA Journal of Guidance, Control, and Dynamics , vol. 13, Jan.- Feb. 1990, p. 183-186.

[13] J. Marec, *Optimal Space Trajectories,* Elsevier Scientific, NY 1979.

[14] H. Schaub, K. Alfriend, "J_2 Invariant Relative Orbits for Spacecraft Formations," In *Goddard Flight Mechanics Symposium,* May 18-20,1999, Paper No. 11.

[15] G. Inalhan, J. How, "Relative Dynamics and Control of Spacecraft Formations in Eccentric Orbits," *Proceedings of the AIAA Guidance, Navigation, and Control Conference and Exhibit*, Denver, CO, Aug. 14-17, 2000, Collection of Technical Papers, Reston, VA, American Institute of Aeronautics and Astronautics, 2000. AIAA Paper 2000-4443.

[16] M. Tillerson, J. How, "Formation Flying Control in Eccentric Orbits," *Proceedings of the AIAA Guidance, Navigation, and Control Conference*, Montreal, Canada, Aug. 6-9, 2001, Collection of Technical Papers, Reston, VA, American Institute of Aeronautics and Astronautics, 2001.

[17] H. Yeh, A. Sparks, "Geometry and Control of Satellite Formations," *Proceedings of the 2000 American Control Conference*, Chicago, IL, June 28-30, 2000. Vol. 1 (A01-12703 01-63), Piscataway, NJ, Institute of Electrical and Electronics Engineers, 2000, p. 384-388.

[18] G. Inalhan, M. Tillerson, J. How, "Relative Dynamics & Control of Spacecraft Formations in Eccentric Orbits," AIAA Journal of Guidance, Control, and Dynamics (0731-5090), vol. 25, no. 1, Jan.-Feb. 2002, p. 48-59.

[19] S. Vadali, S. Vaddi, K. Naik, K. Alfriend, "Control of Satellite Formations," *Proceedings of the AIAA Guidance, Navigation, and Control Conference*, Montreal, Canada, Aug. 6-9, 2001. AIAA Paper 2001-4028.

[20] A. Sparks, "Satellite Formationkeeping Control in the Presence of Gravity Perturbations," *Proceedings of the 2000 American Control Conference*, Chicago, IL, June 28-30, 2000. Vol. 2 (A01-12740 01-63), Piscataway, NJ, Institute of Electrical and Electronics Engineers, 2000, p. 844-848.

[21] A. Robertson, G. Inalhan, J. How, "Formation Control Strategies for a Separated Spacecraft Interferometer," *Proceedings of the 1999 American Control*

Conference, San Diego, CA, June 2-4, 1999, Proceedings. Vol. 6 (A00-15511 02-63), Piscataway, NJ, Institute of Electrical and Electronics Engineers, 1999, p. 4142-4147.

[22] R. Bate, D. Mueller, J. White, *Fundamentals of Astrodynamics,* Dover Publications Inc., NY, 1971.

[23] V. Chobotov, *Orbital Mechanics,* Second Edition, AIAA Educational Series, 1996.

[24] A.I. Solutions, "FreeFlyer User's Guide", Version 4.0, March 1999.

[25] G. Franklin, J. Powell, M. Workman, "Digital Control of Dynamic Systems," Third Edition,Addison-Wesley, 1998.

[26] R. Sedwick, T. Hacker, D. Miller, "Optimum Aperture Placement for a Space-Based Radar System Using Separated Spacecraft Interferometry," *Proceedings of the AIAA Guidance, Navigation, and Control Conference*, Portland, OR, Aug. 9-11, 1999. AIAA Paper 99-4271.

[27] F. Busse, G. Inalhan, How, J. P., "Project ORION: Carrier Phase Differential GPS Navigation For Formation Flying," *Proceedings of the Annual AAS Rocky Mountain Conference*, Breckenridge, CO, Feb. 2-6, 2000 (A00-41276 11-12), San Diego, CA, Univelt, Inc. (Advances in the Astronautical Sciences. Vol. 104), 2000, p.197-212.

[28] F. Busse, J. How, J. Simpson, and J. Leitner, "PROJECT ORION-EMERALD: Carrier Differential GPS Techniques and Simulation for Low Earth Orbit Formation Flying," presented at the *IEEE Aerospace Conference*, Mar 10-17, 2001.

[29] A. Richards, J. How, T. Schouwenaars and E. Feron, "Plume Avoidance Maneuver Planning Using Mixed Integer Linear Programming," *Proceedings of the AIAA Guidance, Navigation, and Control Conference*, Montreal, Canada, Aug. 6-9, 2001. AIAA Paper 2001-4091.

[30] M. Tillerson, G. Inalhan, and J. How, "Coordination and Control of Distributed Spacecraft Systems Using Convex Optimization Techniques," International Journal of Robust and Nonlinear Control, vol 12, Issue 2-3, Feb.-Mar. 2002, p.207-242.

[31] C. Park, P. Ferguson, N. Pohlman, J. How, "Decentralized Relative Navigation for Formation Flying Spacecraft using Augmented CDGPS," *Proceedings of Institute of Navigation GPS Conference*, Salt Lake City, Utah, Sept. 2001.

[32] J. How and M. Tillerson, "Analysis of the Impact of Sensor Noise on Formation Flying Control," *Proceedings of the 2001 American Control Conference*, Arlington, VA, June 25-27, 2001, Proceedings. Vol. 5 (A01-45851 12-63), Piscataway, NJ, Institute of Electrical and Electronic Engineers, 2001, p. 3986-3991.

[33] M. Tillerson, J. How, "Advance Guidance Algorithms for Spacecraft Formation Flying," accepted for *2002 American Control Conference*, Anchorage, AK, May 8-10, 2002, Piscataway, NJ, Institute of Electrical and Electronics Engineers, 2002.

[34] J. P. Vinti. *Orbital and Celestial Mechanics.* AIAA, 1998, pp.196-197.

[35] R. G. Melton, Time Explicit Representation of Relative Motion Between Elliptical Orbits, *JGCD* Vol. 23, No. 4, July - Aug. 2000, pp. 604-610.

[36] Breger, L., Ferguson, P., How, J.P., Thomas, S., McLoughlin, T. and Campbell, M., "Distributed Control of Form. Flying Spacecraft Built on OA," *AIAA GNC Conf.*, August 2003.

[37] Ilgen, Marc R., "Low Thrust OTV Guidance using Lyapunov Optimal Feedback Control Techniques," AAS/AIAA *Astrodynamics Specialist Conference*, Victoria, B.C., Canada, Aug. 16–19 1993, Paper No. AAS 93-680.

[38] Bo Naasz, *Classical Element Feedback Control for Spacecraft Orbital Maneuvers,* S.M. Thesis, Dept. of Aerospace Engineering, Virginia Polytechnic Institute and State University, May 2002.

[39] Mishne, D. "Formation Control of LEO Satellites Subject ot Drag Variations and J_2 Perturbations," AAS/AIAA Astrodynamics Specialist Conference, Monterey, California, August 2002.

[40] P. Gurfil, "Control-Theoretic Analysis of Low-Thrust Orbital Transfer Using Orbital Elements," *AIAA Journal of Guidance, Control, and Dynamics*, vol. 26, no. 6, November-December. 2003, p. 979-983.

[41] T.E. Carter, S.A. Alvarez, "Quadratic-Based Computation of Four-Impulse Optimal Rendezvous near Circular Orbit," *AIAA Journal of Guidance, Control, and Dynamics*, vol. 23, no. 1, January-February. 2000, p. 109-117.

[42] M. Tillerson, L. Breger, J. How, "Distributed Coordination and Control of Formation Flying Spacecraft," Proceedings of *American Control Conference*, June 2003.

[43] Schaub, Hanspeter and Junkins, John L., *Analytical Mechanics of Space Systems,* AIAA Education Series, Reston, VA, 2003.

[44] H. Schaub, K. Alfriend, "Impulsive Feedback Control to Establish Specific Mean Orbit Elements of Spacecraft Formations," *AIAA Journal of Guidance, Control, and Dynamics*, vol. 24, no. 4, July-Aug. 2001, p. 739-745.

[45] L. Mailhe, C. Schiff, and S. Hughes, "Formation Flying in Highly Elliptical Orbits: Initializing the Formation," *Proceedings of the International Symposium on Space Dynamics,* Biarritz, France, CNES, June 26-30, 2000. Paper MS00/21.

[46] Battin, Richard H., *An Introduction to the Mathematics and Methods of Astrodynamics,* AIAA Education Series, New York, 1987.

[47] Greenwood, Donald T., *Advanced Dynamics,* Cambridge University Press, Cambridge, 2003.

[48] K. T. Alfriend, H. Schaub, and D.-W. Gim, "Formation Flying: Accomodating Non-linearity and Eccentricity Perturbations," presented at the 12th *AAS/AIAA Space Flight Mechanics Meeting,* January 27-30, 2002.

[49] J. Guzman and C. Schiff, "A Preliminary Study for a Tetrahedron Formation (Spacecraft Formation Flying)," *AIAA/AAS Astro. Specialists Conf.*, Aug 2002.

[50] P. Robert, A. Roux, C. Harvey, M. Dunlop, P. Daly, and K. Glassmeier, "Tetrahedron Geometric Factors," Analysis Methods for Multi-Spacecraft Data (G. Paschmann and P. Daly, eds.), pp. 323348, Noordwijk, The Netherlands: ISSI Report SR-001, ESA Pub. Div., 1998.

[51] S. Curtis, "The Magnetospheric Multiscale Mission Resolving Fundamental Processes in Space Plasmas," NASA GSFC, Greenbelt, MD, Dec. 1999. NASA/TM2000-209883.

[52] J. R. Carpenter and K. T. Alfriend, "Navigation Accuracy Guidelines for Orbital Formation Flying," AIAA Guidance, Navigation, and Control Confrence, Austin, TX, Aug 11-4, 2003.

[53] D. Bertsimas and J.N. Tsitsiklas, *Introduction to Linear Optimization,* Athena Scientific, Belmont, 1997.

[54] W. Ren, and R. Beard, "Virtual Structure Based Spacecraft Formation Control with Formation Feedback," presented at the *AIAA GN&C Conference,* Aug. 2002.

[55] M. Tillerson, L. Breger, J. How, "Multiple Spacecraft Coordination & Control," Proceedings of the *American Control Conference*, pp. 1740-1745, June 2003.

[56] F. Busse, J. How, J. Simpson, and J. Leitner, "PROJECT ORION-EMERALD: Carrier Differential GPS Techniques and Simulation for Low Earth Orbit Formation Flying," presented at the *IEEE Aerospace Conference*, Mar 10-17, 2001.

[57] F. D. Busse and J. P. How, "Real-Time Experimental Demonstration of Precise Decentralized Relative Navigation for Formation-Flying Spacecraft," *AIAA Guidance, Navigation, and Control Conference,* August 2002, AIAA Paper 2002–5003

[58] A. Robertson, G. Inalhan, and J.P. How, "Spacecraft Formation Flying Control Design for the Orion Mission," in *Proceedings of AIAA/GNC*, August 1999.

[59] A. G. Richards and J. P. How, "Model Predictive Control of Vehicles Maneuvers with Guaranteed Completion Time and Robust Feasibility," American Control Conference, Denver CO, ACC, 2003.

[60] A. G. Richards and J. P. How, "A Computationally-Efficient Technique for Robust Model Predictive Control," submitted to IEEE Transactions on Automatic Control, February 2004.

[61] A. G. Richards and J P How, "Robust Constrained Model Predictive Control with Analytical Performance Prediction," submitted to GNC 2004, available from the authors by request.

[62] E. Kerrigan, Invariant Set Toolbox for Matlab, available at `http://www-control.eng.cam.ac.uk/eck21`, July 2003.

[63] E.C. Kerrigan, "Robust Constraint Satisfaction: Invariant Sets and Predictive Control," PhD Thesis, Cambridge University, November 2000.

[64] I. Kolmanovsky and E. G. Gilbert, "Maximal Output Admissible Sets for Discrete-Time Systems with Disturbance Inputs," American Control Conference, Seattle WA, ACC, 1995, p. 1995.

[65] P.O.M. Scokaert and D.Q. Mayne, "Min-Max Feedback Model Predictive Control for Constrained Linear Systems," *IEEE Transactions on Automatic Control*, vol 43., no 8., Aug. 1998, p.1136.

[66] L. Breger, A.G. Richards, M. Mitchell, and J.P. How, "Model Predictive Control of Spacecraft Formations with Sensing Noise," submitted to GNC 2004, available from the authors by request.

[67] A. G. Richards and J P How, "Robust Constrained Model Predictive Control with Analytical Performance Prediction," submitted to GNC 2004, available from the authors by request.

[68] M. Tillerson, "*C*oordination and Control of Multiple Spacecraft using Convex Optimization Techniques," S.M. Thesis, Massachusetts Institute of Technology, Dept. Aeronautics and Astronautics, June 2002.

[69] M. Mitchell, "*C*DGPS-Based Relative Navigation for Multiple Spacecraft," S.M. Thesis, Massachusetts Institute of Technology, Dept. Aeronautics and Astronautics, June 2004.

[70] F. D. Busse, J. Simpson, and J. P. How, "Demonstration of Adaptive Extended Kalman Filtering for LEO Formation Estimation Using CDGPS," *Navigation* Journal of the Institute of Navigation, Vol. 50, No. 2, Summer 2003, pp. 79–94.

[71] B.W. Parkinson, "Origins, Evolution, and Future of Satellite Navigation," AIAA Journal of Guidance, Control, and Dynamics , vol. 20, Jan.– Feb. 1997, p. 11–25.

[72] R.A. Broucke, "Solution of the Elliptic Rendezvous Problem with the Time as an Independent Variable," AIAA Journal of Guidance, Control, and Dynamics, vol. 26, July.– Aug. 2003, p. 615–621.

[73] J.R. Carpenter, J.A. Leitner, D.C. Folta, and R.D. Burns, "Benchmark Problems For Spacecraft Formation Flying Missions," *AIAA Guidance, Navigation, and Control Conference,* August 2003, AIAA Paper 2003–5364.

[74] N.H. Hamilton, D.C. Folta, and J.R. Carpenter, "Formation Flying Satellite Control Around the L2 Sun-Earth Libration Point," AAS/AIAA Astrodynamics Specialist Conference, Monterey, California, August 2002.

[75] G.W. Hill, "Researches in Lunar Theory," *A*merican Journal of Mathematics, Vol. 1, 1878, pp. 5–26,129–147,24–260.

[76] W.H Clohessy and P.S. Wiltshire, "Terminal Guidance System for Satellite Rendezvous," *J*ournal of Aerospace Sciences, Sept. 1960, pp. 653–658,674.

[77] Carpenter, J.R. and Schiesser, E.R., "Semimajor Axis Knowledge and GPS Orbit Determination," NAVIGATION: Journal of The Institute of Navigation, Vol. 48, No. 1, Spring 2001, p. 57-68.

[78] J. R. Carpenter and K. T. Alfriend, "Navigation Accuracy Guidelines for Orbital Formation Flying," AIAA Guidance, Navigation, and Control Confrence, Austin, TX, Aug 11-4, 2003.

[79] Spirent Communications, Inc., "Multi Channel High Dynamic GPS/SBAS Simulation Systems STR4760 Series." http://www.positioningtechnology.co.uk/datasheets/str4760.html.

[80] NASA Goddard Space Flight Center, "Magnetosphere MultiScale." http://stp.gsfc.nasa.gov/missions/mms/mms.htm.

[81] D.P. Scharf, F.Y. Hadaegh, and S.R. Ploen, "A Survey of Spacecraft Formation Flying Guidance and Control (Part I): Guidance," *2003 American Control Conference*, Denver, CO, June 4-6, 2003, Institute of Electrical and Electronic Engineers, 2003, p. 1733–1739.

[82] V. Kapila, A.G. Sparks, J.M. Buffington, and Q. Yan, "Spacecraft Formation Flying: Dynamics and Control," *2003 American Control Conference*, San Diego, CA, June 2-4, 1999, Institute of Electrical and Electronic Engineers, 1999, p. 4137–4141.

[83] G.E. Piper, J.M. Watkins, and J.P. How, "On the Control Design of the Disturbance Reduction System for the LISA Mission," *Proceedings of the AIAA Guidance, Navigation, and Control Conference*, Monterey, California, Aug. 5-8, 2002, Collection of Technical Papers, Reston, VA, American Institute of Aeronautics and Astronautics, 2002.